VOL. 107 NO. HY2. FEB. 1981

JOURNAL OF THE HYDRAULICS DIVISION

PROCEEDINGS OF
THE AMERICAN SOCIETY
OF CIVIL ENGINEERS

VOL.107 NO.HY2. FEB. 1981

JOURNAL OF THE HYDRAULICS DIVISION

PROCEEDINGS OF THE AMERICAN SOCIETY OF CIVIL ENGINEERS

Copyright© 1981 by
American Society
of Civil Engineers
All Rights Reserved
ISSN 0044-796X

AMERICAN SOCIETY OF CIVIL ENGINEERS

BOARD OF DIRECTION

President
Irvan F. Mendenhall

Past President
Joseph S. Ward

President Elect
James R. Sims

Vice Presidents
Robert D. Bay — Lyman R. Gillis
Francis J. Connell — Albert A. Grant

Directors
Martin G. Abegg — Paul R. Munger
Floyd A. Bishop — William R. Neuman
L. Gary Byrd — Leonard S. Oberman
Larry J. Feeser — John D. Parkhurst
John A. Focht, Jr. — Celestino R. Pennoni
Sergio Gonzalez-Karg — Robert B. Rhode
James E. Humphrey, Jr. — S. Russell Stearns
Richard W. Karn — William H. Taylor
Leon D. Luck — Stafford E. Thornton
Arthur R. McDaniel — Robert E. Whiteside
Richard S. Woodruff

EXECUTIVE OFFICERS

Eugene Zwoyer, *Executive Director*
Julie E. Gibouleau, *Assistant to the Executive Director*
Louis L. Meier, *Washington Counsel/Assistant Secretary*
William H. Wisely, *Executive Director Emeritus*
Michael N. Salgo, *Treasurer*
Elmer B. Isaak, *Assistant Treasurer*

STAFF DIRECTORS

Donald A. Buzzell, *Managing Director for Education and Professional Affairs*
Robert A. Crist, Jr., *Managing Director for Publications and Technical Affairs*
Alexander Korwek, *Managing Director for Finance and Administrative Services*
Alexandra Bellow, *Director, Human Resources*
David Dresia, *Director, Publications Production and Marketing*
Barker D. Herr, *Director, Membership*
Richard A. Jeffers, *Controller*
Carl E. Nelson, *Director, Field Services*
Don P. Reynolds, *Director, Policy, Planning and Public Affairs*
Bruce Rickerson, *Director, Legislative Services*
James M. Shea, *Director, Public Communications*
Albert W. Turchick, *Director, Technical Services*
George K. Wadlin, *Director, Education Services*
R. Lawrence Whipple, *Director, Engineering Management Services*

COMMITTEE ON PUBLICATIONS

Stafford E. Thornton, *Chairman*
Martin G. Abegg — Richard W. Karn
John A. Focht, Jr. — Paul R. Munger
William R. Neuman

HYDRAULICS DIVISION

Executive Committee
Ronald E. Nece, *Chairman*
Rudolph P. Savage, *Vice Chairman*
George E. Hecker — Ralph M. Weaver
Charles S. Mifkovic, *Secretary*
John J. Cassidy, *Management Group D Contact Member*

Publications Committee
Melvin W. Anderson, ***Chairman***
John A. Hoopes, ***Vice Chairman***
Philip H. Burgi, *Hydraulic Structures*
Richard H. (Pete) Hawkins, *Surface Water Hydrology*
John A. Hoopes, *Hydromechanics, General*
Gerhard H. Jirka, *Hydraulic Transport and Dispersion*
Chintu Lai, *Hydromechanics, Open Channels*
Frederick A. Locher, *Hydromechanics, Open Channels*
Donn G. DeCoursey, *Sedimentation*
Bryan R. Pearce, *Tidal Hydraulics*
John A. Roberson, *Hydromechanics, Closed Conduits*
John L. Wilson, *Groundwater Hydrology*
John J. Cassidy, *Exec. Comm. Contact Member*

PUBLICATION SERVICES DEPARTMENT

David Dresia, *Director, Publications Production and Marketing*

Technical and Professional Publications

Richard R. Torrens, *Manager*
Joseph P. Cerami, *Chief Copy Editor*
Linda Ellington, *Copy Editor*
Thea C. Feldman, *Copy Editor*
Meryl Mandle, *Copy Editor*
Joshua Spieler, *Copy Editor*
Shiela Menaker, *Production Co-ordinator*
Richard C. Scheblein, *Draftsman*

Information Services

Elan Garonzik, *Editor*

PERMISSION TO PHOTOCOPY JOURNAL PAPERS

Permission to photocopy for personal or internal reference beyond the limits in Sections 107 and 108 of the U.S. Copyright Law is granted by the American Society of Civil Engineers for libraries and other users registered with the Copyright Clearance Center, 21 Congress Street, Salem, Mass. 01970, provided the appropriate fee is paid to the CCC for all articles bearing the CCC code. Requests for special permission or bulk copying should be addressed to the Manager of Technical and Professional Publications, American Society of Civil Engineers.

CONTENTS

Evaluation of Sand Waves in an Estuary
by B. R. Baliga and Robert T. Hudspeth 161

Total Load Transport in Alluvial Channels
by Kittur G. Ranga Raju, Ramachandra J. Garde, and Ramesh C. Bhardwaj 179

Hazard Assessment of Arch Dam in Seismic Zone
by Donald E. Bowes, Antonio X. Sison, and Alan L. O'Neill 193

Modeling Transverse Mixing in Natural Streams
by Y. Lam Lau and B. G. Krishnappan 209

Overland Flow from Time-Distributed Rainfall
by Allen T. Hjelmfelt, Jr. 227

This Journal is published monthly by the American Society of Civil Engineers. Publications office is at 345 East 47th Street, New York, N.Y. 10017. Address all ASCE correspondence to the Editorial and General Offices at 345 East 47th Street, New York, N.Y. 10017. Allow six weeks for change of address to become effective. Subscription price to members is $16.50. Nonmember subscriptions available; prices obtainable on request. Second-class postage paid at New York, N.Y. and at additional mailing offices. HY.

The Society is not responsible for any statement made or opinion expressed in its publications.

DISCUSSION

Proc. Paper 16004

Gravel Size Analysis from Photographs, by John Adams (Oct., 1979. Prior Discussion: Aug., 1980).
closure 241

Stormwater Detention Basin Sizing,[a] by Kit R. Burton (Mar., 1980).
by Stuart G. Walesh 241

Debris Flow on Prismatic Open Channel, by Tamotsu Takahashi (Mar., 1980).
errata 243

Submerged Radial Hydraulic Jump, by John A. McCorquodale and Abdelkawi M. Khalifa (Mar., 1980).
errata 243

Cavitation Induced by Turbulence in Stilling Basin,[a] by Rangaswami Narayanan (Apr., 1980).
by Ryszard Blazejewski 244

Laboratory Verification of a Dam-Break Flood Model,[a] by Cheng-lung Chen (Apr., 1980).
by Nikolaos D. Katopodes and David R. Schamber 246

Turbulence Prediction in Open Channel Flow,[a] by Ruh-Ming Li, James D. Schall, and Daryl B. Simons (Apr., 1980).
by Darrel M. Temple 249

Linear Reservoirs and Numerical Diffusion,[a] by Victor Miguel Ponce (May, 1980).
by Witold G. Strupczewski and Zbigniew W. Kundzewicz 251

Hydrographs by Single Linear Reservoir Model,[a] by John T. Pedersen, John C. Peters, and Otto J. Helweg (May, 1980).
by James M. Stubchaer 254

Curve-Number Procedure as Infiltration Method,[a] by Allen T. Hjelmfelt, Jr. (June, 1980).
by Richard H. Hawkins 256

[a]Discussion period closed for this paper. Any other discussion received during this discussion period will be published in subsequent Journals.

Steady-State Estimation of Cooling Pond Performance,* by Gerhard H. Jirka and Masataka Watanabe (June, 1980).
by E. Eric Adams 257

INFORMATION RETRIEVAL

The key words, abstract, and reference "cards" for each article in this Journal represent part of the ASCE participation in the EJC information retrieval plan. The retrieval data are placed herein so that each can be cut out, placed on a 3 × 5 card and given an accession number for the user's file. The accession number is then entered on key word cards so that the user can subsequently match key words to choose the articles he wishes. Details of this program were given in an August, 1962 article in CIVIL ENGINEERING, reprints of which are available on request to ASCE headquarters.

*Discussion period closed for this paper. Any other discussion received during this discussion period will be published in subsequent Journals.

16016 EVALUATION OF SAND WAVES IN AN ESTUARY

KEY WORDS: Dissection; **Ecosystems;** Energy; Environmental impact statements; Equilibrium; **Estuaries; Sand waves; Sediment; Spectral analysis;** Turnovers

ABSTRACT: The Bella-Williamson rate of sediment turnover-organic content of sediment (RST-OCS) dissection plane method integrates relevant physical, chemical, and biological analyses in order to estimate the chronic impacts of dredging on estuarine ecosystems. A spectral analysis by a finite Fourier transform of estuarine sand waves is presented which only requires a spatial sand wave record that is relatively easy to measure in contrast to stochastic analyses which require both spatial and temporal observations of sand wave profiles. The total energy content (or, equivalently, the statistical variance of the spatial sand wave profile) and the equilibrium subrange of the wave number spectrum provide readily observable measures of the RST in an estuary; economic savings, promise to be significant. In addition, a uniform "-3 power law" for the wave number equilibrium subrange is presented which offers an opportunity to obtain a sand wave frequency spectrum without a temporal sand wave profile record through a dispersion transformation proportional to the bed shear velocity.

REFERENCE: Baliga, B. R., and Hudspeth, Robert T., "Evaluation of Sand Waves in an Estuary," *Journal of the Hydraulics Division,* ASCE, Vol. 107, No. HY2, **Proc. Paper 16016**, February, 1981, pp. 161-178

16020 TOTAL LOAD TRANSPORT IN ALLUVIAL CHANNELS

KEY WORDS: **Alluvial channels; Bed load; Canals;** Hydraulics; **Rivers; Sediments;** Sediment transport; Shear stress

ABSTRACT: A relationship for computation of total load transport in alluvial channels has been developed by analysis of extensive data from rivers and canals and from laboratory studies. The relationship is extremely simple and is based on logicalpremises. The accuracy of computation of total load from this relationship is quite good in comparison to that obtained from some of the existing relationships.

REFERENCE: Raju, Kittur G. Ranga, Garde, Ramachandra J., and Bhardwaj, Ramesh C., "Total Load Transport in Alluvial Channels," *Journal of the Hydraulics Division,* ASCE, Vol. 107, No. HY2, **Proc. Paper 16020**, February, 1981, pp. 179-191

16012 HAZARD ASSESSMENT OF ARCH DAM IN SEISMIC ZONE

KEY WORDS: **Dams (arch);** Dynamic loads; Earthquake engineering; **Earthquakes; Fault;** Geology; **Seismic properties; Stresses;** Structural engineering; **Vibration**

ABSTRACT: Principal faults in the Green Lake Arch Dam region were examined and an assessment was made of potentially damaging earthquakes. An earthquake which can cause the most severe ground motion at the site (Maximum Credible Earthquake) and another one which has a recurrence interval of 100 yr, were selected for use in design. A dynamic analysis using the time-history method was performed, showing that vertical contraction joints would partially open for short instants under dynamic loading. It was concluded that the dam can resist the Maximum Credible Earthquake without an uncontrolled release of water from the reservoir, and that the dam can withstand the 100-yr earthquake with little or no damage.

REFERENCE: Bowes, Donald E., Sison, Antonio X., and O'Neill, Alan L., "Hazard Assessment of Arch Dam in Seismic Zone," *Journal of the Hydraulics Division,* ASCE, Vol. 107, No. HY2, **Proc. Paper 16012**, February, 1981, pp. 193-208

16048 MODELING TRANSVERSE MIXING IN STREAMS

KEY WORDS: Coordinates; **Discharge;** Dispersion; Dyes; **Field tests; Mixing; Natural streams;** Pollutants; **Solutes**

ABSTRACT: A model of transverse mixing in natural streams has been tested using dye data from a field experiment and has been proven successful. The model uses a natural coordinate system which follows the curvature of the stream and is based on the cumulative discharge concept. In the numerical solutions, different assumptions are used for the factor of diffusion, $(uh^2m_xe_z)$. The best accuracy is found when local values of (uh^2m_x) are used together with a dispersion coefficient e_z which can vary in the downstream direction. The changes in the size of the dye plume can be predicted fairly well, even with an analytical solution. An analysis of available field values for e_z suggests that the dimensionless dispersion coefficient e_z/U_*W can be represented as a function of the width-depth ratio and a variable which characterizes the curvature of the stream. The sinuosity is a possible variable to use. Most of the data are distributed fairly well along one curve which can be used to obtain estimates of e_z for streams with small curvatures.

REFERENCE: Lau, Y. Lam, and Krishnappan, B. G., "Modeling Transverse Mixing in Natural Streams," *Journal of the Hydraulics Division,* ASCE, Vol. 107, No. HY2, **Proc. Paper 16048,** February, 1981, pp. 209-226

16060 OVERLAND FLOW FROM TIME-DISTRIBUTED RAINFALL

KEY WORDS: Kinematics; **Overland flow;** Peak discharge; **Rainfall;** Rainfall-runoff relationships; Thunderstorms; **Time factors; Time of concentration**

ABSTRACT: The influence of time-varying rainfall on overland flow is investigated. The kinematic wave equations for turbulent flow (across a plane, impermeable surface) are solved using a time-varying rainfall appropriate for thunderstorms. The peak discharge is shown to be a function of surface length, total precipitation, storm duration, and time to equilibrium for rainfall of constant intensity. For rainfall durations equal or less than the time-of-concentration, there is little difference between peak discharges estimated using time-varying rainfall and rainfall of constant intensity. For rainfall of long relative duration, the thunderstorm distribution gives much higher peak discharges.

REFERENCE: Hjelmfelt, Allen T., Jr., "Overland Flow from Time-Distributed Rainfall," *Journal of the Hydraulics Division,* ASCE, Vol. 107, No. HY2, **Proc. Paper 16060,** February, 1981, pp. 227-238

JOURNAL OF THE HYDRAULICS DIVISION

EVALUATION OF SAND WAVES IN AN ESTUARY

By B. R. Baliga[1] and Robert T. Hudspeth,[2] M. ASCE

INTRODUCTION

The National Environmental Policy Act (NEPA) establishes continuing environmental responsibilities for agencies of the Federal government [20, Sec 101(b)]. One of these responsibilities is the preparation of environmental impact statements (EIS) for dredging operations which require Federal action [20, Sec 102(2)(C)]. A comprehensive interdisciplinary methodology for identifying the chronic environmental impacts of dredging operations in estuaries has been developed by Bella and Williamson (2). A methodology for incorporating an evaluation of these environmental impacts into an environmental strategy has been outlined by Bella and Overton (1). The power of this diagnostic approach toward the preparation and evaluation of EIS for estuarine dredging lies in its relatively simple methodology for integrating disciplinary data which are easily measured, into a two-dimensional dissection plane from which the chronic impacts of dredging operations may be identified. The Bella-Williamson dissection plane approach should result in significant economic savings due to the elimination of the collection and analyses of irrelevant environmental data from estuaries in which dredging operations are proposed. Included in the Bella-Williamson dissection plane methodology are estuaries in which sand waves are present at the benthic interface; and the collection and analyses of sand wave data by spectral methods are presented in the context of a disciplinary element in the holistic dissection plane approach for diagnosing the environmental impacts of dredging in estuaries.

The two orthogonal dimensions identified by Bella and Williamson (2) for their dissection plane are: (1) The *rate of sediment turnover* (RST abscissa);

[1]Grad. Research Asst., Dept. of Civ. Engrg. and Ocean Engrg. Programs, Oregon State Univ., Corvallis, Oreg. 97331.

[2]Assoc. Prof., Dept. of Civ. Engrg. and Ocean Engrg. Programs, Oregon State Univ., Corvallis, Oreg. 97331.

Note.—Discussion open until July 1, 1981. To extend the closing date one month, a written request must be filed with the Manager of Technical and Professional Publications, ASCE. Manuscript was submitted for review for possible publication on January 24, 1980. This paper is part of the Journal of the Hydraulics Division, Proceedings of the American Society of Civil Engineers, ©ASCE, Vol. 107, No. HY2, February, 1981. ISSN 0044-769X/81/0002-0161/$01.00.

and (2) the *organic content of the sediment* (OCS ordinate). Contours of measures of the various physical, chemical, and biological environmental properties of an estuarine ecosystem may be displayed on this dissection plane with the RST and the OCS as the axes. From these contours on this dissection plane, the environmental impacts from dredging on the estuarine ecosystem may be estimated from known or predicted alterations in the RST and the OCS. Changes in the RST may be diagnosed from the direct influence of the hydrodynamic forces on sand waves at the benthic interface of an estuary. Accordingly, sand waves subjected to hydrodynamic forces due to oscillatory flows in an estuary were observed in order to estimate the RST in a *pristine* estuary. These observations from a *pristine* estuary are also compared with sand waves in an adjacent *developed* estuary.

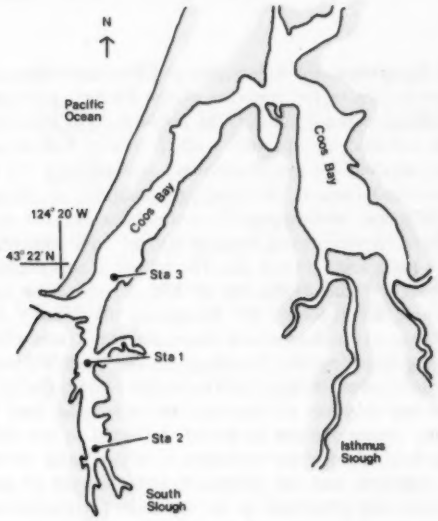

FIG. 1.—Location of Sand Wave Sampling Stations, Coos Bay Estuary, Oregon

The hydrodynamic forces which directly influence the RST at an erodible sediment interface result in an alternating sequence of erosion and deposition. In those instances when this alternating sequence of erosion and deposition result in a wave-like deformation of the sediment boundary, wave propagation theories may be employed to compute the wave celerity, C, wave length, L, and wave period, T, of these waves. In deterministic wave propagation problems, the reciprocal of the interval of periodicity yields the frequency, f, at which the process is periodically repeated and provides an estimate of the RST. Since the benthic interfaces in most estuaries are definitely not purely sinusoidal or strictly periodic, the superposition of many waves may be employed to Fourier analyze the instantaneous profile of this random interface. In addition, the

hydraulic processes which result in erosion and deposition are not, in general, deterministic and the methods of Fourier analyses may be further extended to describe a stochastic process by spectral methods.

In order to demonstrate an application of the relatively simple spectral analysis for estimating the RST in an estuary from the migration of sand waves, sand wave measurements in the South Slough estuary, Coos Bay, Oregon were analyzed. This estuary is located on the southern Oregon coast approx 341 km south of the Columbia river entrance and 702 km north of the San Francisco Bay (see Fig. 1).

Background

The evolution of the various complex analytical models which describe the response of a deformable benthic interface to hydrodynamic forces is eloquently chronicled by Graf (7), Raudkivi (17), and Kennedy (9,10). This evolution follows essentially the same three conceptual areas described by Kinsman (11) for random surface gravity waves, i.e., hydrodynamics, stochastic processes and probability, and Fourier analysis. The evolution of the hydrodynamic concept began with Exner (compare to Ref. 7 or Ref. 17) who assumed that the bottom was initially a sinusoid and that the free surface of the water was sensibly horizontal. Exner's model is capable (at least theoretically) of including the effects of friction in a channel of variable width. The principal contribution of this model is that the instantaneous profile of the bed form results in a faster speed for the crest of the sinusoid compared to the trough and provides a means for estimating an approximate time for this sinusoid to become unstable and to collapse. Experimental verification of this model is lacking, as well as a physical explanation of how the bed initially becomes a sinusoid or what shape it assumes following the instability of breaking.

Others (6,12,15,18,19,21) have extended this model to include a steady flow over a sinusoidal bottom with a corresponding sinusoidal free surface. The linearized potential theory solution derived by these authors yields a disturbing singularity for the special case in which the speed of the free surface sinusoidal profile is exactly equal to the free stream velocity. The existence of this singularity is frequently used to argue that a deformable bedform may not remain flat. Kennedy (9,10) and Reynolds (18) also have included a slowly moving sinusoidal bottom in their model. However, the speed of this motion is considered to be small compared with the speed of the free-stream velocity and is neglected in the mathematical solution.

Mei (14) analyzed steady flow with a periodic free surface over an impermeable stationary bottom which also has a periodic profile. By considering the fully nonlinear boundary conditions and by assuming that the amplitude of the periodic bottom profile was of higher order in the perturbation parameter, he successfully removed the singularity present in the previous linearized studies and was able to determine the conditions required for the existence of a flat bottom. The key to his successful development was to assume that the bottom amplitude was of higher order in the perturbation parameter and that the speed of the free surface wave and the speed of the free-stream flow were *initially* equal.

The major limitations of each of these models for measuring the RST in an estuary with oscillatory flow is that only steady unidirectional flows are

treated and that the benthic boundaries are either impermeable or their motion must be determined empirically. The solution for the motion of an irregular, erodible, and permeable bottom under oscillatory flows does not presently exist.

Lee (13) developed a *stochastic* theory and analyzed the particle movement within a sand dune bed under uni-directional hydrodynamic flows. Lee (13) assumed that the process of alternate erosion and deposition of sand grains is stochastic and that the rest periods and step lengths of the sand particles within the profile are Gamma distributed. The Gamma distribution for the rest periods and the step lengths is a two-parameter positive semidefinite distribution. Once the Gamma distributions are determined for measured sand wave data collected in an estuary, the mode of the distributions of the rest periods, T_m, and the step lengths L_m could be used to estimate the RST in the estuary. The celerity of the sand wave would then be estimated by the relation $C = L_m/T_m$.

Hino (8) developed a *spectral* theory for sand waves also under uni-directional flows. He derived parametric equations for the wave number and frequency domain spectra for sand waves based on a dimensional analysis. The wave number and the wave frequency are related by the celerity for any harmonic of the sand wave profile in an estuary, which is given by

$$C = \frac{f}{k} \quad \ldots\ldots\ldots\ldots\ldots\ldots\ldots\ldots\ldots\ldots\ldots\ldots\ldots\ldots\ldots\ldots\ldots\ldots\ldots\ldots\ldots\ldots (1)$$

in which f = a harmonic frequency in the wave frequency spectrum; and k = a harmonic wave number in the wave number spectrum of the sand waves. The value of the peak frequency of the sand wave sprectrum, f_m, could provide an average estimate of the RST for the sand waves and could be estimated by Eq. 1 from the peak wave number and the celerity. The advantage of the *spectral* method of Hino (8) over the *stochastic* method of Lee (13) is that it would only be necessary to measure a spatial record of the sand wave elevations since the peak frequency of the frequency domain spectrum may be computed from Eq. 1 using a "dispersion" transformation between wave frequencies and wave numbers. In contrast, the *stochastic* method of Lee (13) requires both a temporal and a spatial record of the sand wave profile since no dispersion transformation presently exists between the Gamma distribution for step lengths and rest periods. A great deal of difficulty and expense is involved in obtaining a time-dependent record of a sand wave profile under field conditions since the profile sensor must be introduced into the flow field without significantly disturbing the flow. Furthermore, if the oscillatory motion of the wave-like benthic interface is a slowly-varying function of time, then the profile sensor must either be protected against long-term mechanical and biological degradation or repositioned exactly at the same location at relatively short intervals of time over a number of oscillatory cycles. This second requirement for repositioning may involve expensive navigational positioning systems.

Because of the potential economic savings offered by the *spectral* method of Hino (8) over the *stochastic* method of Lee (13) as a result of eliminating the requirement to measure a temporal record of the sand wave profile, the spectral method was adopted for application to the Bella-Williamson dissection plane approach. The essential theoretical elements from the eloquent derivation

of the Hino spectral method (8) are succinctly summarized for convenience in demonstrating its application.

Spectral Analyses of Sand Waves

The random, irregular shape of estuarine sand wave profiles may be represented by the harmonic analysis of a number of sinusoids of varying frequencies having spectral representation (compare Refs. 4, 5, and 22). Hino (8) derived the parametric equation for a wave number and a wave frequency spectrum for wave numbers; and frequencies within the equilibrium subrange for sand wave values are shown in Fig. 2.

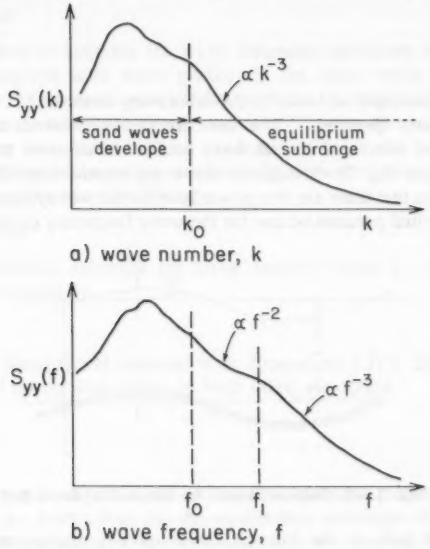

FIG. 2.—Equilibrium Sand Wave Spectra: (*a*) Wave Number Spectrum $S_{yy}(k)$; and (*b*) Wave Frequency Spectrum, $S_{yy}(f)$

For fully-developed (or equilibrium) sand waves, the slope of the sand bed profile may never exceed the angle of repose, ϕ, of the sand. This implies that an upper limit exists for the spectral amplitude values within an equilibrium subrange in which the spectral form is governed predominantly by the angle of repose and some power of the wave number. For lower values of wave numbers below this equilibrium subrange, the sand waves are still growing and the law of equilibrium subrange fails due to an instability mechanism between the sand bed and the flowing water as a result of the continuing transfer of energy from the hydrodynamic shear stress to the deformable sand bed.

Wave Number Spectrum.—The wave *number* spectrum may be estimated from a *spatial* record of a sand wave profile. From a dimensional analysis, Hino (see Ref. 8, Eq. 10) has determined that the spectral density function for a

sand wave profile within the equilibrium subrange is of the form

$$S_{yy}(k) = \alpha(\phi)\, k^{-3}; \quad (k_o << k << d^{-1}) \quad \ldots\ldots\ldots\ldots\ldots\ldots\ldots\ldots (2)$$

in which k = the wave number in cycles per unit length; $\alpha(\phi)$ = a function of the angle of repose of a sand particle (assumed to be a constant); d = the diameter of the sand particle; y = the vertical elevation of the sand wave profile above the horizontal mean at any horizontal coordinate in a spatial sand wave record (see Fig. 3); and k_o = the smallest value for the wave number of the sand wave field in which the interactional instability mechanisms are not important. Analyzing experimental data for uni-directional flow, Hino (8) found that an approximate value for k_o may be estimated from

$$k_o = \frac{0.15}{h} \quad \ldots\ldots\ldots\ldots\ldots\ldots\ldots\ldots\ldots\ldots\ldots\ldots\ldots\ldots (3)$$

in which h = the depth of water in the laboratory channel.

Wave Frequency Spectrum.—The wave frequency spectrum may be estimated from a *temporal* record of a sand wave profile. In contrast to the single "−3 power law" (see Eq. 2) throughout the wave *number* equilibrium subrange, Hino (8) suggests that there are two power laws for the wave *frequency* equilibrium subrange. This dual parametric law for the wave frequency equilibrium subrange

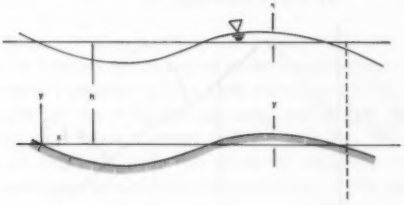

FIG. 3.—Definition Sketch for Sinusoidal Sand Bed

may be due, in part, to the form of the frequency dispersion transformation assumed by Hino (8). An alternate frequency dispersion transformation which removes this dual parametric law for the wave frequency equilibrium subrange is given in Appendix I.

Hino (8) assumes that within the equilibrium subrange, the frequency spectrum follows a "−3 power law" for higher frequencies, and a "−2 power law" for frequencies slightly greater than the spectral peak frequency but less than the "−3 power law" frequencies. In the higher frequency region within the equilibrium subrange, the frequency spectrum for the sand wave profile is assumed from dimensional analysis to be given by

$$S_{yy}(f) = f(\psi)\, V_*^2\, f^{-3}; \quad (f_1 < f < f_\infty) \quad \ldots\ldots\ldots\ldots\ldots\ldots\ldots\ldots (4)$$

in which f = the wave frequency in cycles per unit time; $f(\psi)$ = a function of ψ, which is a nondimensional quantity related to the critical tractive force of the sand bed by $\psi = V_*^2/[(\rho_s/\rho - 1)\, gd]$; V_* = the bed shear velocity; and f_1 and f_∞ = the lower and upper bounds, respectively, of the higher frequency

region within the equilibrium subrange for sand wave frequencies.

The wave number, k, and the wave frequency, f, of a sand wave are related by the wave celerity or rate of translation of the waveform according to

$$f = C(k)\,k \quad \ldots\ldots\ldots\

method for estimating the RST lies in determining the appropriate constant of proportionality, γ, and the angle of repose function, $\alpha(\phi)$.

For application in the Bella-Williamson RST-OCS dissection plane method, it was proposed to use the total energy content of the sand wave number spectral density (or, equivalently, the variance of the spatial profile record) and the wave number equilibrium subrange defined by Hino (8) as measures of the RST in an estuary in which sand waves are present. The relative magnitude of the total energy in the sand wave profile and the equilibrium subrange amplitudes would provide estimates of the relative energy transfer occurring between the hydrodynamic shear stress and the resulting deformation of the migrating benthic interface. For comparison, data were measured in both a *pristine* estuary and an adjacent *developed* (dredged) estuary. The relative ease and low cost involved in acquiring these sand wave records are especially attractive economically and are fundamentally compatible with the philosophy of the Bella-Williamson RST-OCS dissection plane approach in the evaluation and preparation of EIS for dredging operations in estuaries.

Sand Wave Data Acquisition and Analysis

Sand wave profiles were recorded in analog form by a submerged sonic profiler during a two-day period. A rigid steel pipe was mounted vertically to the side of a boat and the sonic transducer was secured to the underwater end approx 0.8 m above the sand bed. The sonic data were recorded directly on FM magnetic tape in analog form by an FM tape recorder aboard the boat. The sonic sampling locations (STA 1, 2, 3) are shown in Fig. 1.

Five buoys were implanted along the channel at each of the sampling stations shown in Fig. 1 and the distances between these buoys were measured by means of a range finder (transit type) on shore. The buoys were moored taut and anchored to the bottom of the estuary in order to minimize their drift. Before recording the sonic data at each station, the boat was driven slowly along the course of the buoys and the time of travel between the buoys was recorded by a stop watch. The speed of the boat was then computed by dividing the known distances between the buoys by the recorded time required for the boat to cover these distances at each station. The speed of the boat was approximately equal to 0.5 m/sec. The speed of the boat at each station was then maintained at approximately a constant value of 0.5 m/sec during each of the subsequent data recording operations. During the two-day data-recording period, two data recordings were taken at STA 1, four at STA 2, and one at STA 3. These seven data measurements are summarized in Table 1.

In order to correlate the *in situ* length of the sand waves with the magnetic tape data, the passing of each buoy by the sampling boat was recorded by voice on the same channel of the magnetic tape as the sonic data. The pulse rate for the sound waves from the sonic profiler was 1/30 second. This rate of data sampling was required to be greater than the speed at which the boat was moving (approx 0.5 m/sec) in order to insure that no sand wave elevation data were omitted from the recordings. In order to eliminate extraneous vertical disturbances to the boat and, consequently, to the data records, data were collected only when the water surface disturbances were minimum. In order to maintain a sufficient draft below the underwater sonic transducer, data were

collected only during the slack periods of high tide.

These sonic sand wave data were recorded in analog form on an FM magnetic tape and were later copied onto an analog strip chart for visual observation and calibration. The total length of each run was computed both in meters and in seconds. The elapsed time between the start and the end of each FM magnetic tape record gave the total length of the record in seconds. The total length of the sand wave records in seconds was required in order to digitize the sand wave record by an analog to digital converter (ADC) through a PDP 11 E10 minicomputer. The spatial resolution, Δx, of each sand wave record was computed by multiplying the tangent of the sonic profiler half-beam angle (5°) by the vertical height of the sonic transducer above the sand bed (approx 0.8 m). The spatial resolution, Δx, computed from the aforementioned method was approximately equal to 0.07 m. This spatial resolution was then compared with the horizontal distance between two consecutive sonic waves to insure that it was greater than the horizontal distance between two consecutive sonic waves.

TABLE 1.—Summary of Sonic Profiler Data

Record number (1)	Length, in meters (2)	Length, in seconds (3)	Variance, in square meters (4)	H_{rms}, in meters (5)	Δk, in meters (6)	k_o, in meters (7)	Sampling location, (see Fig. 1) (8)
1	91.09	236	0.0113	0.30	0.011	0.075	STA 1
2	127.53	471	0.1348	1.04	0.008	0.075	STA 1
3	211.34	675	0.0615	0.70	0.005	0.038	STA 2
4	211.34	400	0.0337	0.52	0.005	0.038	STA 2
5	211.34	402	0.0654	0.72	0.005	0.038	STA 2
6	216.02	540	0.0427	0.58	0.005	0.038	STA 2
7	45.81	270	0.2382	1.38	0.022	0.017	STA 3

This horizontal distance was computed by multiplying the average speed of the boat by the rate at which the sonic waves were sent. Once the spatial resolution of each record was determined, the total number of digitizing values, N, may be computed from the relation

$$N \geq \frac{\mathrm{L}}{\Delta x} \quad \ldots\ldots\ldots\

Fourier transform (FFT) algorithm of base two. For a real-valued sequence, y_n, the discrete FFT pair may be given by

$$y_n = N^{-1} \sum_{m=o}^{N-1} A_m \exp i\left(\frac{2\pi nm}{N}\right); \quad n = 0, 1, 2, \ldots, N-1 \quad \ldots\ldots\ldots \quad (13a)$$

$$A_m = \sum_{n=o}^{N-1} y_n \exp -i\left(\frac{2\pi nm}{N}\right); \quad m = 0, 1, 2, \ldots, N-1 \quad \ldots\ldots\ldots \quad (13b)$$

in which the real and imaginary components of the complex-valued FFT coefficients are identified by

$$A_m = RA_m + i\,IA_m \quad \ldots\ldots\ldots\ldots\ldots\ldots\ldots\ldots\ldots\ldots\ldots\ldots \quad (14)$$

In order for the inverse transform to be exact, we must also require that

$$\Delta t \cdot \Delta k = N^{-1} \quad \ldots\ldots\ldots\ldots\ldots\ldots\ldots\ldots\ldots\ldots\ldots\ldots \quad (15)$$

Only the real part of the complex-valued (y_n) sequence represents the digitized values of the sand wave profiles. The one-sided spectral density function for the sand wave profile may be estimated from the complex-valued FFT coefficients according to

$$S_{yy}(m\Delta k) = \frac{2A_m \cdot A_m^*}{\Delta k}; \quad m = 0, 1, 2, \ldots, \frac{N}{2} \quad \ldots\ldots\ldots\ldots\ldots\ldots \quad (16)$$

in which the superscript asterisk denotes a complex conjugate value. The amplitude spectra for the sand waves recorded at the three stations in Coos Bay estuary are shown in Figs. 4–9. The variance, root-mean-square wave height, H_{rms}, and the equal discrete wave number interval, Δk, are tabulated in Table 1. The variance of the zero-mean spatial sand wave profile is computed from

$$V = \frac{1}{N} \sum_{n=o}^{N-1} y_n^2 \quad \ldots\ldots\ldots\ldots\ldots\ldots\ldots\ldots\ldots\ldots\ldots\ldots \quad (17)$$

and the H_{rms} from

$$H_{rms} = \left\{ 8\,\Delta k \sum_{m=o}^{N/2} S_{yy}(m\Delta k) \right\}^{1/2} \quad \ldots\ldots\ldots\ldots\ldots\ldots\ldots \quad (18)$$

The amplitude spectra of the sand wave records from the South Slough estuary, Coos Bay, Oregon (see Figs. 4–8) demonstrate two important points. First, the total energy (or, equivalently, the statistical variance of the spatial sequence) of the spectra are relatively low (e.g., the minimum $H_{rms} = 0.3$ m for record No. 1 in Fig. 4). Second, most of the energy is contained in the fundamental harmonic component. This indicates that the dynamic migration of these sand waves is a slowly-varying, low-energy process and that the sand bed is a slowly-undulating boundary. In addition, the maximum spectral amplitudes are found at wave numbers which lie below the smallest wave number of the equilibrium subrange given by Hino (8) for uni-directional flow in the laboratory. This indicates that the sand waves in the South Slough estuary are still growing. In estuaries of low sand wave energy, catastrophic events such as storms govern the RST and not the hydrodynamics of the average flow. In the South Slough

estuary data, the rms sand wave height, H_{rms}, varied from 0.30 m–1.04 m.

In contrast, sand waves in the Coos Bay main channel (see Fig. 9) have a higher energy content (variance of the spatial sequence) dispersed over a wider band of wave numbers; however the fundamental harmonic still contains most of the total energy. This is due to the stronger tidal velocities probably

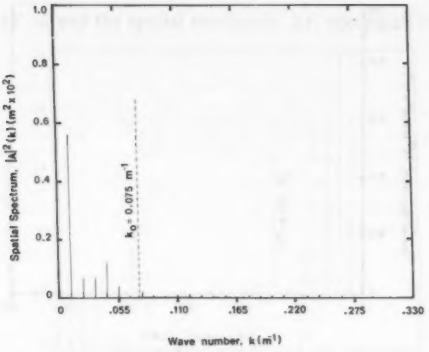

FIG. 4.—Sand Wave Amplitude Spectrum for Record No. 1 (V = 0.0113 m^2; Δk = 0.011 m^{-1})

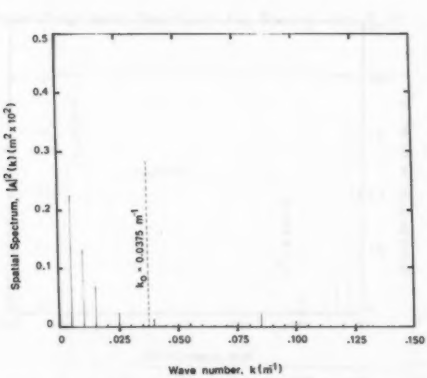

FIG. 5.—Sand Wave Amplitude Spectrum for Record No. 3 (V = 0.0615 m^2; Δk = 0.005 m^{-1})

augmented by the ship propeller disturbances in the main channel. Since this spectral comparison is only a visual comparison, the spectral band width parameter which provides an estimate of the width of the wave frequency spectrum (compare to Ref. 3), should be computed from the wave frequency spectrum in order to obtain the dispersion of the spectrum about the spectral peak. The sand wave frequency spectrum may be obtained from the wave number spectrum

by using a theoretical or empirical transformation between the wave numbers and the wave frequencies. A flow chart for obtaining the RST from a wave number spectrum using a dispersion transformation is shown in Fig. 10.

For the sand wave record from the Coos Bay main channel (see record No. 7 in Fig. 9), the wave number of the maximum spectral amplitude falls very

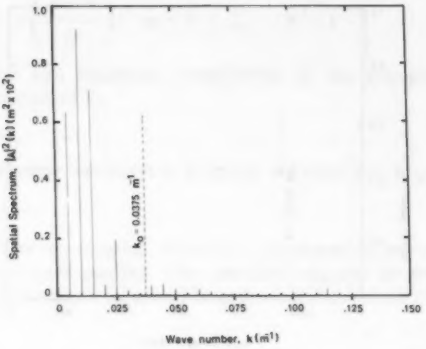

FIG. 6.—Sand Wave Amplitude Spectrum for Record No. 4 (V = 0.0337 m^2; Δk = 0.005 m^{-1})

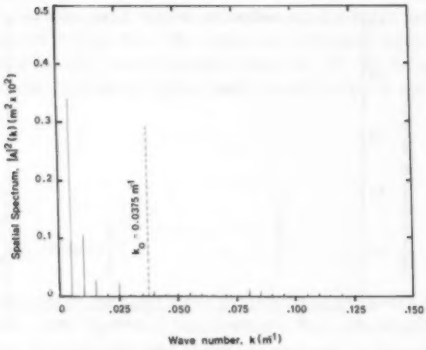

FIG. 7.—Sand Wave Amplitude Spectrum for Record No. 5 (V = 0.0654 m^2; Δk = 0.005 m^{-1})

close to the minimum wave number value for the equilibrium subrange given by Hino (8). We note that the minimum wave number value for the equilibrium subrange, k_o, given by Hino (8) is slightly less than the first harmonic component. This demonstrates that some additional care must be taken when digitizing analog data in order to insure that the value for the minimum wave number for the equilibrium subrange, k_o, will be much greater than the fundamental harmonic component.

For example, if we assume that k_o will appear in the mth harmonic (e.g., $k_o = m\,\Delta k$; $m >> 1$), then the equal discrete wave number interval, Δk, may be estimated from Eq. 3 according to

$$\Delta k = \frac{0.15}{m\,h} \quad \ldots\ldots\ldots\

harmonic, then the equal discrete wave number interval, Δk, may be estimated from Eq. 19 to be $\Delta k = 0.0033\ m^{-1}$. Substituting this equal discrete wave number interval into Eq. 20 yields approx $N \simeq 4{,}096$. Therefore, the spatial sand wave data should have been digitized with at least 4,096 values instead of the 1,024 values used in the present analysis, in order to insure that k_o would be much greater than the fundamental harmonic component and to better resolve the equilibrium subrange.

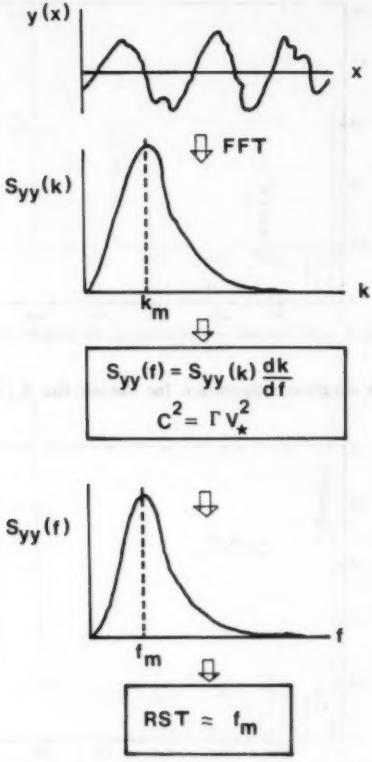

FIG. 10.—Flow Chart for Estimating RST from Wave Number Spectrum by Dispersion Transformation

These amplitude spectra demonstrate the significant differences between the hydrodynamic processes in a *pristine* estuary (South Slough) and a *developed* estuary (Coos Bay Main Channel). The RST in the pristine estuary is a low-energy process, which is storm driven, while the RST in the developed estuary is a high-energy process driven by the hydrodynamics of the average flows. Additional laboratory and field measurements are required, however, to verify

the constants of proportionality for the equilibrium subrange and the dispersion transformation.

Conclusions

The equilibrium subrange and the total energy (variance of the spatial sequence) of the wave number spectrum for sand waves in an estuary may be used to quickly and economically locate the RST in the Bella-Williamson dissection plane method for diagnosing the chronic environmental impacts of dredging in estuaries. A spatial record of a sand wave profile in an estuary may be easily measured by underwater sonic profilers and the wave number spectral amplitude may be quickly estimated by an FFT algorithm. A comparison between the rms wave height (which may be determined from the total energy content computed by the FFT coefficients) with the equilibrium subrange of the theoretical wave number spectrum developed by Hino (8) provides a reasonable estimate for a measure of the RST. Some care must be taken in both recording and digitizing spatial sand wave data and the important analytical relationships between the spatial resolution of the data acquisition equipment, the speed of the sampling boat, and the minimum value of the equilibrium subrange wave number are presented.

The method described in the present analysis may be extended to compute the wave frequency spectrum *without* requiring the measurement of a temporal sand wave profile provided that a dispersion transformation between wave frequencies and wave numbers is known. A uniform "−3 power law" wave frequency spectrum is presented which follows the assumption that the wave celerity is proportional to the bed shear velocity. Additional analytical, or experimental verifications, or both, are required to determine the dimensionless constant of proportionality for oscillatory flows.

The potential economic savings which may be realized in the preparation and evaluation of EIS by the judicious application of the Bella-Williamson dissection approach are tremendously encouraging. A key ingredient in their approach is the successful integration of disciplinary data and analysis which may be rapidly and economically collected and analyzed. The spectral analysis of sand wave profiles by an FFT in an estuary is presented within the context of a disciplinary input to the Bella-Williamson dissection plane method. Details regarding the integration of disciplinary data are given by Bella and Williamson (2). In addition, recommendations are presented for extending the present knowledge of the wave number equilibrium subrange and the wave frequency dispersion transformation for sand waves under oscillatory flows.

Acknowledgments

We are especially grateful for the unique opportunity to provide disciplinary data to D. A. Bella and K. J. Williamson for integration in the development of their pioneering work on the RST-OCS dissection plane approach for diagnosing the chronic impacts of dredging in estuaries which was sponsored by the National Science Foundation-Research Applied to National Needs (NSF-RANN) under Grant No. ENV71-01908. Equally rewarding and professionally stimulating have been the collaborative opportunities with the following NSF-RANN team

members: W. L. Schroeder, L. S. Slotta, D. R. Hancock, C. K. Sollitt, and J. M. Stander. The sonic profiler used in the data acquisition was made available by C. Nordin of the United States Geological Survey, Department of the Interior. Additional financial support (for RTH) was provided by the Oregon State University Sea Grant College Program, National Oceanic and Atmospheric Administration, Office of Sea Grant, Department of Commerce, under Grant No. 04-6-158-44004. We dedicate this effort to the memory of our late NSF-RANN team member J. E. McCauley, benthic biologist, educator, and a good man. It is also a pleasure to extend our appreciation to the reviewers for their valuable suggestions on how to improve both the clarity and accuracy of our efforts.

Appendix I.—Uniform "−3 Power Law" Equilibrium Frequency Spectrum

The equilibrium wave frequency spectra derived by Hino (8) follows a "−3 power law" for the higher frequencies within the equilibrium subrange and a "−2 power law" for frequencies slightly greater than the spectral peak frequency but less than the "−3 power law" frequencies. This indicates that two frequency dispersion relationships are required for the sand waves *within* the wave number equilibrium subrange. Since the wave frequency spectrum is of prime importance in the estimation of the RST, a uniform "−3 power law" is developed for the entire wave frequency equilibrium subrange. This results in a one-to-one correspondence with the wave number equilibrium subrange.

Following the derivation for the equilibrium subrange for surface gravity waves by Phillips (16), we note two important points. First, the constants of proportionality used in his dimensional analysis are dimensionless; and, second, the same dimensional constant used in the parametric equation for the wave frequency spectrum also appears in the frequency dispersion equation (i.e., the gravitational constant). We shall incorporate these two points in our following formulation.

Gradowczyk (6) and Hino (see Ref. 8, Eq. 16) have shown that the celerity of the sand wave profile is proportional to the bed shear velocity. We, therefore, assume the following for the frequency dispersion transformation given by Eq. 8:

$$C^2 = \Gamma V_*^2 \quad \ldots \ldots \ldots

$$f_\infty << \Gamma^{1/2} V_* d^{-1} \quad \ldots \ldots \ldots \ldots \ldots \ldots \ldots \ldots \ldots \ldots \quad (25)$$

and a uniform "−3 power law" for the entire wave frequency equilibrium subrange is now given by

$$S_{yy}(f) = \alpha(\phi)(\Gamma V_*)^2 f^{-3}; \quad (f_o < f < \Gamma^{1/2} V_* d^{-1}) \ldots \ldots \ldots \ldots \quad (26)$$

Appendix II.—References

1. Bella, D. A., and Overton, W. S., "Environmental Planning and Ecological Possibilities," *Journal of the Sanitary Engineering Division*, ASCE, Vol. 98, No. SA3, Proc. Paper 8994, June, 1972, pp. 579–592.
2. Bella, D. A., and Williamson, K. J., "Diagnosis of Chronic Impacts of Estuarine Dredging," *Journal of Environmental Systems*, Vol. 9, 1979–1980, pp. 289–311.
3. Cartwright, D. E., and Longuet-Higgins, M. S., "The Statistical Distribution of the Maxima of a Random Function," *Proceedings Royal Society of London*, Series A, Vol. 237, 1956, pp. 212–232.
4. Cartwright, D. E., "On Submarine Sand-Waves and Tidal Lee-Waves," *Proceedings of Royal Society of London*, Series A, Vol. 253, 1959, pp. 218–240.
5. Crickmore, M. J., and Lean, G. H., "The Measurement of Sand Transport by Means of Radioactive Tracers," *Proceedings of Royal Society of London*, Series A, Vol. 266, 1962, pp. 402–421.
6. Gradowczyk, M. H., "Wave Propagation and Boundary Instability in Erodible-bed Channels," *Journal of Fluid Mechanics*, London, England, Vol. 33, 1968, pp. 93–112.
7. Graf, W. H., *Hydraulics of Sediment Transport*, McGraw-Hill Book Co., Inc., New York, N.Y., 1971, pp. 273–303.
8. Hino, M., "Equilibrium-Range Spectra of Sand Waves Formed by Flowing Water," *Journal of Fluid Mechanics*, London, England, Vol. 34, 1968, pp. 565–573.
9. Kennedy, J. F., "The Mechanics of Dunes and Antidunes in Erodible-Bed Channels," *Journal of Fluid Mechanics*, London, England, Vol. 16, 1963, pp. 521–544.
10. Kennedy, J. F., "The Formation of Sediment Ripples, Dunes and Anti-Dunes," *Annual Review of Fluid Mechanics*, Annual Reviews, Inc., Palo Alto, Calif., 1969, pp. 147–168.
11. Kinsman, B., *Wind Waves*, Prentice-Hall, Inc., Englewood Cliffs, N.J., 1956, pp. 51–112, 325–361, 427–487.
12. Lamb, H., *Hydrodynamics*, 6th ed., Dover Publications, Inc., New York, N.Y., 1945, pp. 398–410.
13. Lee, B. K., "Stochastic Analysis of Particle Movement Over a Dune Bed," thesis presented to Colorado State University, at Fort Collins, Colo., in 1973, in partial fulfillment of the requirements for the degree of Doctor of Philosophy.
14. Mei, C. C., "Steady Free Surface Flow Over Wavy Bed," *Journal of the Engineering Mechanics Division*, ASCE, Vol. 95, No. EM6, Proc. Paper 6967, Dec., 1969, pp. 1393–1402.
15. Milne-Thompson, L. M., *Theoretical Hydrodynamics*, 5th ed., The MacMillan Co., New York, N.Y., 1969, p. 444.
16. Phillips, O. M., *Dynamics of the Upper Ocean*, Cambridge University Press, Cambridge, England, 1966, pp. 109–119.
17. Raudkivi, A. J., *Loose Boundary Hydraulics*, Pergamon Press, Inc., New York, N.Y., 1967, pp. 175–221.
18. Reynolds, A. J., "Waves on an Erodible Bed of an Open Channel," *Journal of Fluid Mechanics*, London, England, Vol. 22, 1965, pp. 113–133.
19. Shinbrot, M., "Water Waves Over Periodic Bottom in Three Dimensions," *Journal Institute Mathematics and Applications*, Vol. 25, 1980, pp. 367–385.
20. *The National Environmental Policy Act*, (PL 91-190), 42 U.S.C. 4321 *et seq*, 1969, Sec. 101(b) and 102(2)(C).
21. Wehausen, J. V., "Surface Waves," *Handbuch der Physik*, Vol. 9, Julius Springer, Berlin, Germany, 1960, pp. 569–570.
22. Winant, C. D., Inman, D. L., and Nordstrom, C. E., "Description of Seasonal Beach Changes Using Empirical Eigenfunctions," *Journal of Geophysical Research*, Vol. 80, No. 15, 1975, pp. 1979–1986.

Appendix III.—Notation

The following symbols are used in this paper:

$A(\cdot)$ = complex finite Fourier transform (FFT) coefficient;
C = celerity of sand wave;
d = diameter of sand particle;
f = sand wave frequency;
f_1, f_∞ = lower and upper frequency bounds for the "−3 power law" equilibrium subrange (8);
f_o = lowest frequency in the equilibrium subrange;
f_m = peak frequency of the wave frequency spectrum;
$f(\psi)$ = a function of ψ;
H_{rms} = root mean square wave height;
h = depth of water in channel;
I = imaginary part of complex FFT coefficient;
$i = \sqrt{-1}$ = imaginary unit number;
k = wave number (cycles/length);
k_o = smallest wave number in the equilibrium subrange;
k_m = peak wave number of the wave number spectrum;
L = length of sand wave record;
L = wave length of a sand wave;
N = total number of digitizing values;
R = real part of a complex FFT coefficient;
$S_{yy}(\cdot)$ = spectral density function for the sand wave profile;
T = total time of the sand wave record;
T = wave period of a sand wave;
V = variance of the sand wave spatial profile;
V_* = shear velocity;
x = horizontal coordinate axis;
y = instantaneous vertical elevation of sand wave profile measured positive upwards from horizontal bottom;
$\alpha(\phi)$ = function of ϕ;
Γ = dimensionless constant of proportionality for frequency dispersion;
γ = dimensional constant of proportionality for frequency dispersion (8);
Δk = equal discrete wave number interval;
Δt = equal discrete time interval;
Δx = equal discrete spatial interval;
ρ = fluid density;
ρ_s = density of sand particles;
ϕ = angle of repose of a sand particle; and
ψ = nondimensional quantity related to the critical tractive force of the sand bed.

JOURNAL OF THE HYDRAULICS DIVISION

TOTAL LOAD TRANSPORT IN ALLUVIAL CHANNELS

By Kittur G. Ranga Raju,[1] Ramachandra J. Garde,[2] M. ASCE, and Ramesh C. Bhardwaj[3]

INTRODUCTION

Many practical problems connected with alluvial rivers and canals require knowledge of the sediment load carried by them or of the load they can safely carry without danger of aggradation of degradation. For example, the loss in storage capacity of a reservoir built on an alluvial river is primarily dependent on the sediment load carried by the river and transport capacity of flow at various sections in the back water reach. Also, the design of a nonscouring, nonsilting alluvial canal requires that only as much sediment be allowed into the canal as it can carry under the given hydraulic conditions. Essentially, therefore, the hydraulic engineer is required to predict the sediment load carried by a channel under equilibrium conditions for given sediment, fluid, and flow characteristics.

Wash load and bed-material load are the two components of the sediment load transported by an alluvial channel (5). It is known that the wash load is poorly related to the hydraulic conditions of the stream, and few attempts have been made in the past at predicting this part of the load, despite the fact that it may form a major part of the load in many channels. The bed-material load is a function of the sediment, fluid, and flow characteristics and is a component amenable to rational analysis. The bed-material load may move entirely as bed load close to the bed, or a part of it may move in suspension as suspended load, if the bed material is fine and the shear stress large enough. Hence the total load as implied in this paper is the sum of the bed load and suspended load of those sediment fractions originating in the bed; in other words, it does not include the wash load.

Total load computations may be made (6) either by computing the bed load and suspended load separately and adding them up, or by using an approach

[1]Prof. of Civ. Engrg., Univ. of Roorkee, Roorkee (U.P.), India.
[2]Prof. and Head of Civ. Engrg., Univ. of Roorkee, Roorkee (U.P.), India.
[3]Asst. Engr., Temporary Construction Div., U.P. Jal Nigam, Itawa (U.P.), India.

Note.—Discussion open until July 1, 1981. To extend the closing date one month, a written request must be filed with the Manager of Technical and Professional Publications, ASCE. Manuscript was submitted for review for possible publication on June 3, 1980. This paper is part of the Journal of the Hydraulics Division, Proceedings of the American Society of Civil Engineers, ©ASCE, Vol. 107, No. HY2, February, 1981. ISSN 0044-796X/81/0002-0179/$01.00.

TABLE 1.—Data Used in Analysis

Number (1)	Source and reference (2)	Median size of sediment, in millimeters (3)	Symbol (4)	Number of data points chosen at random (5)	Range of Depth, in meters		Range of Velocity, in meters per second		Range of Slope, as a percentage	
					Minimum (6)	Maximum (7)	Minimum (8)	Maximum (9)	Minimum (10)	Maximum (11)
1	Kalinske and Hsia (9)	0.011	⊙	9	0.107	0.201	0.380	0.830	0.025	0.100
2	Laursen (9)	0.04	○	8	0.141	0.202	0.515	0.796	0.078	0.117
3	Vanoni and Brooks (9)	0.088	⊕	15	0.057	0.087	0.393	0.760	0.220	0.330
4	Nomicos (9)	0.091	○	10	0.077	0.087	0.373	0.700	0.200	0.250
5	Laursen (9)	0.1	✦	14	0.095	0.290	0.326	0.705	0.043	0.210
6	Sato and Kikkawa (9)	0.1	B	30	0.143	0.366	0.381	0.513	0.031	0.0121
7	Willis (11)	0.1	○	30	0.207	0.378	0.450	0.810	0.027	0.100
8	Znamenlkay (9)	0.104	D	20	0.214	0.360	0.359	0.621	0.104	0.163
9	Nomicos (9)	0.137	○	15	0.071	0.074	0.258	0.807	0.200	0.390
10	Vanoni and Brooks (9)	0.137	◒	10	0.072	0.168	0.390	0.670	0.102	0.278
11	Brooks (9)	0.145	⊖	15	0.055	0.076	0.312	0.717	0.200	0.310
12	Nomicos (9)	0.145	○	10	0.095	0.120	0.355	0.675	0.210	0.340
13	Southampton, A (9)	0.15	∿	20	0.076	0.305	0.244	0.731	0.035	0.251
14	Barton-Lin (9)	0.18	○	30	0.091	0.421	0.216	0.980	0.045	0.170
15	Straub (9)	0.18	○	10	0.063	0.235	0.356	0.790	0.056	0.235
16	USGS (9)	0.19	○	10	0.152	0.323	0.280	1.420	0.028	0.092
17	Vanoni-Hwang (9)	0.206	□	7	0.035	0.30	0.520	0.980	0.589	1.200
18	Znamenskay (9)	0.221	N	15	0.178	0.490	0.555	0.876	0.089	0.205
19	Vanoni-Hwang (9)	0.23	◒	9	0.080	0.092	0.380	0.770	0.231	0.248
20	Franco (9)	0.23	L	10	0.128	0.170	0.361	0.460	0.094	0.169
21	Mutter (9)	0.26	X	15	0.029	0.065	0.126	0.505	0.705	0.360
22	USGS (9)	0.27	◒	25	0.140	0.344	0.406	0.991	0.046	0.163
23	USGS (9)	0.28	●	10	0.135	0.326	0.393	0.933	0.023	0.145
24	Gilbert (9)	0.305	⊠	10	0.021	0.06	0.370	1.350	0.73	1.590
25	USGS (9)	0.32	⊜	15	0.165	0.202	0.370	0.610	0.086	0.214
26	O'Brien (9)	0.36	G	15	0.09	0.13	0.225	0.380	0.063	0.261
27	UBC (9)	0.37	C	15	0.094	0.106	0.201	0.275	1.000	1.000
28	Stein (9)	0.40	ϕ	10	0.183	0.310	0.511	1.300	0.226	1.070
29	USWES (9)	0.42	○	15	0.031	0.056	0.320	0.420	0.1000	0.100
30	USGS (9)	0.45	○	20	0.076	0.133	0.760	1.650	0.490	1.01
31	USGS (9)	0.47	S	28	0.174	0.405	0.350	0.718	0.042	0.32
32	Southampton, B (9)	0.478	A	15	0.152	0.457	0.236	0.701	0.011	0.231
33	Gilbert (9)	0.506	⊠	10	0.019	0.100	0.630	0.856	1.530	2.290
34	USGS (9)	0.54	⊕	10	0.140	0.300	0.512	0.750	0.036	0.121
35	Bharat Singh (9)	0.62	∽	19	0.260	1.042	0.277	0.450	0.100	0.200
36	Gilbert (9)	0.784	⊠	15	0.017	0.102	0.670	0.750	0.750	1.000
37	USGS (9)	0.93	□	15	0.150	0.320	0.500	0.610	0.037	0.130
38	Williams (9)	1.35	M	28	0.087	0.215	0.454	0.821	0.115	0.639
39	Liu (9)	1.48	▲	16	0.059	0.101	0.345	0.550	0.135	0.990
40	Liu (9)	1.7	▲	15	0.021	0.100	0.410	0.562	0.105	1.000
41	Casey (9)	2.26	H	15	0.033	0.060	0.45	0.630	0.491	0.545
42	Liu (9)	2.26	◇	10	0.120	0.165	0.480	0.670	0.185	1.000
43	Hopang-Yung (9)	3.00	○	12	0.171	0.105	0.150	0.580	0.760	0.105
44	Gilbert (9)	3.17	⊠	18	2.530	0.102	0.176	0.651	0.918	1.290
45	Liu (9)	3.25	▲	15	0.025	0.100	0.483	0.740	0.140	0.940
46	Liu (9)	3.60	△	10	0.030	0.090	0.661	1.010	0.500	1.000
47*	Corps of Engineers (9)	0.1 to 0.6	P	50	0.500	10.00	0.850	2.503	0.010	0.022
48*	Colorado River	0.1 to 2.1	◒	40	0.780	8.60	0.750	2.203	0.016	0.033

TABLE 1.—*Continued*

(1)	(2)	(3)	(4)	(5)	(6)	(7)	(8)	(9)	(10)	(11)
49[a]	Indian Canals (9)	0.1 to 0.3	Z	20	1.310	3.079	0.72	1.610	0.012	0.020
50[a]	Niobrara River (3)	0.25	○┘	25	1.400	3.15	0.85	1.513	0.009	0.013
51[a]	Leopold (9)	0.3	K	20	0.850	2.260	0.99	1.500	0.011	0.019
52[a]	Mountain Creek (9)	0.9	⊸●	20	0.930	2.60	0.780	1.450	0.009	0.013
53[a]	Portugal River (9)	2.603	○	30	0.590	1.650	0.785	1.121	0.061	0.091
54[a]	Middle Loup (9)	0.34	⊸○	20	0.315	0.52	0.639	0.829	0.100	1.00

[a]River and canal data.

in which the total load is directly related to the hydraulic and sediment characteristics. A review of the existing methods of both these categories is available (6) and suggests the need for additional work in this field in view of the unsatisfactory accuracy of these computational methods. Hence the writers undertook an investigation with the dual objectives of testing the accuracy of some of the existing computational methods and of proposing an alternative and, if possible, an improved computational technique. The results of that investigation are presented herein.

Data Used

Since a large amount of data collected in flumes and natural streams under equilibrium conditions was available, it was felt unnecessary to carry out any experiments. These data from alluvial rivers, canals, and flume studies were carefully selected to include only those in which information concerning the wash load was available, thereby assuring that the total load used in the analysis excluded the wash load. The data cover a wide range of sediment size and other hydraulic conditions; only data from ripple-dune and transition regimes were chosen for analysis. Antidune data were not included because this regime occurs seldom in the field. The sources of these data and some other relevant details are given in Table 1. Natural sediment with a relative density of 2.65 was used in all these studies.

No correction for bank friction has been applied to the river data, and the depth of flow D has been taken to be the hydraulic radius with respect to the bed R_b. The bed and sides of canals have been assumed to be of the same nature, and the hydraulic radius R was used for R_b. The value of R_b was computed for the flume data adopting the procedure of side wall correction given by Einstein (4).

Concept of Effective Shear Stress

Vittal, et al. (10) found that the dimensionless sediment transport parameter ϕ_T was closely related to the dimensionless shear stress for flow with a plane bed, i.e., for a flow in which the bed is free from undulations. The relationship obtained by them is shown in Fig. 1, and

$$\phi_T = \frac{q_T}{\gamma_s}\sqrt{\frac{\rho_f}{\Delta\gamma_s}}\,\frac{1}{\sqrt{gd^3}} \quad \ldots\ldots\ldots\

$$\tau_* = \frac{\tau_o}{\Delta\gamma_s \cdot d} \quad \ldots\ldots\ldots\

During the course of this investigation a check was made on the adequacy of the $\tau_t/(\Delta\gamma_s \cdot d)$ and τ'_* relation. The data listed in Table 1 indicated that there is no unique relation between the foregoing parameters, and accuracy of predicting q_T from Fig. 1 is significantly affected by the errors in the prediction of τ_t. Therefore the writers attempted to provide a better predictor for τ_t on the following lines.

Functional Relationship for τ_t.—Vittal, et al. (10) have shown that τ_t is greater than τ'_o in case of ripple and dune beds, if suspended load is present. This was ascribed to the fact that part of the form drag would be effective in throwing material into suspension, although it would not help in bed-load movement. At very low values of u_*/ω in which u_* = shear velocity equal to $\sqrt{gR_bS}$, and ω = fall velocity of the sediment in still fluid), that is, when there is no suspended load movement and yet the bed shear stress is greater than the critical shear stress leading to bed-load movement, τ_t would be equal to τ'_o. At high values of u_*/ω, τ_t/τ'_o may be expected to depend on u_*/ω. Furthermore, when the bed is plane, τ'_o tends to τ_o and τ_t tends to τ'_o; but when undulations are present τ_t/τ'_o may be expected to depend on τ'_o/τ_o also. Thus the functional relationship based on this physical reasoning may be written as

$$\frac{\tau_t}{\tau'_o} = f\left(\frac{\tau'_o}{\tau_o}, \frac{u_*}{\omega}\right) \quad \ldots\ldots\ldots\ldots\ldots\ldots\ldots\ldots\ldots\ldots\ldots\ldots\ldots\ldots (5)$$

Eq. 5 may also be obtained from principles of dimensional analysis as follows: $\tau_t = f(\rho_f, d, \mu, \tau_o, U, \gamma_s, \gamma_f)$, in which μ = dynamic viscosity of fluid. Recognizing that ω depends on d, ρ_f, and μ, and also that U is related to τ'_o through a Chezy-type resistance equation, one may write $\tau_t = f(\rho, \omega, \tau_o, \tau'_o)$, which obviously reduces to Eq. 5.

Variation of τ_t/τ'_o *with* τ'_o/τ_o *and* u_*/ω.—The fall velocity of the sediment has been calculated using Rubey's equation, that is

$$\omega = \sqrt{\frac{36\mu^2}{\rho_f^2 d^2} + \frac{2}{3}\frac{\Delta\gamma_s \cdot d}{\rho_f}} - \frac{6\mu}{\rho_f d} \quad \ldots\ldots\ldots\ldots\ldots\ldots\ldots\ldots\ldots\ldots\ldots\ldots (6)$$

The data listed in Table 1 were then grouped into different ranges of u_*/ω and Fig. 2 was prepared in accordance with Eq. 5. It can be seen clearly that τ_t/τ'_o increases with increase in u_*/ω for any given τ'_o/τ_o. This is rather significant because τ'_o generally increases with increase in u_* and the increase of τ_t/τ'_o with increase in u_*/ω suggests a large increase in τ_t as the tendency towards suspension increases. Further, τ_t/τ'_o decreases with increase in τ'_o/τ_o for any value of u_*/ω. Detailed examination of Fig. 2 indicates that the relationship for τ_t can be expressed as

$$\frac{\tau_t}{\tau'_o} = \left(\frac{\tau'_o}{\tau_o}\right)^{-m} \quad \ldots\ldots\ldots\ldots\ldots\ldots\ldots\ldots\ldots\ldots\ldots\ldots\ldots\ldots (7)$$

in which m = function of u_*/ω. When suspended load is absent, τ_t/τ' is equal to unity; in other words $m = 0$. It is known (6) that suspended load is negligible when $u_*/\omega \leq 0.5$. Thus

$$m = 0 \quad \text{if} \quad \frac{u_*}{\omega} \leq 0.5 \quad \ldots\ldots\ldots\ldots\ldots\ldots\ldots\ldots\ldots\ldots\ldots\ldots\ldots\ldots (8)$$

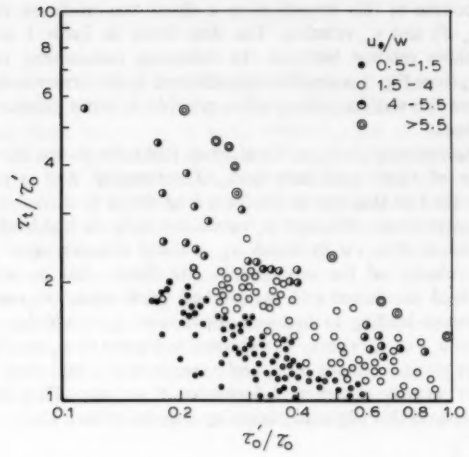

FIG. 2.—Variation of τ_t/τ_o' with τ_o'/τ_o and u_*/ω

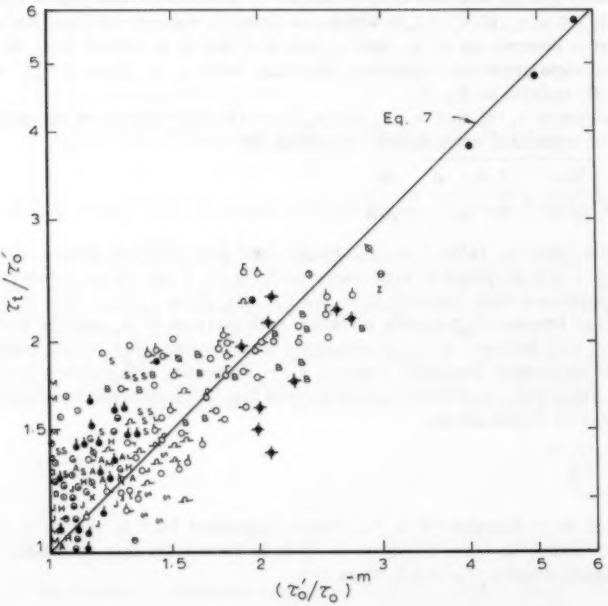

FIG. 3.—Variation of τ_t/τ_o' with $(\tau_o'/\tau_o)^{-m}$

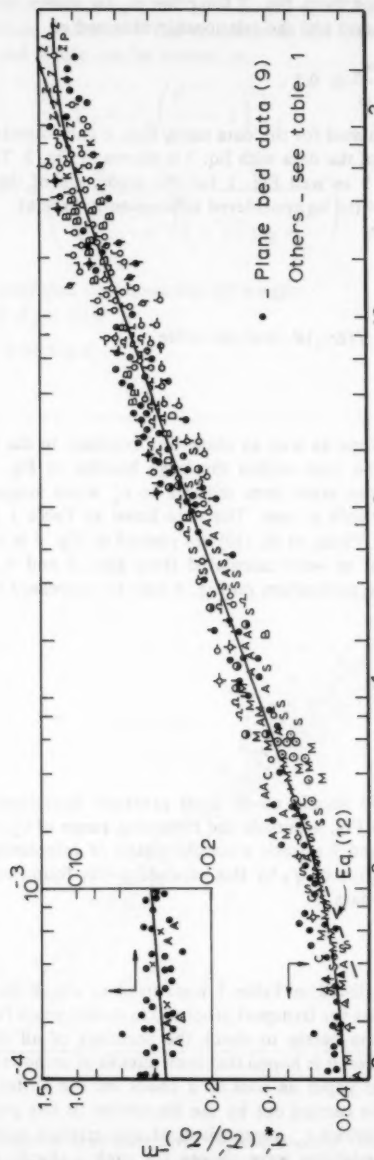

FIG. 4.—Sediment Transport Law for Plane, Ripple, and Dune Beds

The values of m determined from Fig. 2 for other u_*/w values were plotted against u_*/ω (not shown here) and the relationship obtained as

$$m = 0.2\frac{u_*}{\omega} - 0.10 \quad \text{for} \quad \frac{u_*}{\omega} \geq 0.5 \quad \ldots\ldots\ldots\ldots\ldots\ldots\ldots\ldots\ldots\ldots (9)$$

The values of m were calculated for the data using Eqs. 8 and 9, and $(\tau_o'/\tau_o)^{-m}$ computed. The agreement of the data with Eq. 7 is shown in Fig. 3. The over-all error in using Eqs. 8 and 9 as well Fig. 1 for the prediction of the transport rate is apparent from Fig. 4 (to be considered subsequently herein).

Eq. 7 can also be written

$$\frac{\tau_t}{\Delta\gamma_s \cdot d} = \tau_*' \left(\frac{\tau_o'}{\tau_o}\right)^{-m} \quad \ldots\ldots\ldots\ldots\ldots\ldots\ldots\ldots\ldots\ldots\ldots\ldots (10)$$

Since ϕ_T is a function of $\tau_t/(\Delta\gamma_s)d$, one can write

$$\phi_T = f\left[\tau_*' \left(\frac{\tau_o'}{\tau_o}\right)^{-m}\right] \quad \ldots\ldots\ldots\ldots\ldots\ldots\ldots\ldots\ldots\ldots\ldots\ldots (11)$$

Eq. 11 is valid for ripple-dune as well as plane bed regimes; in the latter case τ_o' and τ_o are equal and the term within the large bracket in Eq. 11 merely reduces to τ_*. Note that the same term reduces to τ_*' when suspended load is absent, since $m = 0$ in such a case. The data listed in Table 1 along with the plane bed data used by Vittal, et al. (10) are plotted in Fig. 4 in accordance with Eq. 11. The values of m were calculated from Eqs. 8 and 9. The good correlation between the two parameters on Fig. 4 may be expressed by

$$\phi_T = 60\,\tau_*'^3 \left(\frac{\tau_o'}{\tau_o}\right)^{-3m} \quad \ldots\ldots\ldots\ldots\ldots\ldots\ldots\ldots\ldots\ldots\ldots\ldots (12)$$

in the range of

$$0.05 \leq \tau_*' \left(\frac{\tau_o'}{\tau_o}\right)^{-m} \leq 1.0 \quad \ldots\ldots\ldots\ldots\ldots\ldots\ldots\ldots\ldots\ldots\ldots\ldots (13)$$

The range given by Eq. 13 should cover most practical situations. One can use the mean line drawn in Fig. 4 outside the foregoing range of $\tau_*'(\tau_o'/\tau_o)^{-m}$. Eq. 12 along with Eqs. 8 and 9 affords a simple means of calculating the total load. The error in computation of q_T by this procedure was found to be within ±40% for over 80% of the data.

Check on Existing Relations

The various sets of data listed in Table 1 were used to check the accuracy of a few of the many relations for transport proposed in recent years (1,2,3,5,7,8, 12,13). It is not the intention herein to check the accuracy of all the existing transport relationships. In fact, it is hoped that such checks of some relationships using the data listed in this paper as well as a check on the writers' relation using additional data will be carried out by the discussers to this paper. Some conclusions could also be drawn by comparison of one relation with another. Hence only the following relations were chosen for such a check: (1) Ackers

and White (1); (2) Engelund and Hansen (5); and (3) Graf and Acaroglu (7).

Ackers-White Relation.—The relationship for total load transport proposed by Ackers and White can be written as

$$\left(\frac{u_*}{U}\right)^{C_1} \frac{\gamma_f}{\gamma_s} \cdot \frac{D}{d} \cdot C_T = C_2 \left(\frac{F_1}{C_3} - 1\right)^{C_4} \quad \ldots\ldots\ldots\ldots\ldots\ldots\ldots\ldots (14)$$

in which $$F_1 = \left(\frac{u_*^{C_1}}{\sqrt{\frac{\Delta\gamma_s}{\rho_f} d}}\right)\left(\frac{U}{\sqrt{32}\log\frac{10D}{d}}\right)^{1-C_1} \quad \ldots\ldots\ldots\ldots\ldots (15)$$

and C_T = total load concentration by weight.

For $1.0 \le d_* \le 60.0$

$$C_1 = 1.0 - 0.56 \log d_* \quad \ldots\ldots\ldots\ldots\ldots\ldots\ldots\ldots\ldots\ldots (16a)$$

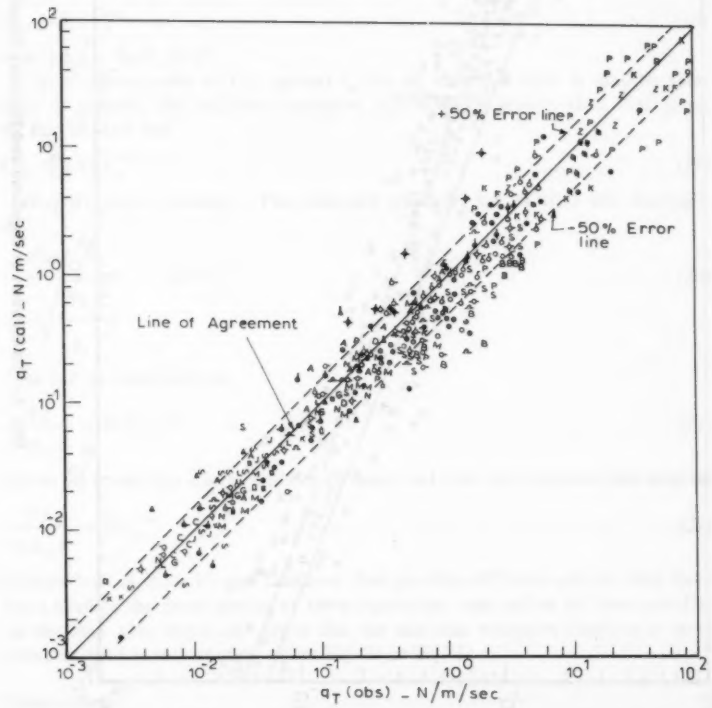

FIG. 5.—Observed Transport Rate Plotted Against Transport Rate Calculated by Ackers-White Method (1)

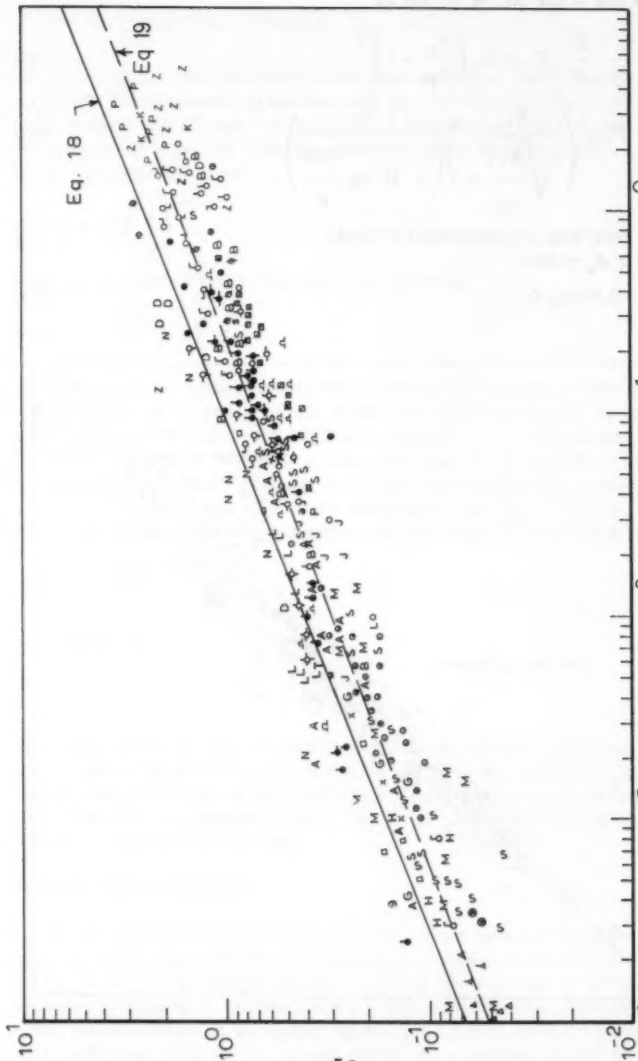

FIG. 6.—Verification of Engelund and Hansen's Equation (5)

$$\log C_2 = 2.86 \log d_* - (\log d_*)^2 - 3.53 \quad \ldots\ldots\ldots\ldots\ldots\ldots \quad (16b)$$

$$C_3 = \frac{0.23}{d_*^{1/2} + 0.14} \quad \ldots\ldots\ldots\ldots\ldots\ldots\ldots\ldots \quad (16c)$$

$$C_4 = \frac{9.66}{d_* + 1.34} \quad \ldots\ldots\ldots\ldots\ldots\ldots\ldots\ldots\ldots \quad (16d)$$

For $d_* > 60.0$

$$C_1 = 0, \quad C_2 = 0.025, \quad C_3 = 0.17 \quad \text{and} \quad C_4 = 1.50 \quad \ldots\ldots\ldots\ldots \quad (17)$$

in which $d_* = (\Delta\gamma_s/\rho_f\nu^2)^{1/3}\, d$, ν being the kinematic viscosity. The values of C_T were calculated for all the data using Eqs. 14 through 17, and hence q_T was computed. The computed values are plotted against the observed transport rates in Fig. 5. The error in the predicted transport rate is within ±50% for 80% of the data.

Engelund-Hansen Relation.—Engelund and Hansen gave the total load equation

$$f\phi_T = 0.1\,\tau_*^{5/2} \quad \ldots\ldots\ldots\ldots\ldots\ldots\ldots\ldots\ldots \quad (18)$$

in which $f = 8gR_bS/U^2$.

Fig. 6 shows a plot of $f\phi_T$ against τ_* for all dune-bed data. It may be seen that, in general, the sediment transport rate is much greater than that given by Eq. 18, and that

$$f\phi_T = 0.25\,\tau_*^{8/3} \quad \ldots\ldots\ldots\ldots\ldots\ldots\ldots\ldots\ldots \quad (19)$$

Graf-Acaroglu Relation.—The sediment transport law of Graf and Acaroglu is

$$\frac{C_T \cdot U R_b}{\gamma_s \sqrt{\dfrac{\Delta\gamma_s}{\rho_f} d^3}} = 10.39\,\tau_*^{2.52} \quad \ldots\ldots\ldots\ldots\ldots\ldots \quad (20)$$

This can be expressed as

$$\frac{q_T}{\gamma_s u_* d} = 10.39\,\tau_*^{2.02} \quad \ldots\ldots\ldots\ldots\ldots\ldots\ldots\ldots \quad (21)$$

Garde (6) found that a large amount of flume and field data followed the relation

$$\frac{q_T}{\gamma_s u_* d} = 16\,\tau_*^{4.0} \quad \ldots\ldots\ldots\ldots\ldots\ldots\ldots\ldots \quad (22)$$

Comparison of Eqs. 21 and 22 shows that possibly different sets of data have been used in the development of these equations, and neither of them satisfies all the data. One might also argue that the sediment transport function is more complex than is indicated by either Eq. 21 or Eq. 22.

Conclusions

The total load transported by an alluvial channel can be expressed in functional form as $\phi_T = f(\tau'_*, \tau'_o/\tau_o, u_*/\omega)$.

Available data from canals, rivers, and flume studies, for regimes other than the antidune regime, indicate that Eq. 12, which is based on the foregoing functional relationship, is a satisfactory sediment transport relation for the commonly encountered regimes of flow. This relationship appears to be more accurate than some of the existing total load equations.

Appendix I.—References

1. Ackers, P., and White, W. R., "Sediment Transport—New Approach and Analysis," *Journal of the Hydraulics Division*, ASCE, Vol. 99, No. HY11, Proc. Paper 10167, Nov., 1973, pp. 2041–2058.
2. Bagnold, R. A., "An Approach to the Sediment Transport Problem from General Physics," Professional Paper 422-I, U.S. Geological Survey, 1966.
3. Colby, B. R., and Hembree, C. H., "Computation of Total Sediment Discharge, Niobrara River near Cody, Nebraska," Water Supply Paper 1357, U.S. Geological Survey, 1955.
4. Einstein, H. A., "Formulas for the Transportation of Bed Load," *Transactions*, ASCE, Vol. 107, 1942, pp. 561–597.
5. Engelund, F., and Hansen, E., "A Monograph on Sediment Transport in Alluvial Streams," Teknisk Forlag, Denmark, 1967.
6. Garde, R. J., and Ranga Raju, K. G., "Mechanics of Sediment Transportation and Alluvial Stream Problems," Wiley Eastern Ltd., New Delhi, India, 1977.
7. Graf, W. E., and Acaroglu, E. R., "Sediment Transport in Conveyance System," *Bulletin of International Association of Scientific Hydrology*, Vol. 13, No. 2, 1968.
8. Pazis, G. C., and Graf, W. H., "Weak Sediment Transport," *Journal of the Hydraulics Division*, ASCE, Vol. 103, No. HY7, Proc. Paper 13032, July, 1977.
9. Peterson, A. W., and Howells, R. F., "A Compendium of Solids Transport Data for Mobile Boundary Channels," Report No. Hy-1973-ST3, Department of Civil Engineering, University of Alberta, Canada.
10. Vittal, N., Ranga Raju, K. G., and Garde, R. J., "Sediment Transport Relations Using Concept of Effective Shear Stress," *Proceedings*, International Association for Hydraulic Research, International Symposium on River Mechanics, Bangkok, Thailand, Jan., 1973, pp. 489–499.
11. Willis, C. J., Neil, L. C., and Wilbert, M. E., "Laboratory Study of Transport of Fine Sand," *Journal of the Hydraulics Division*, ASCE, Vol. 98, No. HY3, Proc. Paper 8765, Mar., 1972, pp. 489–501.
12. Yang, C. T., "Incipient Motion and Sediment Transport," *Journal of the Hydraulics Division*, ASCE, Vol. 99, No. HY10, Proc. Paper 10067, Oct., 1973, pp. 1679–1704.
13. Yang, C. T., and Stall, J. B., "Applicability of the Unit Stream Power Equation," *Journal of the Hydraulics Division*, ASCE, Vol. 102, No. HY5, Proc. Paper 12103, May, 1976, pp. 559–568.

Appendix II.—Notation

The following symbols are used in this paper:

C_1, C_2, C_3, C_4 = constants;
C_T = total load concentration by weight;
D = depth of flow;
d = median diameter of sediment;
f = Darcy-Weisbach friction factor;
g = gravitation acceleration;
m = constant;
n = Manning's roughness coefficient;
q_T = total sediment rate, in weight per unit width of channel;

R_b' = hydraulic radius with respect to grain roughness;
S = energy slope;
U = average velocity over the cross section;
u_* = shear velocity;
γ_f = unit weight of fluid;
γ_s = unit weight of sediment;
$\Delta\gamma_s$ = $\gamma_s - \gamma_f$;
μ = dynamic viscosity;
ν = kinematic viscosity;
ρ_f = mass density of fluid;
τ_o = average bed shear stress;
τ_o' = average bed shear stress corresponding to grain roughness;
τ_t = effective shear stress;
τ_*' = dimensionless grain shear stress;
ϕ_T = dimensionless total load transport; and
ω = fall velocity of sediment in still fluid.

JOURNAL OF THE HYDRAULICS DIVISION

HAZARD ASSESSMENT OF ARCH DAM IN SEISMIC ZONE[a]

By Donald E. Bowes,[1] Antonio X. Sison,[2] and Alan L. O'Neill,[3]

INTRODUCTION

The serious consequences of a failure of a dam structure make it imperative that these structures be designed appropriately for all possible hazards. The occurrence of strong earthquakes and the resulting damage that had occurred to some structures has drawn attention to hazards posed by earthquakes.

Construction of the concrete-arch Green Lake Dam in one of North America's highly seismic areas required an assessment of the hazards and risks associated with this level of seismicity. This was evaluated by a determination of anticipated bedrock acceleration at the dam site, determination of the response behavior of the dam, and a detailed stress analysis to ensure that the stress levels in the dam would be within generally acceptable limits.

The Green Lake Hydroelectric Project is located in Southeast Alaska about 12 air miles (19 km) southeast of Sitka on the west side of Baranof Island (see Fig. 1). The project is being constructed by the city and borough of Sitka, Alaska. The arch dam is located across the Vodopad River at the mouth of Green Lake, an existing glacial lake at approximate El. 240 ft (73 m), which drains to tidewater at Silver Bay some 2,000 ft (610 m) downstream. The reservoir will have a total storage capacity of 90,000 acre-ft (111×10^6 m^3) at the normal maximum reservoir, El. 390 ft (119 m). Water for power generation will be conveyed to the powerhouse at tidewater by an 8-ft (2.4-m) diam concrete-lined tunnel, 1,900 ft (580 m) long. The powerhouse will contain two vertical axis

[a]Presented at the April 14–18, 1980, ASCE Convention and Exposition, held at Portland, Oreg., (Preprint 80-055).

[1]Partner, R. W. Beck and Assocs., Tower Building, 7th Avenue at Olive Way, Seattle, Wash. 98101.

[2]Executive Engr., R. W. Beck and Assocs., Tower Building, 7th Avenue at Olive Way, Seattle, Wash. 98101.

[3]Vice Pres., Converse, Ward, Davis, Dixon, Inc., San Francisco, Calif.

Note.—Discussion open until July 1, 1981. To extend the closing date one month, a written request must be filed with the Manager of Technical and Professional Publications, ASCE. Manuscript was submitted for review for possible publication on June 10, 1980. This paper is part of the Journal of the Hydraulics Division, Proceedings of the American Society of Civil Engineers, ©ASCE, Vol. 107, No. HY2, February, 1981. ISSN 0044-796X/81/0002-0193/$01.00.

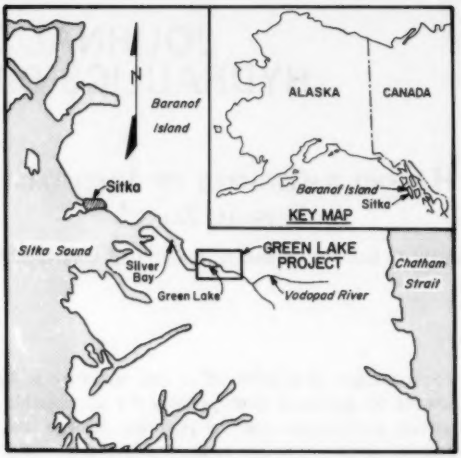

FIG. 1.—Location Map

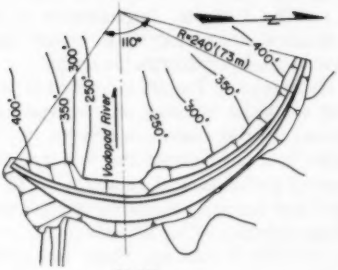

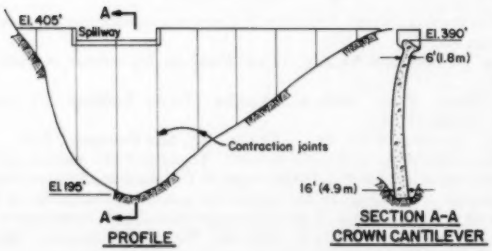

FIG. 2.—Green Lake Dam

Francis turbines connected to two generators with a total rated capacity of 16,500 kW.

The dam, currently under construction, will be a concrete double curvature arch, as shown in Fig. 2. The crest length along the axis will be 450 ft (137 m), subtending an angle of 110°. The dam will be 210 ft (64 m) high, 6 ft (1.8 m) thick at the crest, and 16 ft (4.9 m) thick at the base of the crown cantilever. The total volume of concrete in the dam will be 26,000 cu yd (19,900 m^3).

Seismic records indicate that approx 25 earthquakes have been recorded within 100 miles (160 km) of the site between 1899 and 1976. The records suggest that at least one of those earthquakes may have caused significant ground motion at the dam site. Recognizing that the record of seismicity in Southeast Alaska is very short, and likely deficient with some inaccuracies, it was concluded that a study was necessary to realistically assess the seismic hazards and risk at the site and that the design of the arch dam should take into account the anticipated seismic ground motions identified by the study.

Geology

Green Lake dam site is located on the west side of Baranof Island. Foundation rock for the dam is very competent, slightly metamorphosed greywacke. The topography is precipitous, rising approx 4,000 ft (1,200 m) within 1-1/2 miles (2.4 km) of the shoreline. The core of the island consists largely of Jurassic and Cretaceous-age, 70,000,000-yr–180,000,000-yr before present (ybp), granitic rocks which have intruded and metamorphosed older stratified sedimentary rocks on the east and west sides of the island. Subsequent deformation of the rocks occurred, including folding and movement by strike slip and vertical motion along faults. The period of major deformations probably terminated more than 10,000,000 ybp.

Baranof Island was intensely glaciated during Pleistocene time (between 10,000 ybp–2,000,000 ybp). The continental ice sheet covered the island to about El. 3,000 (915 m). The last ice probably disappeared about 10,000 ybp leaving elevated terraces, rounded rock lips (Green Lake dam site), *U*-shaped valleys (Green Lake drainage basin), and deep *V*-shaped fiords (Silver Bay).

Faulting and Seismicity

Southeast Alaska is presently the site of major plate convergence and its associated tectonics. The plate boundary between the North American plate and the Pacific plate is along the Fairweather-Queen Charlotte Islands Fault which lies about 35 miles (56 km) southwest of the dam site (see Fig. 3). That fault has been associated with numerous earthquakes, several of which fall into the "great earthquake" (8+ magnitude) category.

Baranof Island is bounded by three major faults, the Fairweather-Queen Charlotte Islands to the southwest, the Peril Strait to the northeast, and the Chatham Strait-Lynn Canal to the east and southeast (see Fig. 3). The Chichagof-Sitka Fault traverses part of the island near Sitka and its trace passes within 1/2 mile (0.8 km) of the dam site. These faults were considered to be the major tectonic structures along which, if earthquakes occurred, potentially

damaging ground motion could occur at the dam site. Therefore, they were the subject of evaluation during the study. For purposes of this study a fault was assumed to be capable if there was evidence of movement within the last 35,000 yr.

Clearly, the Fairweather-Queen Charlotte Islands Fault is the most important capable fault in Alaska since it acts as the boundary between the North American and Pacific plates. The fault is assumed to be as long as 470 miles (752 km) (6,20).

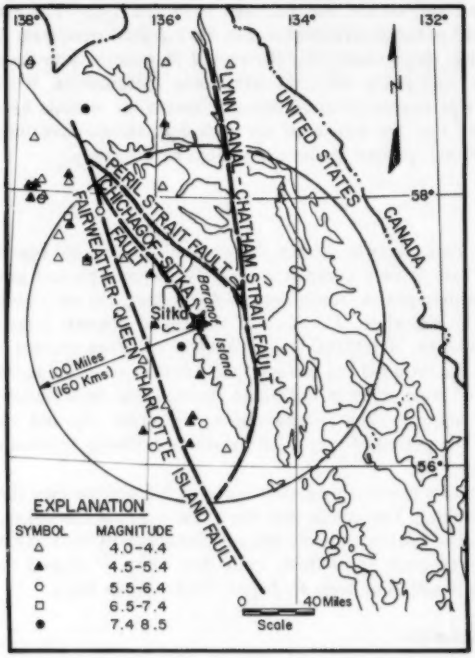

FIG. 3.—Earthquake Epicenters and Faults

The Peril Strait Fault is about 110 miles (176 km) in length (6). Major movement on the fault appears to have occurred prior to the Miocene age (25,000,000 ybp) (13); however some low level seismicity recorded to the north could be associated with the fault and therefore it was assumed capable.

The Chatham Strait-Lynn Canal Fault was conservatively classified as capable on circumstantial evidence consisting of a small amount of microseismicity which could be associated with the fault. Also, toward the south end, the literature reports interpretations of marine geophysical surveys which indicate deformations and faulted sediments of the Holocene age (less than 10,000 ybp) along its

trace (26). The fault is believed by some to be the southeast continuation of the major active Denali fault system to the north, giving it a combined length of greater than 265 miles (424 km) (13).

The Chichagof-Sitka Fault has three major segments with a combined length of between 100 miles (160 km) and 125 miles (200 km) (13). The major movement occurred over 25,000,000 ybp. There is no known geologic evidence or historic seismicity to suggest activity during the past 35,000 yr. Therefore, this fault was considered noncapable. A short fault which splays from the Chichagof-Sitka Fault and passes through Green Lake about 1/2 mile from the dam site was carefully inspected from the air and on the ground. Evidence to indicate movement within the past 35,000 yr along that fault or other possible capable faults was not detected; thus they were considered to be noncapable.

Evaluation of fault capability included aerial flights at different sun angles for evaluation of lineaments and to detect if there were other significant faults which had geomorphic evidence of young movement. Geologic mapping and foundation exploration at the dam site, as well as the aerial reconnaissance, revealed no faults passing through the foundation; therefore permanent dam foundation ground displacement was not a seismic consideration for the design of the arch dam.

Maximum Credible Earthquake

The maximum credible earthquake (MCE) for a given fault is defined as the largest magnitude event, independent of time, which can be reasonably postulated to occur based upon existing geologic and seismologic evidence. Lacking other parameters, maximum credible earthquakes were estimated for the fault rupture length assuming that one half of the surface mapped length could rupture during a single event. Based on the maximum credible earthquake determined for each capable fault, the maximum horizontal ground acceleration at the dam site was established using the attenuation curves of Schnabel and Seed (22); duration of shaking was determined from Bolt et al. (2) and Housner (10). A summary of the maximum credible earthquakes and estimated rock motion parameters for the dam site is given in Table 1.

TABLE 1.—Green Lake Dam Site Maximum Credible Earthquakes and Horizontal Rock Motion Parameters

Fault name (1)	Minimum site distance, in miles (2)	Maximum credible earthquake magnitude (3)	Rock Surface Motion Parameters	
			Maximum rock acceleration (22), *g* (4)	Duration of strong shaking seconds (2,10) (5)
Chatham Strait-Lynn Canal (26)	16	8+	0.40	45
Peril Strait (29)	18	7.3	0.28	26
Fairweather-Queen Charlotte Islands (53)	33	8+	0.25	40

Although the frequency of earthquakes from the Fairweather-Queen Charlotte Fault is greater, a MCE from the Chatham Strait-Lynn Canal Fault would cause the maximum peak bedrock acceleration at the dam site.

Seismic Risk Evaluation

Seismic risk evaluations were carried out after the methods outlined by Marachi and Dixon (14). Earthquakes occurring within a 100-mile (160-km) radius circle about the site (see Fig. 3), formed the data bank for the historic analysis. Two methods of analysis proved valuable in comparing the seismic risk in terms of return intervals; those methods were the site region model and fault model.

The site region model assumes the random occurrence of earthquakes in space and the independence of events; results from this method should be regarded as an average for a particular area. Attenuation areas were developed based on the curves of Schnabel and Seed (22).

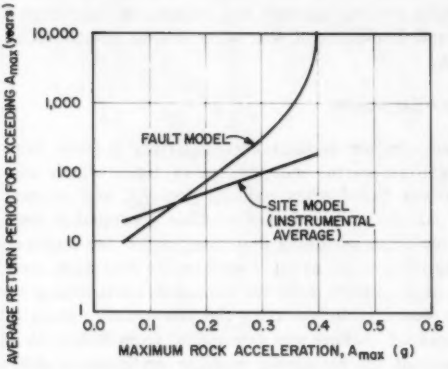

FIG. 4.—Average Recurrence of Horizontal Rock Surface Acceleration

The fault model only included data from the Fairweather-Queen Charlotte Islands Fault Zone due to the lack of sufficient geologic/seismic information for other regional faults. The magnitude recurrence relationship was based on earthquakes instrumentally recorded along the 470-mile (752-km) length of the fault.

Recurrence intervals for the two methods of analyses were interpreted (see Fig. 4). The site region model assumes the random distribution of earthquakes in both time and space and is best suited to analyze a seismic environment in which earthquakes are uniformly distributed over relatively large areas. Conversely, the fault model assumes that the earthquakes originate only on known fault traces. Fig. 3 indicates that recorded earthquakes are not uniformly distributed throughout Southeast Alaska and there is a preference for most earthquakes to be associated with known faults. The fault model appeared best suited for evaluation of the seismic risks for the Green Lake Dam, even though it is recognized that epicenter locations could be mislocated along a single fault

trace and the Fairweather-Queen Charlotte Islands Fault Zone could be 20 miles (32 km) or more wide adjacent to the site.

Ground Motion

Two earthquakes were selected for consideration in design. They are termed the Class I and Class II earthquakes. The Class I earthquake is the MCE. The dam was designed to ensure that the structure could withstand the loads

TABLE 2.—Green Lake Dam Site Horizontal Bedrock Ground Motion Parameters

Variable (1)	Earthquake parameter: CLASS I, Fault Name: Chatham Strait (2)	Earthquake parameter: CLASS II, Fault Name: Fairweather-Queen Charlotte Islands (3)
Richter magnitude	8+	8+
Site distance to fault, in miles (kilometers)	16 (26)	33 (53)
Maximum peak rock acceleration, g	0.40	0.23–0.30
Probability of exceedance in 100 yr, as a percentage	1	63
Duration of strong ground shaking, in seconds	45	40

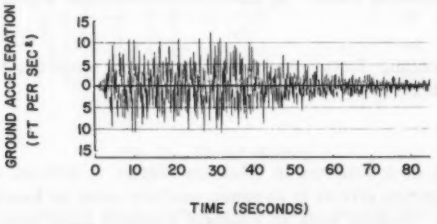

FIG. 5.—Class I Earthquake Time History

from the Class I earthquake without an uncontrolled release of water from the reservoir. The Class II earthquake can reasonably be expected to occur once on the average every 100 yr during the life of the project. The dam was designed to withstand the loads from the Class II earthquake and remain functional.

The important characteristics of ground motion are the amplitude of acceleration, duration of strong shaking, and the frequency with which the acceleration traces cross the time axis which may cause stress reversals. Table 2 summarizes the important characteristics of the Class I and Class II earthquakes selected.

The frequency with which the direction of acceleration changes may be seen in Fig. 5. From these rock motion parameters, accelerograms were developed based on the simulated M8+ (A-1) ground motion accelerogram reported by Jennings et al (11). The Class I and Class II ground accelerations were scaled to 0.4 *g* and 0.23 *g*, respectively. Both upstream-downstream and cross-canyon horizontal components were considered. The time history for one component of horizontal rock surface motion of the Class I earthquake is presented in Fig. 5.

Hydrodynamic Loads

Hydrodynamic loads were found to be a significant portion of the total dynamic loads. The method used to account for hydrodynamic interaction is the widely accepted "virtual mass" approach developed by Westergaard. Recent studies of a model arch dam subjected to low-level excitations have shown reasonable agreement between measured pressures and those obtained using Westergaard's solution (17). The volume of water considered to interact with the dam had a parabolic cross section with a base width equal to 7/8 the height of the

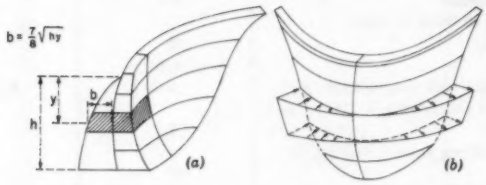

FIG. 6.—Hydrodynamic Forces: (a) Upstream-Downstream Motion; and (b) Cross-Canyon Motion

dam. Hydrodynamic forces were applied in the upstream-downstream and cross-canyon directions (see Fig. 6).

Damping

The damping of a structure in vibratory motion is difficult to evaluate and inclusion of damping effects in dynamic analyses must be based on experience and judgement. Shaking tests to evaluate damping have been performed for concrete dams in Japan, Italy, and the United States, using both model and prototype structures. Low level excitations produced small displacements. Damping ratios from 6%–10% were obtained from tests on arch dams using large excitations (4,7). These tests indicate that energy losses increase as displacements become large. Because of the anticipated opening of contraction joints in the Green Lake Dam during vibration, a damping ratio of 10% was judged to be appropriate for the magnitude of the ground motions for which the dam was designed.

Foundation and Material Properties

Modeling of foundation-arch dam interaction is very complex because of an

arch dam's three-dimensional geometry. Studies made for Auburn Dam showed that rock modulus had little effect on the dynamic characteristics of the dam (25). Green Lake Dam's foundation is hard and not complex and an infinite instantaneous rock modulus was considered appropriate for the dynamic analysis.

The increase in concrete modulus during dynamic loading is well documented by laboratory tests. An instantaneous concrete modulus of elasticity of 4,000,000 psi (27,560 MPa) was used, as compared to the static modulus of 3,000,000 psi (20,670 MPa). Dynamic strength values are dependent on the rate of loading. Under dynamic testing, compressive strengths 20%–30% above static values and tensile strengths of 30%–66% over static values have been cited (25). A comparison between static and dynamic values used in the design is shown in Table 3.

TABLE 3.—Green Lake Dam Static and Dynamic Properties

Variable, in pounds per square inch (1)	Static (2)	Dynamic (3)
Rock deformation modulus	2,000,000	Infinite
Concrete modulus of elasticity	3,000,000	4,000,000
Concrete ultimate compressive strength	4,000	4,800
Concrete ultimate flexural strength	360	540

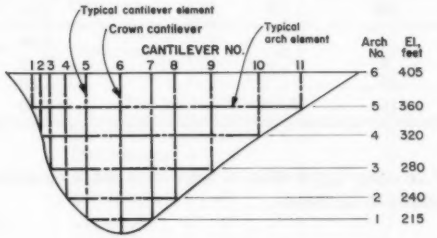

FIG. 7.—Model of Dam

Horizontal construction joints were considered to remain uncracked provided that the ultimate flexural strength was not reached, but vertical contraction joints were assumed to have negligible tensile capacity.

Method of Analysis

The trial load method was utilized in the design analysis. The dam was divided into a system of cantilever and arch elements (see Fig. 7), each set of elements occupying the entire volume of the dam. During vibration, the dam was considered to deflect dynamically as a group of fixed end arches and vertical cantilevers. The loads on the dam are divided between the arch and cantilever elements in such a manner so that the strains at the common nodes are identical.

Static Loading Conditions

The dam was designed for the following conditions: (1) A normal full reservoir with low concrete temperatures; (2) a minimum design reservoir elevation with high concrete temperatures; (3) an absolute minimum reservoir elevation with average concrete temperatures; (4) a probable maximum flood with average concrete temperatures; (5) a design earthquake with Case 1; and (6) a maximum credible earthquake with Case 1.

Modal Sensitivity Analysis

In general, for structures with uncomplicated geometry, the higher vibration modes contribute less to the total response than do the lower modes. A modal sensitivity analysis was performed to determine the lowest mode of vibration above which no significant change in stress is encountered. In Table 4, the relation of stress value to the number of modes considered is shown for a node common to Arch 5 and Cantilever 6. The stress based on a 12-mode analysis was normalized to 1. It is seen that no significant stress change occurred

TABLE 4.—Green Lake Dam Effect of Number of Modes on Stress Values

Number of modes (1)	Stress value (2)
4	0.84
8	0.91
12	1.00
16	1.00

when modes of an order higher than 12 were included. Consequently, the design analysis was limited to 12 modes.

Evaluation of Results

A time history analysis of an arch dam results in an enormous amount of data which have to be evaluated systematically. Of particular interest are: (1) The maximum compressive and tensile stresses; (2) whether high stresses occur over large regions or isolated areas; (3) the duration of stress above a certain level; (4) whether the tensile stresses occur on the upstream or downstream face; and (5) the magnitude and nature of the other stresses occurring in the same region at the same instant.

The first step in the evaluation was to list the compressive and tensile stresses in descending order, and also their locations and times of occurrence. The next step was to plot stress-time histories at points where stresses were significant. From these plots the frequency and duration above any given stress level were determined. At critical instants, stress "snapshots" were taken. These "snapshots" showed the stresses over the entire dam at a given instant and areas of high compressive and tensile stresses were mapped. Also, by taking stress

"snapshots" at successive instants, the pattern of stress change over the entire dam was obtained. Adjustments in the dam configuration were made until the design analysis results indicated acceptable performance.

Stresses Due to Class II Earthquake

Since ground motion varies as a function of time, stresses at various points in the dam also vary with time. Table 5 shows the arch and cantilever stresses

TABLE 5.—Class II Earthquake Stresses at Time When Maximum Compression Occurs, +Compression, −Tension, in pounds per square inch

Arch number (1)	Elevation, in feet (2)	Surface (3)	Cantilever Number 2 (4)	4 (5)	6 (6)	8 (7)	10 (8)
		(*a*) Arch Stresses					
6	405	Upstream	112	−18	788	254	173
		Downstream	272	387	−321	166	187
5	360	Upstream	170	119	923 (Maximum)	463	207
		Downstream	487	561	−146	328	241
4	320	Upstream	133	233	866	461	283
		Downstream	567	478	−5	335	102
3	280	Upstream		208	769	264	
		Downstream		440	−10	350	
2	240	Upstream		88	550	83	
		Downstream		291	−79	269	
		(*b*) Cantilever Stresses					
6	405	Upstream	0	0	0	0	0
		Downstream	0	0	0	0	0
5	360	Upstream	174	76	−32	123	233
		Downstream	−98	5	120	−39	−156
4	320	Upstream	63	134	−56	117	237
		Downstream	77	16	225	40	−123
3	280	Upstream		190	1	−53	
		Downstream		6	241		
2	240	Upstream		155	106	−6	
		Downstream		60	91	181	
	195	Upstream			−11		
		Downstream			354 (Maximum)		

at the upstream and downstream face of the dam at the instant when maximum compression occurred. Similarly, Table 6 shows the stresses when maximum tension occurred. The maximum compressive stress of 923 psi (6.36 MPa) (arch stress), shown in Table 5, and the cantilever tensile stress of 132 psi (0.91 MPa) in Table 6, indicate that an adequate factor of safety was attained. The computed arch tensile stresses shown in the tables need further explanation for proper evaluation.

Since vertical contraction joints have negligible tensile capacity, the computed

negative arch stresses merely indicate that the particular vertical contraction joints were partially open at the instant reflected in the analysis. Physically, when the joints partially open for very short periods (fractions of seconds) the stiffness of the arch is somewhat reduced and the arch load is redistributed as a cantilever load for a fraction of a second. Fortunately, this condition only occurs in the upper arches where the cantilever stresses are small and therefore the redistributed arch load does not result in excessive cantilever stresses. Based on the results shown in Tables 5 and 6, it was concluded that the dam would

TABLE 6.—Class II Earthquake Stresses at Time When Maximum Tension Occurs, +Compression, −Tension, in pounds per square inch

Arch number (1)	Elevation, in feet (2)	Surface (3)	Cantilever Number 2 (4)	4 (5)	6 (6)	8 (7)	10 (8)
			(*a*) Arch Stresses				
6	405	Upstream	46	−80	558	24	116
		Downstream	77	201	−358 (Maximum)	94	17
5	360	Upstream	138	74	678	245	171
		Downstream	292	364	−204	223	108
4	320	Upstream	100	199	635	345	179
		Downstream	413	298	−37	222	87
3	280	Upstream		197	582	249	
		Downstream		306	−3	241	
2	240	Upstream		65	465	83	
		Downstream		240	−46	221	
			(*b*) Cantilever Stresses				
6	405	Upstream	0	0	0	0	0
		Downstream	0	0	0	0	0
5	360	Upstream	169	54	−18	142	210
		Downstream	−93	28	106	−58	−132 (Maximum)
4	320	Upstream	63	119	−56	177	186
		Downstream	77	31	228	21	−71
3	280	Upstream		202	8	36	
		Downstream		−7	233	160	
2	240	Upstream		175	165	36	
		Downstream		38	129	134	
	195	Upstream			35		
		Downstream			303		

not sustain damage under the Class II earthquake which would disrupt normal operation of the project.

Stresses Due to Class I Earthquake

When considering the effects of the loading of a 0.40 *g* Class I earthquake, it should be borne in mind that its occurrence would be an extremely rare event and that minor damage to the structure can be tolerated. However, the damage would not result in an uncontrolled release of water from the reservoir. The maximum compressive stress for the Class I earthquake is about 40% higher than for the Class II, and the stress pattern is similar. Fig. 8 shows the arch

TABLE 7.—Class I Earthquake Stresses at Time When Maximum Compression Occurs, +Compression, −Tension, in pounds per square inch

Arch number (1)	Elevation, in feet (2)	Surface (3)	Cantilever Number 2 (4)	4 (5)	6 (6)	8 (7)	10 (8)
			(*a*) Arch Stresses				
6	405	Upstream	26	−141	1,200	235	183
		Downstream	399	590	−536	287	270
5	360	Upstream	159	26	1,289 (Maximum)	492	213
		Downstream	641	811	−290	481	268
4	320	Upstream	195	193	1,066	478	398
		Downstream	612	649	−65	426	8
3	280	Upstream		198	850	256	
		Downstream		508	−47	414	
2	240	Upstream		100	576	83	
		Downstream		308	−105	298	
			(*b*) Cantilever Stresses				
6	405	Upstream	0	0	0	0	0
		Downstream	0	0	0	0	0
5	360	Upstream	197	48	−139	110	320
		Downstream	−122	34	229	−25	−244
4	320	Upstream	52	116	−181	116	378
		Downstream	89	35	353	42	−267
3	280	Upstream		192	−62	−83	
		Downstream		5	307	283	
2	240	Upstream		151	82	−29	
		Downstream		65	217	207	
	195	Upstream			−28		
		Downstream			373 (Maximum)		

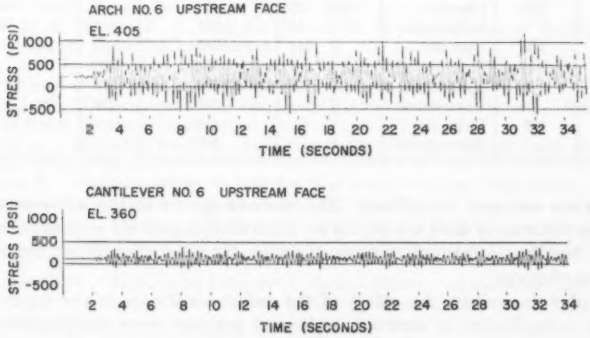

FIG. 8.—Stress Time History Due to Class I Earthquake

stress time history at the crown near the crest. Typically, the stresses were flexural in nature with joint openings taking place intermittently as indicated by the tensile stresses. Compressive stresses were well below the ultimate concrete compressive strength of 4,800 psi (33,100 kPa), and the region of high compression is localized at the crown section on the upper half (see Table 7). Joint openings took place in the upper arches as indicated by the tensile stresses, as shown in Table 8. The duration of these joint openings were approx 0.08 sec. Complete separation of joints was not indicated. As the contraction joints opened and closed, arch and cantilever stresses were redistributed to varying degrees as

TABLE 8.—Class I Earthquake Stresses at Time When Maximum Tension Occurs, +Compression, −Tension, in pounds per square inch

Arch number (1)	Elevation, in feet (2)	Surface (3)	Cantilever Number 2 (4)	4 (5)	6 (6)	8 (7)	10 (8)
			(*a*) Arch Stresses				
6	405	Upstream	491	533	−627 (Maximum)	505	173
		Downstream	−42	−264	531	−249	0
5	360	Upstream	235	554	−283	531	219
		Downstream	113	−236	472	−158	255
4	320	Upstream	−102	442	333	496	−62
		Downstream	589	−8	268	110	480
3	280	Upstream		257	675	311	
		Downstream		321	130	227	
2	240	Upstream		62	552	89	
		Downstream		284	−14	216	
			(*b*) Cantilever Stresses				
6	405	Upstream	0	0	0	0	0
		Downstream	0	0	0	0	0
5	360	Upstream	84	209	383	172	−78
		Downstream	−7	−130	−301 (Maximum)	−88	160
4	320	Upstream	108	220	454	91	−256
		Downstream	31	−74	−298	66	382
3	280	Upstream		164	262	−12	
		Downstream		33	−29	210	
2	240	Upstream			139	44	
		Downstream			157	126	
	195	Upstream			−3		
		Downstream			345		

the arches changed in stiffness. The state-of-the-art in the analysis of arch dams unfortunately does not permit an exact modeling of the nonlinear response of the dam due to the dam's changing elastic characteristics during the duration of an earthquake.

In order to evaluate the effect of the reduced stiffness in the upper arches on the redistribution of stresses, additional analyses were made adjusting the stiffness of the central portion of the upper arch to 25% of that used in the previous analysis. As expected, the stresses in the upper arches were reduced and additional load was taken by the cantilevers. The increased cantilever stresses were well below the ultimate values allowed. Based on these analyses, it was

concluded that the dam can withstand the MCE and will function without causing uncontrolled releases of water from the reservoir. Minor repairs to the dam, such as spalled concrete, should be anticipated.

Summary and Conclusions

Construction of an arch dam in an active seismic zone required a careful assessment of the hazards associated with seismicity. The geology of the region was reviewed and an assessment was made of the hazards posed by the presence of three major faults. The hazards were quantified and expressed as ground motions. The dam was analyzed for two magnitudes of earthquakes, called Class I and Class II. Analyses indicated that the vertical contraction joints partially open during vibration, which results in redistribution of stresses within the structure. The results showed that the dam will remain functional and not disrupt normal operation after a Class II earthquake, and after a Class I earthquake minor damage such as spalling of concrete should be expected, but the dam will remain intact and an uncontrolled release of water from the reservoir will not occur.

Acknowledgment

The authors acknowledge the help and assistance provided by R. W. Beck and Associates and Converse, Ward, Davis, Dixon, Inc., in the preparation of this paper and also thank their special consultant Merlin D. Copen who provided advice and consultation during the design.

Appendix.—References

1. Bell, J. M., and Hoffman, R. A., "Design Earthquakes Based on Geologic Evidence," *Earthquake Engineering and Soil Dynamics*, Vol. 1, ASCE, 1978, pp. 231–271.
2. Bolt, B. A., Horn, W. L., Macdonald, G. A., and Scott, R. F., *Geological Hazards*, Julius Springer, Berlin, Germany, 1975, pp. 52–53.
3. Brew, D. A., Loney, R. A., and Muffler, L. J., *Tectonic History of Southeastern Alaska*, United States Geologic Survey.
4. Enzo, L., "Dynamic Features of a Recent Italian Arch Dam," *Proceedings*, Eighth International Congress on Large Dams, Edinburgh, Scotland, 1964.
5. Fabry, J. W., "Laboratory Tests of Foundation Rock Core for Auburn Dam," *GR-12-75*, United States Bureau of Reclamation, Denver, Colo., Oct., 1975.
6. Grantz, A., "Strike-Slip Faults in Alaska," *open-file report 267*, United States Geologic Survey, 1966, p. 26, 38–41.
7. Hatano, T., "Aseismic Design Criteria for Arch Dams in Japan," *Proceedings*, Ninth International Congress on Large Dams, Istanbul, Turkey, 1967.
8. Housner, G. W., "Intensity of Earthquake Ground Shaking Near the Causative Fault," *Proceedings of the Third World Conference on Earthquake Engineering*, Vol. I, Session III, 1965, p. 94.
9. Housner, G. W., "Engineering Estimates of Ground Shaking and Maximum Earthquake Magnitude," *Proceedings of the Fourth World Conference on Earthquake Engineering*, A-1, 1969, pp. 1, 13.
10. Housner, G. W., "Strong Ground Motion and Design Spectra," *Earthquake Engineering*, R. L. Wiegel, ed., Prentice-Hall, Inc., Englewood Cliffs, N.J., 1970, chapters 4 and 5.
11. Jennings, P. C., Housner, G. W., and Tsai, N. C., "Simulated Earthquake Motions," *Earthquake Engineering Research Laboratory Report*, California Institute of Technology, Pasadena, Calif., 1968.

12. Lemke, R. W., "Reconnaissance Engineering Geology of the Ketchikan Area, Alaska, with Emphasis on Evaluation of Earthquake and Other Geologic Hazards," *open-file report 75-250,* United States Geologic Survey, 1975, p. 17–29.
13. Loney, R. A., Brew, D. A., Muffler, L. J., and Pomeroy, J. S., "Reconnaissance Geology of Chichagof, Baranof and Kruzof Islands, Southeastern Alaska," *Professional Paper 792,* United States Geologic Survey, 1975.
14. Marachi, N. D., and Dixon, S. J., "A Method for Evaluation of Seismicity," *Proceedings of the International Conference on Microzonation,* Oct., 1972.
15. Milne, W. G., and Davenport, A. G., "Distribution of Earthquake Risk in Canada," *Bulletin of the Seismological Society of America,* Vol. 59, No. 2, Apr., 1969, pp. 729–754.
16. Milne, W. G., Rogers, G. C., Riddihough, R. P., McMeehan, G. A., and Hydman, R. D., "Seismicity of Western Canada," *Canadian Journal of Earth Sciences,* Department of Energy, Mines, and Resources, Sidney, British Columbia, Canada, 1978.
17. Norman, C. D., Crowson, R. D., and Balsara, J. P., "Dynamic Response Characteristics of a Model Arch Dam," *Technical Report N-76-3,* United States Army Engineer Waterways Experiment Station, Vicksburg, Miss., Mar., 1976.
18. Page, R., and Lahr, J., "Measurements for Fault Slip on Denali, Fairweather and Castle Mountain Faults, Alaska," *Journal of Geophysical Research,* Vol. 76, No. 35, 1971, pp. 8538–8540.
19. Plafker, G., Hudson, T., and Rubin, M., "Late Holocene Offset Features Along the Fairweather Fault," *USGS Circular 733,* United States Geological Survey, 1975, p. 57.
20. Plafker, G., Hudson, T., Rubin, M., and Bruns, T., "Late Quaternary Offsets Along the Fairweather Fault and Crustal Plate Interactions in Southern Alaska," United States Geological Survey, 1978.
21. Richter, C. R., *Elementary Seismology,* W. H. Freeman and Company, San Francisco, Calif., 1958.
22. Schnable, P. B., and Seed, H. B., "Accelerations in Rock for Earthquakes in the Western United States," *Bulletin of the Seismological Society of America,* Vol. 63, No. 2, 1973, pp. 501–506.
23. Trifunac, M. D., and Brady, A. G., "Correlations of Peak Acceleration, Velocity and Displacement with Earthquake Magnitude, Distance and Site Conditions," *Earthquake Engineering and Structural Dynamics,* Vol. 4, 1976, pp. 455–471.
24. Twenhofel, W. S., and Sainsbury, C. L., "Fault Patterns in Southeastern Alaska," *Bulletin of Geologic Society of America,* Vol. 69, 1958, pp. 1434–1438.
25. *Design and Analysis of Auburn Dam,* Vol. IV, United States Department of the Interior, Bureau of Reclamation, Denver, Colo., 1978.
26. Yehle, L. A., "Reconnaissance Engineering Geology of Sitka and Vicinity, Alaska, with Emphasis on Evaluation of Earthquake and other Geologic Hazards," *open-file report 74-53,* United States Geological Survey, 1974, pp. 34–41.
27. Yehle, L. A., "Reconnaissance Engineering Geology of the Metlakatta Area, Annette Island, Alaska, with Emphasis on Evaluation of Earthquakes and other Geologic Hazards," *open-file report 77-272,* United States Geological Survey, 1977, pp. 28–38.

JOURNAL OF THE HYDRAULICS DIVISION

MODELING TRANSVERSE MIXING IN NATURAL STREAMS

By Y. Lam Lau[1] and B. G. Krishnappan[2]

INTRODUCTION

The transverse mixing of a neutrally buoyant solute that is discharged into an open-channel flow has been the subject of many investigations. For uniform flow in straight, prismatic channels, the advective-diffusion equation describing the depth-averaged concentration under steady-state conditions can be simplified to only two terms, expressing the balance between the longitudinal advection and the transverse dispersion of the solute. For this type of flow, the variance of the concentration-transverse distance distribution increases linearly with downstream distance, in direct proportion to the dispersion coefficient. Thus, the dispersion coefficient can be evaluated from measured concentration distributions. However, when the velocity and depth are not uniform or when the channel is not straight, there is transport of solute by the transverse velocities. This transverse advection must be included in the advective-diffusion equation and must be accounted for when the dispersion coefficient is evaluated from experimental data. Taking this into consideration, Holley, et al. (5) introduced the generalized change-of-moment method for evaluating the dispersion coefficient from second moments of the distributions of solute flux. Their method was derived from the advective-diffusion equation written in rectangular Cartesian coordinates.

Yotsukura and Sayre (13) generalized this approach by writing the continuity and advective-diffusion equations in a general orthogonal curvilinear coordinate system in which the x-axis follows the meander of the river. Then, by using the cumulative discharge to replace the transverse distance coordinate, they showed that the equation for steady, two-dimensional mixing can again be

[1]Head, Environmental Hydr. Section, Hydr. Research Div., National Water Research Inst., Canada Center for Inland Waters, 867 Lakeshore Rd., Burlington, Ontario, L7R 4A6, Canada.

[2]Environmental Hydr. Section, Hydr. Research Div., National Water Research Inst., Canada Center for Inland Waters, 867 Lakeshore Rd., L7R 4A6, Canada.

Note.—Discussion open until July 1, 1981. To extend the closing date one month, a written request must be filed with the Manager of Technical and Professional Publications, ASCE. Manuscript was submitted for review for possible publication on March 6, 1980. This paper is part of the Journal of the Hydraulics Division, Proceedings of the American Society of Civil Engineers, ©ASCE, Vol. 107, No. HY2, February, 1981. ISSN 0044-796X/81/0002-0209/$01.00.

simplified to include only two terms, similar to the equation for straight, prismatic channels. The advantage of this approach is that the effects of changes in channel width and depth as well as channel curvature can be readily included in a "diffusion factor," making it particularly suitable for natural streams. These effects are much more difficult to handle if rectangular Cartesian coordinates are used.

This paper presents a numerical model based on the equation derived by Yotsukura and Sayre (13). The applicability of the model is tested using data from a field experiment. Simulations using different assumptions for the diffusion factor are compared. Finally, the dependence of the transverse mixing coefficient on stream variables is investigated using published values for natural streams.

Analytical Considerations

When the solute has mixed fairly well over the flow depth, the two-dimensional continuity and advective-diffusion equations in an orthogonal curvilinear coordinate system can be written as

$$m_x m_z \frac{\partial h}{\partial t} + \frac{\partial}{\partial x}(m_z h u) + \frac{\partial}{\partial z}(m_x h v) = 0 \quad \ldots\ldots\ldots\ldots\ldots\ldots (1)$$

and

$$m_x m_z \frac{\partial (hc)}{\partial t} + \frac{\partial}{\partial x}(m_z h u c) + \frac{\partial}{\partial z}(m_x h v c) = \frac{\partial}{\partial x}\left(\frac{m_z}{m_x} h e_x \frac{\partial c}{\partial x}\right) + \frac{\partial}{\partial z}\left(\frac{m_x}{m_z} h e_z \frac{\partial c}{\partial z}\right) \quad \ldots\ldots\ldots\ldots\ldots\ldots\ldots\ldots (2)$$

in which t = time; x, z = longitudinal and transverse distance coordinates in the orthogonal, curvilinear system; u, v = depth-averaged velocity components in the x, z directions; h = local flow depth; c = depth-averaged concentration; e_x, e_z = turbulent mixing or dispersion coefficients in the x, z directions; and m_x, m_z = metric coefficients for the coordinate system. Details for the derivation of Eqs. 1 and 2 have been given in Ref. 13. In this study, the x-axis has been chosen to coincide with the right bank (looking downstream), and z is measured across the stream, orthogonal to the x-axis (see Fig. 1).

When the channel discharge and the solute inflow rate are both steady, the time dependent terms can be dropped. The longitudinal dispersion term has very little influence on the transverse mixing under this condition and can also be neglected (8). Eqs. 1 and 2 are then reduced to

$$\frac{\partial}{\partial x}(m_z h u) + \frac{\partial}{\partial z}(m_x h v) = 0 \quad \ldots\ldots\ldots\ldots\ldots\ldots\ldots\ldots (3)$$

and

$$m_z h u \frac{\partial c}{\partial x} + m_x h v \frac{\partial c}{\partial z} = \frac{\partial}{\partial z}\left(\frac{m_x}{m_z} h e_z \frac{\partial c}{\partial z}\right) \quad \ldots\ldots\ldots\ldots\ldots (4)$$

Introducing a variable called the cumulative discharge q_c in which

$$q_c = \int_0^z m_z h u dz \quad \ldots\ldots\ldots\ldots\ldots\ldots\ldots\ldots\ldots (5)$$

and using q_c in place of the variable z, the advective-diffusion equation (Eq. 4) is transformed into

$$\frac{\partial c}{\partial x} = \frac{\partial}{\partial q_c}\left(uh^2 m_x e_z \frac{\partial c}{\partial q_c}\right) \quad \ldots\ldots\ldots\ldots\ldots\ldots\ldots\ldots\ldots\ldots (6)$$

Eq. 6 is the equation presented by Yotsukura and Sayre (13) and can be shown to be the general form of the stream tube models derived in earlier papers (2,3,9,12).

Defining a dimensionless cumulative discharge $\eta = q_c/Q$, in which Q = the total discharge of the channel, Eq. 6 can be written as

$$\frac{\partial c}{\partial x} = \frac{1}{Q^2}\frac{\partial}{\partial \eta}\left[D_z(x,\eta)\frac{\partial c}{\partial \eta}\right] \quad \ldots\ldots\ldots\ldots\ldots\ldots\ldots\ldots\ldots\ldots (7)$$

At the left bank, $\eta = 0$ and at the right bank, $\eta = 1$. The term $D_z = (uh^2 m_x e_z)$ is called the factor of diffusion. It includes the turbulent mixing coefficient

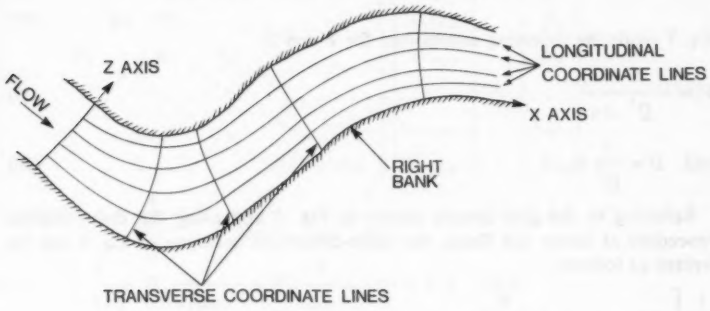

FIG. 1.—Curvilinear Coordinate System

e_z as well as the term $(uh^2 m_x)$ which reflects local changes in depth, velocity, and stream curvature, If D_z is assumed to be constant, then Eq. 7 can be solved analytically. However, for accurate simulations, it is necessary to use local values for D_z and solve Eq. 7 numerically. As will be shown later, different approximations for D_z can be used, depending on the accuracy desired.

Numerical Method

An implicit finite-difference scheme proposed by Stone and Brian (11) to solve the advective-diffusion type equations was adopted for the present work. When the right hand side of Eq. 7 is expanded and terms are rearranged, it takes the form which was analyzed by Stone and Brian for numerical oscillations and dispersion. The form of the equation is:

$$\frac{\partial c}{\partial x} + V\frac{\partial c}{\partial \eta} = D\frac{\partial^2 c}{\partial \eta^2} \quad \ldots\ldots\ldots\ldots\ldots\ldots\ldots\ldots\ldots\ldots (8)$$

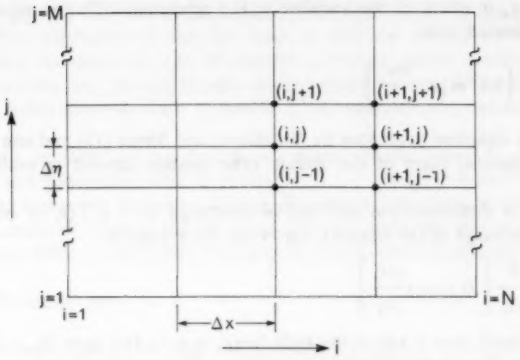

FIG. 2.—Grid System for the Numerical Scheme

Eq. 7 yields the following expressions for V and D:

$$V = -\frac{1}{Q^2}\frac{\partial D_z}{\partial \eta} \quad \ldots \ldots \ldots

No weighting coefficients are used for approximating the second derivative $\partial^2 c/\partial \eta^2$. A Crank-Nicolson type approximation is used to discretize it.

Stone and Brian have shown that the preceding numerical scheme yields solutions closer to the analytical solutions (for the case of constant V and D) when the weighting coefficients take the following optimum values:

$$g = \frac{2}{3}; \quad \frac{\theta}{2} = m = \frac{1}{6}; \quad a = b = d = \frac{\epsilon}{2} = \frac{1}{4} \ldots\ldots\ldots\ldots\ldots\ldots (14)$$

They recommended the use of the preceding values for the weighting coefficients for the general case when V and D are not constants.

When the concentration distribution at an initial station, say i, is known, then the concentration distribution at the next station, $i + 1$, can be calculated using Eq. 11 for a specific boundary condition at the sidewalls. For a no-flux boundary condition at the sidewalls, Eq. 11 can be expanded and written in matrix notation as follows:

$$\begin{bmatrix} q_2 & -r_2 & & & & \\ -p_3 & q_3 & -r_3 & & & \\ & -p_4 & q_4 & -r_4 & & \\ & & \ddots & \ddots & \ddots & \\ & & & & -r_{M-1} & \\ & & & -p_M & q_M & \end{bmatrix} \begin{bmatrix} c_{i+1,2} \\ c_{i+1,3} \\ c_{i+1,4} \\ \\ c_{i+1,M-1} \\ c_{i+1,M} \end{bmatrix} = \begin{bmatrix} S_2 \\ S_3 \\ S_4 \\ \\ S_{M-1} \\ S_M \end{bmatrix} \ldots\ldots (15a)$$

in which $q_j = \dfrac{g}{\Delta x} + D_{i,j}\dfrac{1}{(\Delta\eta)^2} + V_{i,j}\dfrac{1}{\Delta\eta}(d - b), \quad (j = 2, 3 \ldots M);$

$$p_j = -\frac{\theta}{2}\frac{1}{\Delta x} + D_{ij}\frac{1}{2(\Delta\eta)^2} + V_{i,j}\frac{1}{\Delta\eta}d, \quad (j = 3, 4 \ldots M);$$

$$r_j = -\frac{m}{\Delta x} + D_{ij}\frac{1}{2(\Delta\eta)^2} - V_{i,j}\frac{1}{\Delta\eta}b, \quad (j = 2, 3 \ldots M - 1);$$

and $S_j = c_{i,j-1}\left[\dfrac{\theta}{2}\dfrac{1}{\Delta x} + D_{i,j}\dfrac{1}{2(\Delta\eta)^2} + V_{i,j}\dfrac{\epsilon}{2\Delta\eta}\right] + c_{i,j}\left[\dfrac{g}{\Delta x}\right.$

$$\left. - D_{i,j}\frac{1}{(\Delta\eta)^2} - V_{i,j}\frac{1}{\Delta\eta}\left(\frac{\epsilon}{2} - a\right)\right] + c_{i,j+1}\left[\frac{m}{\Delta x} + D_{i,j}\frac{1}{2(\Delta\eta)^2}\right.$$

$$\left. - V_{i,j}\frac{a}{\Delta\eta}\right], \ (j = 2, 3 \ldots M) \ldots\ldots\ldots\ldots\ldots\ldots\ldots\ldots (15b)$$

When calculating the terms $V_{i,j}$, the derivative of D_z with respect to η is evaluated in the same manner as the derivative of c with respect to η. The coefficients of the tridiagonal matrix can be evaluated from the known values of V and D and the weighting coefficients. The system of equations is then solved using the Gauss-Seidal method (10) of successive substitutions.

As a check of the accuracy of the numerical scheme, the numerical solution

was compared with an analytical solution which can be obtained when D_x is a constant. The initial condition used was a concentration distribution at $x = 0$ which decreased linearly from a maximum at $\eta = 0$ to zero at $\eta = 0.5$. There were no detectable differences between the two solutions.

Description of Field Test

A field experiment was carried out on the Grand River, just south of Kitchener, Ontario to collect data for use with the model. The study reach was 1,500-m long with two bends at the lower portions (Fig. 3). The streambed was primarily sand and gravel with some large rocks. Measurements were made at six transects which were spaced 250-m apart along the right bank. The stream characteristics

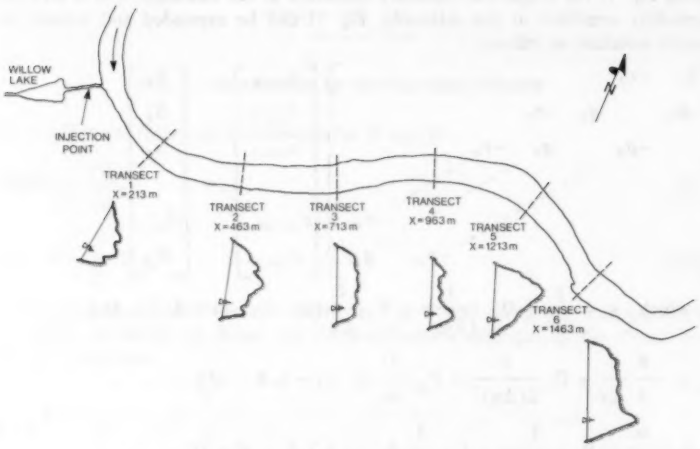

FIG. 3.—Test Reach, Grand River Below Kitchener, Ontario

measured at these six transects are given in Table 1. The average width, depth, and velocity of the reach were 59.2 m, 0.506 m, and 0.353 m/s respectively.

The tracer used was a Rhodamine B dye which was injected into a small tributary (3 m wide) located about 230 m upstream from the first transect. A 2.5% solution of Rhodamine B was injected at about 100 ml/min using a constant-rate diaphram pump. The tributary has negligible momentum compared to the main flow. The dye was mixed throughout the tributary and, on entering the river, formed a small line source at the right bank.

A Turner model 111 fluorometer was used at the first transect to monitor the dye concentration. After making sure that steady-state conditions had been reached, measurements of dye concentration, velocity, and depth were made at 3-m intervals across the transect, using a marked cable that was stretched across the stream as a guide. Velocity measurements were taken at 0.2 and 0.8 depths using an Ott meter. The fluorometer readings were adjusted for

background concentration and also temperature corrected. After completing all the measurements at the first transect, the field party moved to the next transect downstream and the whole operation was repeated. Similar measurements were made at all six transects.

Analysis of Results

Using the measurements of depth and velocity, the discharge through each 3-m wide segment of the stream was calculated. From these, the cumulative discharge with cross-stream distance was calculated at each transect. Next, the flow distribution curves (q_c versus z and η versus z) were constructed. Using these curves, the variations of u, h, and c with η at all the transects were obtained. The only other piece of information required for the solution of Eq. 7 is the variation of m_x with η at each transect.

Values for the metric coefficient m_x were obtained graphically. The metric coefficient m_x is equal to the ratio between distances measured along the longitudinal coordinate lines and those measured along the x-axis. Therefore,

TABLE 1.—Hydraulic Data

Transect number (1)	Distance from source, in meters (2)	Channel width, W, in meters (3)	Average depth, H, in meters (4)	Mean velocity, U, in meters per second (5)	Mean shear velocity, U_*, in meters per second (6)
1	213	49.3	0.47	0.46	0.067
2	463	60.0	0.57	0.29	0.074
3	713	60.0	0.42	0.42	0.063
4	963	55.7	0.28	0.70	0.052
5	1213	57.0	0.65	0.29	0.079
6	1463	79.5	0.55	0.23	0.072

by definition, $m_x = 1.0$ along the x-axis (right bank). For convenience, the longitudinal coordinate lines were chosen to coincide with lines of constant η. On a 1:1,200 map of the river reach, the points of constant η were marked at intervals of 0.1 along every transect. Curves of constant η were drawn through these points. Distances were then measured along all the lines of constant η and the ratios with distances along the x-axis were computed. In this manner, the variation of m_x with η at each transect was obtained.

The dye flux at each transect was calculated and compared with the dye flux at the injection point. For the first five transects, the dye recovery ratio varied from 97%–86%. For the last transect, the recovery ratio dropped to 77%. No apparent reason for this change can be found. The dye concentration readings were normalized by dividing by the recovery ratio so that the flux at each transect was equal to the input flux.

Eq. 7 was solved with the numerical scheme described previously, using the c-η curve obtained for the first transect downstream of the discharge as the initial condition. Concentration versus η distributions for the downstream

transects were then obtained by simulation. These were converted to concentration versus tranverse distance plots using the η-z curves and were compared with the measured concentration distributions.

The factor of diffusion D_z in Eq. 7 is the product of two terms: e_z and (uh^2m_x). The term e_z is the transverse mixing coefficient which accounts for the turbulent diffusive transport as well as the transport caused by differential advection. The term (uh^2m_x) accounts for the local variations in velocity, depth, and curvature. Different assumptions or approximations can be used for both of these terms. The term e_z can be assumed to be constant for the whole reach or can be allowed to vary from transect to transect. One can use local values of (uh^2m_x) at every point or use an average for the transect or an average value for the whole reach. In solving Eq. 7, these approximations were tried so that their effects on the simulated results could be compared. The different forms of D_z which were used are listed in the following:

1. $D_z = (uh^2m_x)\bar{e}_z(x)$—local values for (uh^2m_x). The term e_z is assumed to be constant for a transect but is allowed to vary with each transect and D_z varies with x and z.
2. $D_z = (uh^2m_x)\bar{\bar{e}}_z$—local values for (uh^2m_x). The term e_z is assumed to be a constant, $\bar{\bar{e}}_z$, for the whole reach and D_z varies as the variation in (uh^2m_x).
3. $D_z = \overline{(uh^2m_x)}\bar{e}_z$—Cross-sectional average of (uh^2m_x) is used. The term e_z is constant for the reach and D_z is constant for a transect but varies for different transects.
4. $D_z = \overline{(uh^2m_x)}\bar{\bar{e}}_z$—Averages for the whole reach are used for both (uh^2m_x) and e_z. The term D_z is constant throughout.
5. $D_z = (uh^2m_x)(\alpha U_* h)$—The term e_z is assumed to vary across the stream as the product of the local depth and the mean shear velocity U_*. Local values for (uh^2m_x) are used.

Simulations were carried out for all five cases listed in the foregoing. In case 1, in which $D_z = (uh^2m_x)\bar{e}_z$, different values for $\bar{e}_z$ were tried to find the value which gave the best match between simulated and measured concentrations at the first transect to be simulated. The solution then proceeded to the next transect when different values for $\bar{e}_z$ were again tried. In this manner, a value for $\bar{e}_z$ was obtained for every transect. The values for $\bar{e}_z$ varied from 0.013 m^2/s–0.006 m^2/s. The simulated concentrations are compared with the measured ones in Fig. 4(*a*). The agreement can be considered to be very good.

In case 2, the transverse dispersion coefficient was assumed to be a constant, $\bar{\bar{e}}_z$, for the whole reach. The value chosen for $\bar{\bar{e}}_z$ was 0.009 m^2/s, which was obtained from averaging the values of $\bar{e}_z$ found in case 1. The simulated concentrations are also shown in Fig. 4(*a*). It can be seen that, except for the first transect which seems to require a larger value for e_z, the agreement between the simulations and the data is very good and is not too different from that for case 1.

In the first two cases, the transverse dispersion coefficient, e_z, remained constant across the stream. Case 5 was used to investigate the effect of allowing e_z to vary across the stream. In this case, e_z was assumed to be equal to $(\alpha U_* h)$, with α being a constant for the whole reach. Different values for

α were tried and the value which gave the closest fit was 0.26. The simulated results, shown in Fig. 4(*a*), are very much the same as those for case 2, in which e_z was assumed to be constant everywhere throughout the reach.

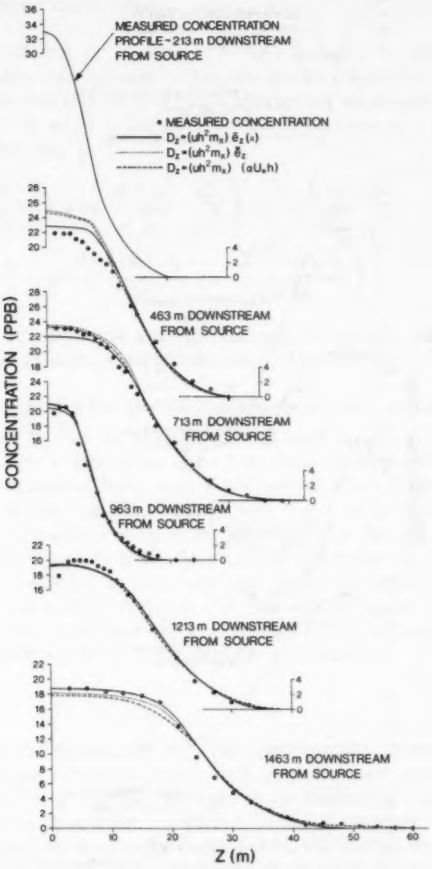

FIG. 4(*a*).—Comparison of Simulated and Measured Dye Concentration Profiles (Case 1, Case 2, and Case 5)

The last two simulations which were tried involved using average values of (uh^2m_x) instead of the local values. In case 3, an average value of (uh^2m_x) was obtained for each transect by plotting the curves of (uh^2m_x) versus η and obtaining the averages graphically. These values were then averaged to obtain

an average value for the reach, $(\overline{uh^2 m_z})$, for use in case 4. The simulated profiles for these two cases, for the sake of clarity, are plotted in Fig. 4(*b*)

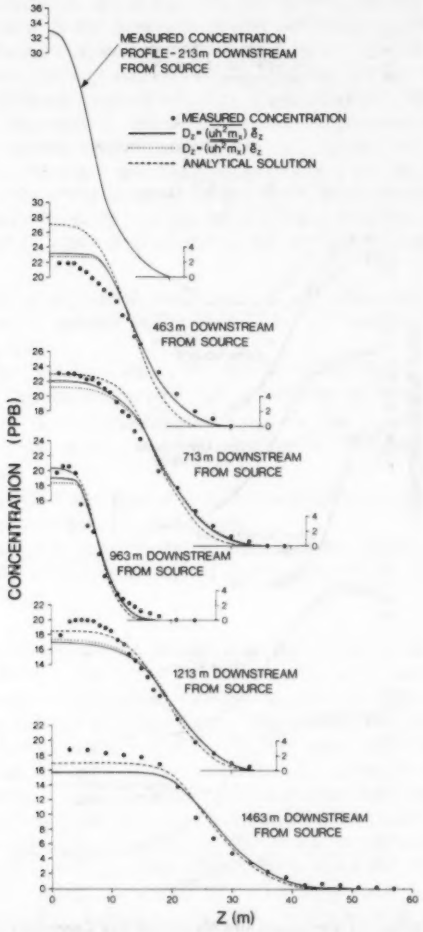

FIG. 4(*b*).—Comparison of Simulated and Measured Dye Concentration Profiles (Case 3, Case 4, and Analytical Solution)

which is a separate but identical plot to Fig. 4(*a*). It can be seen from Fig. 4(*b*) that the resulting profiles from these two simulations are very much the same. Their agreement with the measured profiles can be considered to be

satisfactory, as far as comparison with field data is concerned. However, the agreement is not as good as the three cases shown in Fig. 4(*a*), especially in the last two transects.

Comparison with Analytical Solution

If the diffusion factor D_z is assumed to be a constant for the whole reach, Eq. 7 can be solved analytically. When the tracer enters the stream from a tributary, as with the present case, it is appropriate to assume the boundary conditions at $x = 0$ to be a line source located between $\eta = 0$ and $\eta = w$. A solution for this case is

$$\frac{C}{C_\infty} = \frac{1}{2w}\left[\operatorname{erf}\frac{w-\eta}{\sqrt{2\xi}} + \operatorname{erf}\frac{w+\eta}{\sqrt{2\xi}} + \sum_{n=1}^{\infty}\left(\operatorname{erf}\frac{2n+w-\eta}{\sqrt{2\xi}}\right.\right.$$

$$\left.\left. + \operatorname{erf}\frac{2n+w+\eta}{\sqrt{2\xi}} - \operatorname{erf}\frac{2n-w-\eta}{\sqrt{2\xi}} - \operatorname{erf}\frac{2n-w+\eta}{\sqrt{2\xi}}\right)\right] \quad \ldots\ldots\ldots \quad (16)$$

in which C_∞ = concentration after the tracer is completely mixed across the stream; w = width of source (in η coordinate); and $\xi = 2D_z x/Q^2$, a dimensionless distance.

Concentration profiles for the various transects were calculated using Eq. 16. The value for D_z was the same as the one used in case 4, i.e., $\overline{(uh^2 m_z)}\,\bar{e}_z$ C_∞ = 3.99 ppb and w was taken to be 0.1. These profiles are shown in Fig. 4(*b*) with the simulations from case 3 and case 4. Overall the agreement of the analytical solution with the measured data is just as good as those of case 3 and case 4. It actually gives a better agreement for the last three transects but, at the second transect and the first transect, the errors are quite large.

Basically, the analytical solution and case 4 are the same thing. However, case 4 used the measured profile at the first transect as an initial condition while this condition could not be accommodated by the analytical solution. This is why the two solutions in Fig. 4(*b*) are not identical.

Analysis

The results of the simulations show that the cumulative-discharge model can indeed simulate the transverse mixing in a natural stream quite satisfactorily. The river reach being studied had fairly large transverse velocities at some sections. This is very evident from the fact that between x = 713 m and x = 963 m, the dye plume actually decreased in width from about 42 m–21 m. Even at x = 713 m, the plume was still not as wide as at x = 713 m. All of the cases tested, including the analytical solution, were able to predict the changes in the size of the plume quite well. If one were to use the conventional advective-diffusion equation such as Eq. 4, one would have to measure all the transverse velocities. If these are not taken into account, one can easily obtain negative values for the dispersion coefficient.

From a comparison of all the solutions, it appears that variations of the dispersion coefficient in the downstream direction have a bigger influence on the accuracy of the simulations than the possible variations across the stream.

The best results were obtained using local values of (uh^2m_x) together with a transverse dispersion coefficient $\bar{e}_z$ which was constant for a transect but could vary with each transect. However, allowing e_z to vary across the stream as the local depth did not produce results which were any better than when an average value was used for the whole reach.

When average values (transect average or reach average) of (uh^2m_x) were used instead of their local values, the simulation results were definitely less accurate, especially at the transects furthest downstream. Thus, it appears that, for accurate simulations, one must incorporate the local variations in u, h, and m_x. This conclusion is different from that of Yotsukura and Cobb (12) who performed numerical experiments using a constant value as well as varying distributions for (uh^2e_z) and found little difference in the results. A possible cause of this discrepancy is that the distributions of (uh^2e_z) used by Yotsukura and Cobb were symmetrical about $\eta = 0.5$, being maximum in the middle and zero at the edges. The line source was located near the middle and the concentration distribution was also nearly symmetrical. Therefore, the lowest and highest of (uh^2e_z) occurred either where the concentration was very small or where the concentration gradient was very small and thus their effects on flux of concentration were very small. Where the concentration gradient was large, the (uh^2e_z) distribution had a value close to the average. Under those situations, it was possible that a varying (uh^2e_z) distribution would give much the same results as a constant value for (uh^2e_z). However, in the present study with the source at the bank, the area of high concentration gradient occurs mainly where the value of (uh^2m_x) is lower than the average and the results are seen to be significantly different.

The analytical solution using a constant diffusion factor D_z produced results which were just as good as the numerical simulations using average values of (uh^2m_x), except very close to the source. This is another advantage of the cumulative-discharge model—it allows one to use an analytical solution to obtain reasonable predictions even for natural streams.

Thus, for accurate simulations of the transverse mixing in natural streams, one should use local values of (uh^2m_x) together with an average transverse dispersion coefficient $\bar{e}_z$ which can vary in the downstream direction. If one is only interested in the size of the plume and approximate values of the concentrations, the analytical solution of Eq. 7 may be sufficient.

Transverse Dispersion Coefficient for Natural Streams

In order to use a numerical model such as the one described in this paper to predict concentration distributions in a natural stream, it is necessary to know the value of the transverse dispersion coefficient e_z. Of course, if one can perform a dye test, the value of e_z can always be obtained from the dye data. However, this is not always feasible and some method is required for chosing an average e_z for a given reach using only bulk stream variables.

Many measurements of transverse dispersion have been made in laboratory channels. Most of the data had been summarized by the writers (6) who studied the dependence of the dimensionless dispersion coefficient on the bulk hydraulic variables. It was shown that the dimensionless dispersion coefficient, E_z, was a function of two variables: the friction factor f and the aspect ratio W/H.

TABLE 2.—Summary of Field Data for Transverse Dispersion Coefficient

Data source (1)	Width, W, in meters (2)	W/H (3)	Average velocity, U, in meters per second (4)	Shear velocity, U_*, in meters per second (5)	Friction factor, f (6)	Dispersion coefficient, e_z, in meters squared per second (7)	e_z/U_*W (8)	e_z/U_*H (9)	Sinuosity S (10)
Yotsukura and Cobb (12) Missouri River near Blair	183.0	66.7	1.74	0.073	0.014	0.101	7.5×10^{-3}	0.50	1.1
Yotsukura and Cobb (12) South River	18.3	46.2	0.18	0.040	0.220	0.0046	6.3×10^{-3}	0.29	1.0[a]
Yotsukura and Cobb (12) Aristo Feeder Canal	18.3	27.3	0.67	0.062	0.069	0.0093	8.2×10^{-3}	0.22	1.0[a]
Yotsukura and Cobb (12) Bernado Conveyance Channel	20.1	28.7	1.25	0.061	0.020	0.013	10.6×10^{-3}	0.30	1.0[a]
Beltaos (1), Athabasca below Fort McMurray	373.0	170.0	0.95	0.056	0.028	0.092	4.4×10^{-3}	0.75	1.0[a]
Beltaos (1), Athabasca River below Athabasca	320.0	156.0	0.86	0.079	0.067	0.066	2.6×10^{-3}	0.41	1.2
Beltaos (1), North Saskatchewan River below Edmonton	213.0	137.0	0.58	0.080	0.152	0.031	1.8×10^{-3}	0.25	1.0[a]
Beltaos (1), Bow River at Calgary	104.0	104.0	1.05	0.139	0.143	0.085	5.9×10^{-3}	0.61	1.1
Beltaos (1), Beaver River near Cold Lake	42.7	44.6	0.50	0.044	0.062	0.042	22.4×10^{-3}	1.00	1.3
Sayre and Yeh (9) Missouri River below Cooper Generation Station	234.0	59.1	1.98	0.085	0.015	1.110	55.8×10^{-3}	3.30	2.1
Lau and Krishanppan (6) Grand River below Kitchener	59.2	117.0	0.35	0.069	0.314	0.009	2.2×10^{-3}	0.26	1.1

[a]Approximate values, channels are either straight or have very small curvatures.

W is the channel width and H is the average depth. The coefficient E_z can take several different forms, such as e_z/U_*W, e_z/UW, or e_z/U_*H. It was found that the data could be best correlated when e_z/U_*W was plotted against W/H. The effect of f was small and all the data collapsed on one curve. However, this curve is not too useful for selecting values of e_z for natural streams because most of the laboratory data were for W/H less than 30 while for natural streams the W/H values are generally much higher.

It was decided to investigate if the same type of dependence could be found for field data of e_z. In reviewing the published values of e_z for natural streams, only those in which the effects of depth-averaged transverse advection, v, had been separated from e_z were considered. It is quite clear that, for natural streams, e_z values which are obtained without accounting for such net transverse advection

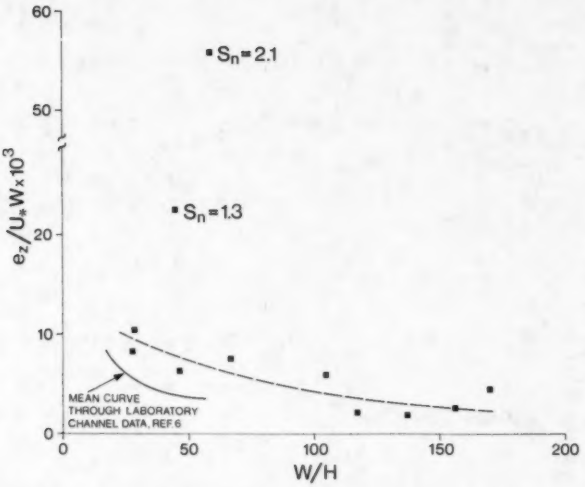

FIG. 5.—Variation of e_z/U_*W with W/H

are very unreliable. The narrowing of the dye plume in the present test is evidence to that fact. Therefore, the data which are summarized in Table 2 are the ones which have been derived from either the generalized change-of-moment method (5) or some kind of stream-tube model similar to the one presented here. Only 11 data points were found, including the one from the present study. The various forms of E_z are calculated and are shown in Table 2 with other pertinent data.

In Fig. 5, e_z/U_*W is plotted against W/H. The mean curve through the laboratory channel data summarized by the writers is also shown. It can be seen that, with the exception of two points, the field data are distributed about a curve somewhat above the laboratory data. There is apparently little dependence on f, which varies from 0.015–0.375, and the scatter of the data is reasonably small. However, the two points which do not conform with the rest have values

which are three times and nine times as large as those given by the mean curve. Some explanation of this behavior is required.

In straight laboratory channels, e_z represents the diffusive transport due to turbulence as well as the dispersion resulting from differential advective transport due to secondary currents which are driven by the variations in bed shear across the channel. In natural streams, e_z also has to account for the dispersive transport due to the secondary circulations which are caused by the stream curvature. As natural streams inevitably have some degree of curvature, it is reasonable to expect that the transverse dispersion due to differential advection for natural streams will be higher, and the values of e_z/U_*W will be somewhat larger than in straight laboratory channels. Thus, it is quite possible that E_z is not governed by f and W/H alone but that an additional variable characterizing the curvature of the particular river reach is required. It is difficult to say what is the best variable to use. For a wide stream rounding a long bend in which the centrifugal force driving the secondary circulation can be assumed to be in equilibrium with the pressure forces and turbulent shear stresses, the radial velocity component can be shown to be inversely proportional to the radius of curvature of the bend. One may thus be tempted to use the radius of curvature as the additional variable. However, river bends are generally not long enough or regular enough for the equilibrium conditions to be established. A more important factor is that a river reach would often consist of straight stretches together with bends of different radii of curvature. Therefore the radius of curvature does not seem to be a practical variable to characterize a stretch of a natural stream. One possible variable which is relatively easy to obtain is the sinuosity which can be defined as the ratio between the thalweg length and the down valley distance (7). Using the symbol S_n to denote sinuosity, the equation for E_z may be written as

$$E_z = \phi\left(f, \frac{W}{H}, S_n\right) \quad \ldots\ldots\ldots\ldots\ldots\ldots\ldots\ldots\ldots\ldots\ldots\ldots \quad (17)$$

The values of the sinuosity are also listed in Table 2. Because of lack of complete information, the values for the Aristo Feeder Canal and the Bernardo Conveyance Channel are listed as 1.0. However, even though these channels have straight sides, the thalwegs are not necessarily straight and for the Aristo Feeder Canal it has been reported as meandering from side to side (4). Thus, it is likely that their values of sinuosity are slightly larger than 1.0. The same holds true for the South River. The values of S_n for the Missouri River near Blair and the Missouri River near Cooper Nuclear Station (9) are calculated using measurements from a map. Because the cross sections are not known, the channel length is taken to be the thalweg length. Therefore, the actual S_n values may be slightly higher.

Inspection of the values of sinuosity shows that the two points in Fig. 5 which do not conform to the mean curve indeed have the largest values of sinuosity. The one with the largest e_z/U_*W has the largest sinuosity of 2.1. The other one has S_n equal to 1.3. All the other points which are distributed about the mean curve have sinuosity $\approx$1.0 or 1.1. One point has a value of 1.2. Although this evidence cannot be regarded as conclusive, this is a good indication that some variable which characterizes the stream curvature, such

as the sinuosity, is important in determining the value of E_z in natural streams. More field data are required, especially for streams with large values of sinuosity, before any more conclusions can be made. There are some published data obtained from sinuous laboratory channels but these have very small W/H ratios (mostly <10) and would not be very useful for natural streams.

A commonly used form of E_z is e_z/U_*H. This form is plotted in Fig. 6 against W/H. There is no discernable dependence on f or W/H. The data can be considered to be distributed about $e_z/U_*H \approx 0.5$, although the scatter is larger than the curve for e_z/U_*W. Again the same two points with the high values of sinuosity do not conform with the other points.

There is, at present, no method for predicting the values of e_z for natural streams. Therefore, for streams which are relatively free of large bends or

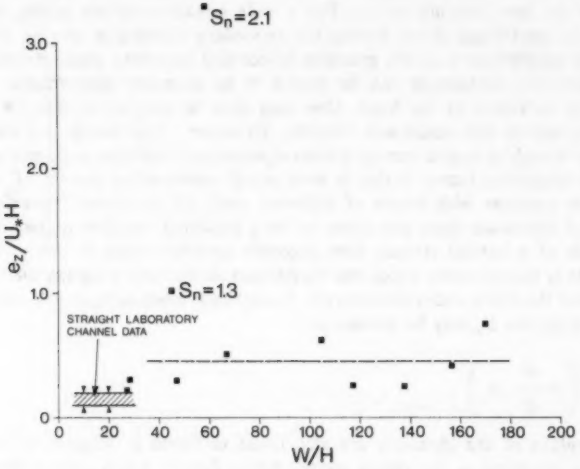

FIG. 6.—Variation of e_z/U_*H with W/H

other structures such as groins which can increase the mixing, the mean curve in Fig. 5 should give a good estimate of e_z.

Summary and Conclusions

A numerical model of the transverse mixing of a neutrally buoyant solute in natural channels has been presented. The model equation is based on the stream-tube or cumulative discharge concept presented by Yotsukura and Sayre (13) and can account for changes in river geometry and curvature quite easily. The validity of this model for use in natural streams has been verified using data from a field test. Simulations of the dye concentration at various transects downstream from the source were carried out, using different assumptions for the factor of diffusion. The simulations all reproduced the narrowing and widening

of the concentration profiles very well. For accurate simulation of the profiles, it is best to use local values of the velocity, depth, and metric coefficient together with a transverse dispersion coefficient which can vary in the downstream direction. However, even an analytical solution of the model equation can give a good approximate estimate of how the concentration profiles will change along the reach.

Published data of the transverse dispersion coefficient for natural streams have been summarized. For these data points, the effects of depth-averaged transverse advection have been accounted for and are not lumped with the dispersion coefficient. The dimensionless dispersion coefficient e_z/U_*W appears to depend primarily on the width-depth ratio W/H and does not seem to be governed by the friction factor. All the data points except two seem to fall reasonably well on one curve. It is suggested that another variable which describes the stream curvature, such as the sinuosity, also governs the dimensionless dispersion coefficient and is responsible for the two points not falling near the curve.

For streams which have small curvatures, the curve presented in Fig. 5 can be used to obtain a reasonable estimate of the transverse dispersion coefficient.

Appendix I.—References

1. Beltaos, S., "Mixing Processes in Natural Streams," *Proceedings of the Transport Processes and River Modelling Workshop*, National Water Research Institute, Burlington, Ontario, Canada, 1978.
2. Chang, Y. C., "Lateral Mixing in Meandering Channels," thesis presented to the University of Iowa, at Iowa City, Iowa, in 1971, in partial fulfillment of the requirements for the degree of Doctor of Philosophy.
3. Fischer, H. B., "Longitudinal Dispersion in Laboratory and Natural Streams," *Report No. KH-R-12*, W. M. Keck Laboratory of Hydraulics and Water Resources, California Institute of Technology, Pasadena, Calif., 1966.
4. Fischer, H. B., "Transverse Mixing in a Sand-Bed Channel," *United States Geological Survey Professional Paper 575-D*, 1967, pp. 267–272.
5. Holley, E. R., Siemons, J., and Abraham, G., "Some Aspects of Analyzing Transverse Dispersion in Rivers," *Journal of Hydraulic Research*, Vol. 10, No. 1, 1972, pp. 27–57.
6. Lau, Y. L., and Krishnappan, B. G., "Transverse Dispersion in Rectangular Channels," *Journal of the Hydraulics Division*, ASCE, Vol. 103, No. HY10, Proc. Paper 13294, Oct., 1977, pp. 1173–1189.
7. Leopold, L. B., Wolman, M. G., and Miller, J. P., *Fluvial Processes in Geomorphology*, 1st ed., W. H. Freeman and Company, San Francisco, Calif., 1964.
8. Sayre, W. W., and Chang, F. M., "A Laboratory Investigation of Open-Channel Dispersion Processes for Dissolved, Suspended and Floating Dispersants," *United States Geological Survey Professional Paper 433E*, 1968.
9. Sayre, W. W., and Yeh, T. P., "Transverse Mixing Characteristics of the Missouri River Downstream from the Cooper Nuclear Station," *IIHR Report 145*, Iowa Institute of Hydraulics Research, University of Iowa, Iowa City, Iowa, 1975.
10. Smith, G. D., "Numerical Solution of Partial Differential Equations," Oxford University Press, Oxford, England, 1965, pp. 20–22.
11. Stone, H. L., and Brain, P. L. T., "Numerical Solution of Convective Transport Problems," *American Institute of Chemical Engineering Journal*, Vol. 9, 1963, pp. 681–688.
12. Yotsukura, N., and Cobb, E. D., "Transverse Diffusion of Solutes in Natural Streams," *United States Geological Survey Professional Paper 582-C*, 1972.
13. Yotsukura, N., and Sayre, W. W., "Transverse Mixing in Natural Channels," *Water Resources Research*, Vol. 12, No. 4, Aug., 1976, pp. 695–704.

Appendix II.—Notation

The following symbols are used in this paper:

a, b = weighting coefficients;
c = depth-averaged concentration;
c_m = fully mixed concentration;
D_z = factor of diffusion;
d = weighting coefficient;
E_z = dimensionless transverse dispersion coefficient;
e_x, e_z = turbulent dispersion coefficient in x and z directions;
$\bar{e}_z$ = cross-sectional average value of e_z;
$\bar{\bar{e}}_z$ = reach-average value of e_z;
f = friction factor;
g = weighting coefficient;
H = average flow depth;
h = local flow depth;
m = weighting coefficient;
m_x, m_z = metric coefficients;
Q = total discharge;
q_c = cumulative discharge;
S_n = sinuosity;
t = time;
U_* = mean shear velocity;
u, v = depth-averaged velocities in x, z directions;
W = width of channel;
w = width of line source;
x = longitudinal coordinate;
z = transverse coordinate;
α = constant;
ϵ = weighting coefficient;
η = dimensionless cumulative discharge;
θ = weighting coefficient;
ξ = dimensionless longitudinal distance; and
ϕ = function.

JOURNAL OF THE HYDRAULICS DIVISION

OVERLAND FLOW FROM TIME-DISTRIBUTED RAINFALL

By Allen T. Hjelmfelt, Jr.,[1] M. ASCE

INTRODUCTION

The study of hydrology of small agricultural and urban watersheds has progressed along different lines than that for medium to large size watersheds. The approach has been a more physically based analysis of infiltration, overland flow, and channel routing. Current techniques for flow analysis are often based on kinematic wave theory, whereas formerly, they were based on the overland flow equation derived by Horton (6). Horton's equation might be considered a quasiunsteady analysis because, although he used the same basic equations as those for kinematic wave theory, he assumed that the water surface profile was always geometrically similar to the equilibrium profile.

Detailed design procedures for small basins have been developed using both analytical methods. Hicks (5) and Hathaway (4) based their work on the Horton equation. Kinematic wave procedures have been described by Overton and Tsay (12) and by Chen and Evans (1). These approaches use rainfall-intensity-frequency distributions to establish the rainfall input. The average intensity for the time-of-concentration is used as rainfall of constant intensity with the Horton or the kinematic wave flow equations. Using this approach, the rainfall intensity decreases as time-of-concentration increases; thus, a correct time is necessary. Hathaway (4) showed how rainfall duration influences peak discharge. Time-of-concentration depends on watershed characteristics, but also varies with rainfall intensity which in turn varies with time, so time-of-concentration is determined by trial and error. Ragan and Duru (13) presented a nomograph to aid in solving the kinematic wave relation. Kerby (8) empirically obtained an equation based on results computed by Hathaway that is apparently appropriate for a particular rainfall frequency.

[1]Hydr. Engr., United States Dept. of Agric., Science and Education Administration, Agric. Research North Central Region, Watershed Research Unit, 207 Business Loop 70 East, Columbia, Mo. 65201.

Note.—Discussion open until July 1, 1981. To extend the closing date one month, a written request must be filed with the Manager of Technical and Professional Publications, ASCE. Manuscript was submitted for review for possible publication on November 14, 1979. This paper is part of the Journal of the Hydraulics Division, Proceedings of the American Society of Civil Engineers, ©ASCE, Vol. 107, No. HY2, February, 1981.

These previous efforts have used rainfall of constant intensity to estimate the overland flow hydrograph. Because constant intensity rainfall is unlikely, it is of interest to determine the influence of time distribution of rainfall on the hydrograph of overland flow. The kinematic wave equations for turbulent flow across a plane, impermeable surface are solved using a time-varying rainfall appropriate for thunderstorms. Peak discharge is shown to be a function of surface length, total precipitation, storm duration, and the time to equilibrium for an equivalent rainfall of constant intensity.

Flow Equations

The flow per unit width across an impermeable plane surface is described by the continuity equation

$$\frac{\partial h}{\partial t} + \frac{\partial q}{\partial x} = i \quad \ldots \ldots \ldots

the solution to which may be determined using the variable τ such that, by the chain rule of differentiation,

$$\frac{dh}{d\tau} = \frac{\partial h}{\partial t}\frac{dt}{d\tau} + \frac{\partial h}{\partial x}\frac{\partial x}{\partial \tau} = i \quad \ldots\ldots\ldots\ldots\ldots\ldots\ldots\ldots\ldots\ldots (6)$$

Eqs. 5 and 6 are identical if

$$\frac{dt}{d\tau} = 1; \quad \frac{dx}{d\tau} = \frac{3}{2}\alpha h^{1/2} \quad \ldots\ldots\ldots\ldots\ldots\ldots\ldots\ldots\ldots\ldots (7)$$

$$\text{or} \quad t - t_o = \tau - \tau_o \quad \ldots\ldots\ldots\ldots\ldots\ldots\ldots\ldots\ldots\ldots (8)$$

$$\text{and} \quad x - x_o = \frac{3}{2}\alpha \int_{\tau_o}^{\tau} h^{1/2}\, d\tau \quad \ldots\ldots\ldots\ldots\ldots\ldots\ldots\ldots\ldots\ldots (9)$$

Eq. 6 yields the relation of the depth of flow, h, to rainfall intensity, i, along a coordinate τ. The coordinate τ is related to the physical time and space coordinates through Eqs. 8 and 9. To solve Eqs. 6, 8, and 9 an expression must be established for rainfall intensity.

Thunderstorm Rainfall

As a result of extensive studies of thunderstorms, the United States Weather Bureau (14) published average time distributions for rainfall within 1-h, high-in-

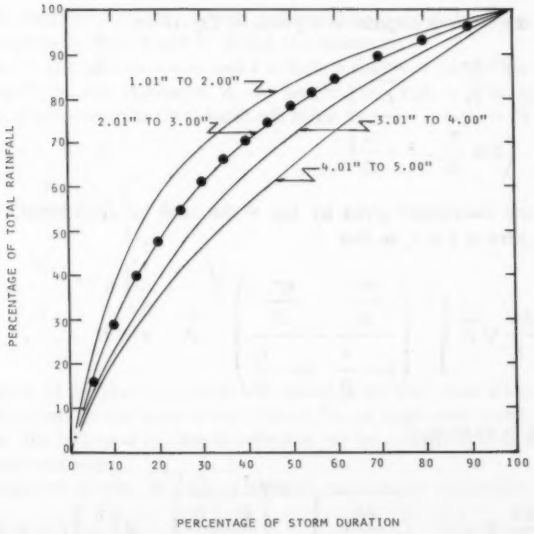

FIG. 1.—Time Distribution of Rainfall in 1-h Storms [Points Determined Using Eq. 10 with $a = 1.37$ and $b = 0.37$; Curves from United States Weather Bureau (14)]

tensity storms (Fig. 1). The relation

$$\frac{P_t}{P} = \frac{\frac{at}{D}}{b + \frac{t}{D}} \quad \ldots\ldots\ldots\ldots\ldots\ldots\ldots\ldots\ldots\ldots\ldots\ldots\ldots\ldots \quad (10)$$

in which P_t = rainfall accumulation at time $t(L)$; P = total rainfall (L); D = storm duration (T); and a, b = constants can be used to describe the curves. The value $a = 1.37$ and $b = 0.37$ fit the 2.01 in./h–3.00 in./h curve quite well, as indicated by the points on Fig. 1. This relationship will be used to describe storms of all short duration.

Solution of Flow and Rainfall Equations

The depth of flow is determined by integration of Eq. 6:

$$h - h_o = \int_{\tau_o}^{\tau} i d\tau \quad \ldots\ldots\ldots\ldots\ldots\ldots\ldots\ldots\ldots\ldots\ldots\ldots\ldots\ldots \quad (11)$$

If t_o and τ_o are made to coincide, the integral is the accumulated precipitation at time, τ, less the accumulated precipitation at time, τ_o, or

$$h - h_o = P_\tau - P_{\tau_o} \quad \ldots\ldots\ldots\ldots\ldots\ldots\ldots\ldots\ldots\ldots\ldots\ldots\ldots\ldots \quad (12)$$

During the storm precipitation is given by Eq. 10 so

$$h - h_o = P\left(\frac{\frac{a\tau}{D}}{b + \frac{\tau}{D}} - \frac{\frac{a\tau_o}{D}}{b + \frac{\tau_o}{D}}\right); \quad \tau < D \quad \ldots\ldots\ldots\ldots\ldots\ldots\ldots \quad (13)$$

The location coordinate given by Eq. 9 can now be determined. The depth of flow is zero at $\tau = \tau_o$ so that

$$x - x_o = \frac{3\alpha}{2}\sqrt{P}\int_{\tau_o}^{\tau}\left(\frac{\frac{a\tau}{D}}{b + \frac{\tau}{D}} - \frac{\frac{a\tau_o}{D}}{b + \frac{\tau_o}{D}}\right)^{1/2} d\tau\,; \quad \tau < D \quad \ldots\ldots\ldots \quad (14)$$

which can be expressed

$$x - x_o = \frac{3\alpha}{2} D\sqrt{P}\sqrt{\frac{ab}{b + \frac{\tau_o}{D}}}\int_{\tau_o/D}^{\tau/D}\left(\frac{\frac{\tau}{D} - \frac{\tau_o}{D}}{\frac{\tau}{D} + b}\right)^{1/2} d\left(\frac{\tau}{D}\right); \quad \tau < D \quad (15)$$

Integration of Eq. 15 results in

$$x - x_o = \frac{3\alpha}{2} D\sqrt{P} \sqrt{\frac{ab}{b + \frac{\tau_o}{D}}} \left[\sqrt{\left(\frac{\tau}{D} - \frac{\tau_o}{D}\right)\left(\frac{\tau}{D} + b\right)} \right.$$

$$\left. - \left(b + \frac{\tau_o}{D}\right) \log \left(\sqrt{\frac{\tau}{D} + b} + \sqrt{\frac{\tau}{D} - \frac{\tau_o}{D}} \right) \right]_{\tau_o/D}^{\tau/D}; \quad \tau < D \quad \ldots\ldots\ldots \quad (16)$$

Evaluating at the limits and rearranging terms results in

$$x - x_o = \frac{3\alpha}{2} D\sqrt{P} \sqrt{\frac{ab}{b + \frac{\tau_o}{D}}} \left[\sqrt{\left(\frac{\tau}{D} - \frac{\tau_o}{D}\right)\left(\frac{\tau}{D} + b\right)} \right.$$

$$\left. - \left(b + \frac{\tau_o}{D}\right) \log \left(\frac{\sqrt{\frac{\tau}{D} + b} + \sqrt{\frac{\tau}{D} - \frac{\tau_o}{D}}}{\sqrt{\frac{\tau_o}{D} + b}} \right) \right]; \quad \tau < D \quad \ldots\ldots\ldots \quad (17)$$

Eqs. 13 and 2 describe the water surface profile and hydrograph for the space-time coordinates given by Eqs. 8 and 17 during the rainstorm.

When $\tau = D$, the rainfall ceases and i in Eqs. 6 and 11 is zero. This indicates that the depth, h, and discharge, q, no longer vary with τ. The space-time coordinates of this constant flow depth are given by

$$t - t_o = \tau - \tau_o; \quad \tau < D \quad \ldots\ldots\ldots\ldots\ldots\ldots\ldots\ldots\ldots\ldots \quad (18)$$

and $$x - x_o = \frac{3\alpha}{2} h^{1/2} \int_{\tau_o}^{\tau} d\tau; \quad \tau > D$$

or $$x - x_o = \frac{3\alpha}{2} h^{1/2} D \left(\frac{\tau}{D} - \frac{\tau_o}{D}\right); \quad \tau > D \quad \ldots\ldots\ldots\ldots\ldots \quad (19)$$

Results

Examination of the results is more convenient if the equations are nondimensionalized in terms of the time to equilibrium for an equivalent steady rainfall. In this form, the influence of time distribution can be compared with a constant intensity approximation.

A total amount of rain, P, falls in time, D, so that the equivalent intensity is

$$i_{equiv} = \frac{P}{D} \quad \ldots\ldots\ldots\ldots\ldots\ldots\ldots\ldots\ldots\ldots\ldots\ldots\ldots\ldots \quad (20)$$

The time to equilibrium for this steady rainfall is [see, e.g., Eagleson (2) or Overton and Meadows (11)]

$$t_e = \frac{L^{2/3}}{\left(\frac{P}{D}\right)^{1/3} \alpha^{2/3}} \quad \ldots\ldots\ldots\ldots\ldots\ldots\ldots\ldots\ldots\ldots\ldots\ldots\ldots\ldots\ldots\ldots (21)$$

in which L = the length of the plane. The kinematic approximation for the momentum equation (Eq. 2) can be divided by LP/D to obtain

$$\frac{q}{\frac{LP}{D}} = \alpha \frac{\sqrt{P}\, D}{L} \left(\frac{h}{P}\right)^{3/2} = \left(\frac{\alpha^{2/3} P^{1/3}}{D^{1/3} L^{2/3}}\right)^{3/2} D^{3/2} \left(\frac{h}{P}\right)^{3/2} \quad \ldots\ldots\ldots\ldots (22)$$

or using the relation for t_e, Eq. 21, this becomes

$$\frac{q}{\frac{LP}{D}} = \left(\frac{D}{t_e} \frac{h}{P}\right)^{3/2} \quad \ldots\ldots\ldots\ldots\ldots\ldots\ldots\ldots\ldots\ldots\ldots\ldots\ldots\ldots\ldots\ldots (23)$$

The quantity q/L, sometimes called the runoff intensity, is the flow rate divided by the watershed area. The quantity, P/D, is the equilibrium runoff intensity for rainfall of constant intensity.

The time coordinate is given by

$$\frac{t}{D} - \frac{t_o}{D} = \frac{\tau}{D} - \frac{\tau_o}{D} \quad \ldots\ldots\ldots\ldots\ldots\ldots\ldots\ldots\ldots\ldots\ldots\ldots\ldots\ldots\ldots\ldots (24)$$

and the space coordinate by

$$\frac{x - x_o}{L} = \frac{3}{2} \left(\frac{\alpha^{2/3} D P^{1/3}}{D^{1/3} L^{2/3}}\right)^{3/2} \sqrt{\frac{ab}{b + \frac{\tau_o}{D}}} \left[\sqrt{\left(\frac{\tau}{D} - \frac{\tau_o}{D}\right)\left(\frac{\tau}{D} + b\right)} \right.$$

$$\left. - \left(b + \frac{\tau_o}{D}\right) \log \left(\frac{\sqrt{\frac{\tau}{D} + b} + \sqrt{\frac{\tau}{D} - \frac{\tau_o}{D}}}{\sqrt{\frac{\tau_o}{D} + b}} \right) \right] ; \quad \frac{\tau}{D} < 1$$

$$\text{or} \quad \frac{x - x_o}{L} = \frac{3}{2} \left(\frac{D}{t_e}\right)^{3/2} \sqrt{\frac{ab}{b + \frac{\tau_o}{D}}} \left[\sqrt{\left(\frac{\tau}{D} + b\right)\left(\frac{\tau}{D} - \frac{\tau_o}{D}\right)} \right.$$

$$-\left(b+\frac{\tau_o}{D}\right)\log\left(\frac{\sqrt{\frac{\tau}{D}+b}+\sqrt{\frac{\tau}{D}-\frac{\tau_o}{D}}}{\sqrt{\frac{\tau_o}{D}+b}}\right)\Bigg]\;;\quad \frac{\tau}{D}<1 \quad\ldots\ldots\ldots\ldots\quad (25)$$

during the rainstorm. After rainfall stops, the space coordinate is given by

$$\frac{x-x_o}{L}=\frac{3}{2}\left(\frac{D}{t_e}\right)^{3/2}\sqrt{\frac{h}{P}}\left(\frac{\tau}{D}-\frac{\tau_o}{D}\right);\quad \frac{\tau}{D}>1 \quad\ldots\ldots\ldots\ldots\quad (26)$$

This form uses the storm duration for the time scale factor, the watershed length, L, for the length scale factor, total precipitation as a fluid length scale factor, and the time to equilibrium for the equivalent uniform rainfall to represent the physical characteristics of the watershed.

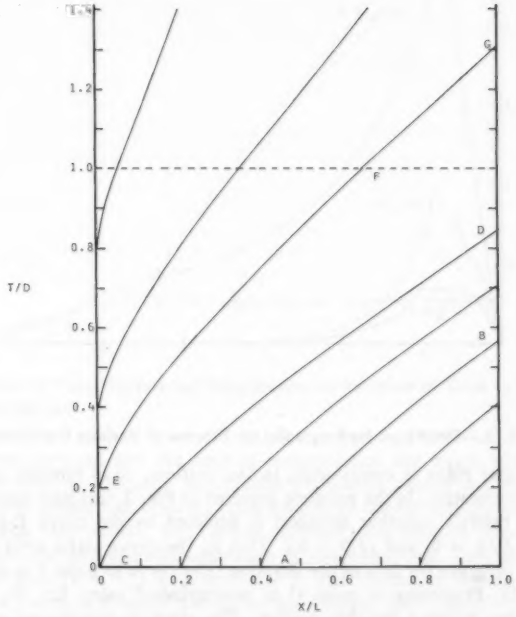

FIG. 2.—Relation between X/L and t/D for $D/t_e = 1$

The outfall hydrograph is determined using the preceding equations in the following manner. A location near the outfall with location x_o is selected. At the start of rainfall, the time t_o, and thus τ_o, is zero. The point indicated by A in Fig. 2 is an example. Values of time, τ, are selected and X/L is

determined, using Eq. 25, until the end of the plane, $X/L = 1$, is reached (unless rainfall stops before this is achieved). This is indicated as point B on Fig. 2. The time associated with point B is used to determine the stage using the nondimensional form of Eq. 13, which is

$$\frac{h - h_o}{P} = \frac{\dfrac{a\tau}{D}}{b + \dfrac{\tau}{D}} - \frac{\dfrac{a\tau_o}{D}}{b + \dfrac{\tau_o}{D}}; \quad \tau < D \ldots\ldots\ldots\ldots\ldots\ldots\ldots\ldots (27)$$

and the nondimensional discharge, $q/(LP/D)$, is determined using Eq. 23. Of particular interest is the curve on Fig. 2 that starts at $X/L = \tau/D = 0$, i.e., curve C-D. The time at which this curve reaches $X/L = 1$ is the time at

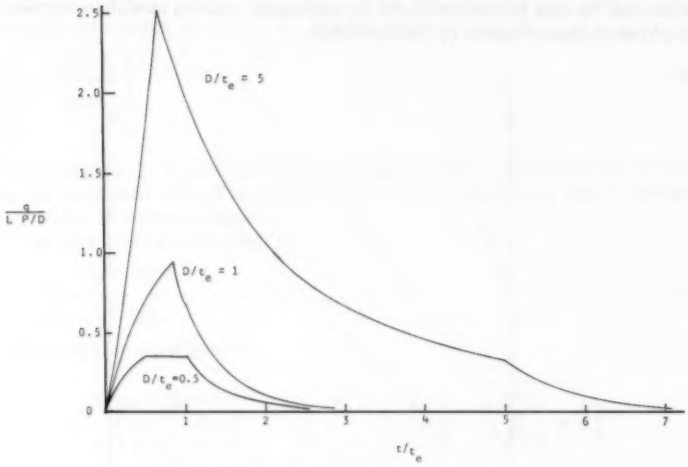

FIG. 3.—Discharge Hydrographs for Storms of Various Durations

which the total plane is contributing to the outflow, so is termed, herein, the time-of-concentration. In the example depicted in Fig. 2, this time occurs before the end of rainfall. Another situation is depicted by the curve E-F-G which starts with $X/L = 0$, and $\tau/D = 0.2$. That is, the curve starts after the storm has been in progress for 20% of the duration. The curve to point F is determined using Eq. 25. Projecting to point G is accomplished using Eq. 26, however, as rainfall has stopped for this portion. The stage is determined at point G using Eq. 27 and the discharge using Eq. 23.

Rainstorms that stop before the time-of-concentration is achieved, have flat peaks. This results because the curve starting $X/L = \tau/D = 0$ will intersect the $\tau/D = 1$ line before reaching $X/L = 1$. Considering the water surface profile at $\tau/D = 1$, indicates that the depth of flow to the right of the C-D equivalent is constant, thus, the flat peak.

Discharge hydrographs at the outfall of the plane are shown in Fig. 3. Storms of long duration are depicted by the hydrograph for $D/t_e = 5$. The total watershed is contributing before the end of the storm. The peak occurs at the time-of-concentration. The hydrograph then recedes, due to the diminution of rainfall intensity. At the end of rainfall, $D/t_e = 5$, a second recession limb appears as detention storage forms the sole source of runoff.

Storms of short duration are indicated, in Fig. 3, by $D/t_e = 0.5$. In this case, the storm ends before the total watershed is contributing to the discharge. The peak is the discharge at the end of the storm. The hydrograph remains at that discharge until the water that started at $x = 0$, $t = 0$ leaves the plane, after which the falling limb appears.

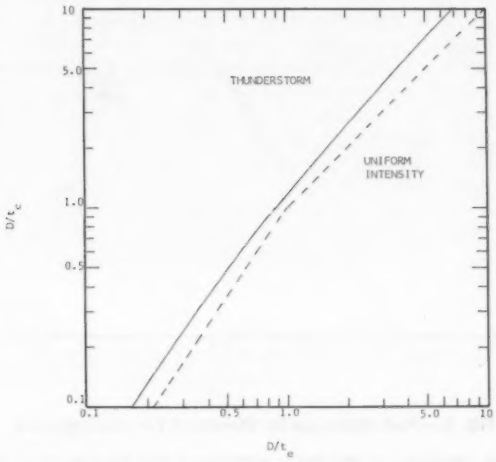

FIG. 4.—Time for Total Watershed Contribution as Function of Time to Equilibrium for Uniform Rainfall

The storm duration and the time-of-concentration are equal when D/t_e is about 0.87. That is, the time distribution of rainfall causes the watershed to respond more rapidly than does the same amount of rainfall distributed uniformly over the same time period. The time-of-concentration depends upon the storm duration and the physical characteristics of the watershed. This time is given by Eq. 25 with $(x - x_o) = L$ and $\tau_o = 0$, the results of which are shown in Fig. 4. An explicit solution cannot be determined. The time-of-concentration for thunderstorm rainfall is always less than for rainfall of constant intensity. This results from the high rainfall intensity early in the thunderstorm coupled with the nonlinear flow relation.

The peak discharge varies with D/t_e, as shown in Fig. 5. The time distribution of rainfall has no influence on the peak discharge if the rainfall duration is less than the time-of-concentration. For the range of time, $0.87 \leq D/t_e \leq 1.08$, the uniform rainfall leads to a peak greater than the thunderstorm distribution.

This results because the slower time for total watershed contribution with uniform rainfall allows more water to accumulate. Storms of longer duration, however, yield higher peaks when distributed according to the thunderstorm pattern. This

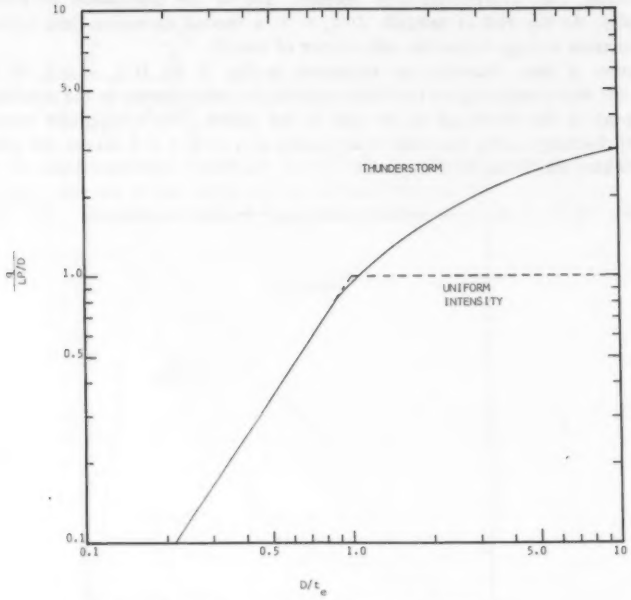

FIG. 5.—Peak Discharge for Storms of Various Durations

is because the intensity of the early portion of the thunderstorm distribution is greater than that used for the equivalent uniform rainfall. The peak discharge is determined only by this early portion.

Application

The object of this effort was to evaluate the influence of time distribution of rainfall on estimates of peak discharge. Although this can be inferred from Fig. 5, an example is helpful.

Consider a watershed with a length of 500 ft (152.4 m). The parameter $\alpha = C\sqrt{S}$ is estimated to be 1.78 $ft^{1/2}/sec$ (0.983 $m^{1/2}/s$). This is subjected to 2 in. (5.1 cm) of thunderstorm rainfall in 1 h. The time to equilibrium for this intensity is determined using Eq. 21:

$$t_e = \frac{L^{2/3}}{\left(\frac{P}{D}\right)^{1/3} \alpha^{2/3}} = \frac{(500)^{2/3}}{\left[\frac{\frac{2}{12}}{1\,(3{,}600)}\right]^{1/3} (1.78)^{2/3}} = 1{,}200 \text{ sec.} \quad \ldots\ldots\ldots \quad (28)$$

Thus, $t_e = 20$ min so that $D/t_e = 3$. Using Fig. 5

$$\frac{q_{max}}{\frac{LP}{D}} = 2.05 \quad \ldots \ldots \ldots \ldots \ldots \ldots \ldots \ldots \ldots \ldots \ldots \ldots \ldots \ldots \ldots \ldots \quad (29)$$

$$\text{so} \quad \frac{q_{max}}{L} = 2.05\frac{P}{D} = 2.05\,(2) = 4.10 \text{ in./h } (10.4 \text{ cm/h}) \quad \ldots \ldots \ldots \ldots \quad (30)$$

Conclusion

The object of this study was to determine the influence of time distribution of rainfall on peak discharge. Usual design procedures use rainfall of constant intensity for a duration equal to the time to equilibrium. This analysis indicates that the peak discharge at the design condition will be slightly greater for rainfall of constant intensity than for rainfall with a thunderstorm time distribution. A correct value of the time to equilibrium is essential, however, for estimation of peak discharge. Difficulty in estimating this time parameter limits any value in considering the time distribution of rainfall in design applications.

The constant intensity approximation is valid for rainfall durations approximately equal to the time to equilibrium or less. As the relative duration increases, the approximation becomes less valid. Thus, an erroneous value for time to equilibrium can lead to significant under design.

Acknowledgment

This work is a contribution of the United States Department of Agriculture, Science, and Education Administration.

Appendix I.—References

1. Chen, C.-N., and Evans, R. F., "Application of Kinematic Wave Method to Predict Overland Peak Flows," *Proceedings of the International Symposium on Urban Hydrology, Hydraulics and Sediment Control*, 1977.
2. Eagleson, P. S., *Dynamic Hydrology*, McGraw-Hill Book Co., Inc., New York, N.Y., 1970.
3. Foster, G. R., Huggins, L. F., and Meyer, L. D., "Simulation of Overland Flow on Short Field Plots," *Water Resources Research*, Vol. 4, No. 6, 1968.
4. Hathaway, G. A., "Military Airfields: A Symposium, Design of Drainage Facilities," *Transactions*, ASCE, Vol. 110, Paper No. 2247, 1945, pp. 697–733.
5. Hicks, W. L., "A Method of Computing Urban Runoff," *Transactions*, ASCE, Vol. 109, Paper No. 2230, 1944, pp. 1217–1253.
6. Horton, R. E., "The Interpretation and Application of Runoff Plot Experiments with Reference to Soil Erosion Problems," *Proceedings of the Soil Science Society of America*, Vol. 3, 1938.
7. Izzard, C. F., "Hydraulics of Runoff from Developed Surfaces," *Proceedings of the Highway Research Board*, Vol. 26, 1946.
8. Kerby, W. S., "Time of Concentration for Overland Flow," *Civil Engineering*, Vol. 74, 1959.
9. Morgali, J. R., "Laminar and Turbulent Overland Flow Hydrographs," *Journal of the Hydraulics Division*, ASCE, Vol. 96, No. HY2, Proc. Paper 7069, Feb., 1970, pp. 441–460.

10. Morris, E. M., and Woolhiser, D. A., "Unsteady One-dimensional Flow over a Plane: Partial Equilibrium and Recession Hydrographs," *Water Resources Research*, Vol. 16, No. 2, Apr., 1980.
11. Overton, D. E., and Meadows, M. E., *Stormwater Modeling*, Academic Press, New York, N.Y., 1976.
12. Overton, D. E., and Tsay, C. G., "A Kinematic Method of Urban Peak Runoff Design Using SCS Curve Numbers," *Research Series No. 25*, University of Tennessee, Knoxville, Tenn., 1974.
13. Ragan, R. M., and Duru, J. O., "Kinematic Wave Nomograph for Time of Concentration," *Journal of the Hydraulics Division*, ASCE, Vol. 98, No. HY10, Proc. Paper 9275, Oct., 1972, pp. 1765–1771.
14. "Thunderstorm Rainfall," *Hydrometeorological Report No. 5*, United States Weather Bureau, 1947.
15. Woolhiser, D. A., and Liggett, J. H., "Unsteady, One-Dimensional Flow over a Plane—The Rising Hydrograph," *Water Resources Research*, Vol. 3, No. 3, 1967.

Appendix II.—Notation

The following symbols are used in this paper:

a = rainfall intensity parameter;
b = rainfall intensity parameter;
C = Chezy constant;
D = thunderstorm duration;
F_o = Froude number at outfall with maximum discharge;
H_o = normal depth at outfall with maximum discharge;
h = depth of flow;
h_o = depth at τ_o;
i = rainfall intensity;
i_{equiv} = uniform rainfall intensity needed to yield P units in duration D;
k = kinematic wave number = $SL/(H_o\mathrm{F}_o^2)$;
L = length of plane;
m = parameter in kinematic wave equation;
P = total storm rainfall;
P_t = rainfall accumulated to time t;
q = discharge per unit width;
$q_{\max}$ = peak discharge per unit width;
R = hydraulic radius;
S = land slope;
t = time;
t_e = time to equilibrium;
t_o = origin of characteristic curve;
V = flow velocity;
x = spatial location;
x_o = origin of characteristic curve;
α = parameter in kinematic wave equation = $C\sqrt{S}$;
τ = variable used in integration of kinematic wave equation; and
τ_o = origin of characteristic curve.

JOURNAL OF THE
HYDRAULICS DIVISION

DISCUSSION

Note.—This paper is part of the Journal of the Hydraulics Division, Proceedings of the American Society of Civil Engineers, ©ASCE, Vol. 107, No. HY2, February, 1981. ISSN 0044-796X/81/0002-0241/$01.00.

Discussions

Discussions may be submitted on any Proceedings paper or technical note published in any *Journal* or on any paper presented at any Specialty Conference or other meeting, the *Proceedings* of which have been published by ASCE. Discussion of a paper/technical note is open to anyone who has significant comments or questions regarding the content of the paper/technical note. Discussions are accepted for a period of 4 months following the date of publication of a paper/technical note and they should be sent to the Manager of Technical and Professional Publications, ASCE, 345 East 47th Street, New York, N.Y. 10017. The discussion period may be extended by a written request from a discusser.

The original and three copies of the Discussion should be submitted on 8-1/2-in. (220-mm) by 11-in. (280-mm) white bond paper, typed double-spaced with wide margins. The length of a Discussion is restricted to two *Journal* pages (about four typewritten double-spaced pages of manuscript including figures and tables); the editors will delete matter extraneous to the subject under discussion. If a Discussion is over two pages long it will be returned for shortening. All Discussions will be reviewed by the editors and the Division's or Council's Publications Committees. In some cases, Discussions will be returned to discussers for rewriting, or they may be encouraged to submit a paper or technical note rather than a Discussion.

Standards for Discussions are the same as those for Proceedings Papers. A Discussion is subject to rejection if it contains matter readily found elsewhere, advocates special interests, is carelessly prepared, controverts established fact, is purely speculative, introduces personalities, or is foreign to the purposes of the Society. All Discussions should be written in the third person, and the discusser should use the term "the writer" when referring to himself. The author of the original paper/technical note is referred to as "the author."

Discussions have a specific format. The title of the original paper/technical note appears at the top of the first page with a superscript that corresponds to a footnote indicating the month, year, author(s), and number of the original paper/technical note. The discusser's full name should be indicated below the title (see Discussions herein as an example) together with his ASCE membership grade (if applicable).

The discusser's title, company affiliation, and business address should appear on the first page of the manuscript, along with the *Proceedings* paper number of the original paper/technical note, the date and name of the *Journal* in which it appeared, and the original author's name.

Note that the discusser's identification footnote should follow consecutively from the original paper/technical note. If the paper/technical note under discussion contained footnote numbers 1 and 2, the first Discussion would begin with footnote 3, and subsequent Discussions would continue in sequence.

Figures supplied by the discusser should be designated by letters, starting with A. This also applies separately to tables and references. In referring to a figure, table, or reference that appeared in the original paper/technical note use the same number used in the original.

It is suggested that potential discussers request a copy of the *ASCE Authors' Guide to the Publications of ASCE* for more detailed information on preparation and submission of manuscripts.

Gravel Size Analysis from Photographs[a]

Closure by John Adams[3]

I thank C. J. Posey for his discussion and agree that the method need not be restricted to river bed gravels. For the sizing of the stockpiles: (1) The photograph should be taken normal to the surface of the pile; (2) the surface area photographed needs to be representative of sizes within the pile (note that rocks at the front of a pile are commonly larger than the average); and (3) intermediate *b* axes should be measured from the photographs to reduce the importance of rock shape. These cautionary points should also be considered during other applications of the method.

Stormwater Detention Basin Sizing[b]

Discussion by Stuart G. Walesh,[2] M. ASCE

The author presents a mathematical technique for more effective application of a basic hydrologic method commonly used for sizing detention/retention facilities. The method is sometimes referred to as the modified rational method and various ways of applying it are discussed in Refs. 1, 2, 3, 4, and 5.

The modified rational method and variations on it, such as that presented by the author, are subject to a potentially serious limitation. The method is always used with the implicit or explicit assumption that the period of rainfall averaging used in the method is equal to the duration of storm. The author explicitly makes and states this assumption. In the writer's opinion, this is not a technically correct use of intensity-duration-frequency relationships and, more importantly, may lead to significant underestimates of required stormwater storage.

---

[a]October, 1979, by John Adams (Proc. Paper 14908).

[3]Visiting Fellow, Earth Physics Branch, 1 Observatory Crescent, Ottawa, Canada, K1A 0Y3.

[b]March, 1980, by Kit R. Burton (Proc. Paper 15229).

[2]Mgr.—Water Resources Services, Donohue & Associates, Inc., 600 Larry Court, P.O. Box 256, Waukesha, Wisc. 53187.

Intensity-duration-frequency relationships provide average rainfall intensity for periods of rainfall and not for discrete storms. For example, assume that one enters a 10-yr recurrence interval intensity-duration curve for a time period of 30 min and reads an intensity of 3.0 in./h. This means that once on the average of every 10 yr (or with a 10% probability in any given year) there will be a 30 min period of continuous rainfall during which the average intensity will be 3.0 in./h or more. It does not mean that there will be a 30-min storm with an average intensity of 3.0 in./h or more. Although this 30-min storm is possible, it is very unlikely. The most probable situation is one in which the 30-min period during which rainfall averages 3.0 in./h or more will be immediately preceded and followed by additional rainfall.

The assumption that the rainfall averaging time is equal to the duration of the storm may have serious implications when rational method concepts are used to calculate the required volume of a detention/retention facility. Because the method does not account for rainfall that occurs immediately before and after the rainfall averaging period, it follows that the corresponding volume of rainfall runoff associated with the preceding and subsequent rainfall is not reflected in the calculated storage obtained with this method. Therefore, this method is likely to underestimate the required volume of storage for the specified or intended design recurrence interval.

The extent to which storage volume is likely to be underestimated is not generally known. However, the writer's experience in applying the modified rational method and comparing the results to other sizing methods suggests that a significant underestimation of storage may occur. Therefore, potential users of the modified rational method, and of specific techniques for applying the method such as that presented by the author, are cautioned to carefully evaluate the results obtained with this technique.

Appendix.—References

1. Baker, W. R., "Storm Water Detention Basin Design for Small Drainage Areas," *Public Works*, Mar., 1977.
2. "Information Pamphlet—Detailed Steps for Determining Allowable Release Rate and Required Flood Storage," Metropolitan Sanitary District of Greater Chicago, Chicago, Ill., 1972.
3. Kao, T. Y., "Hydraulic Design of Storm Water Detention Basin," Mini Course No. 3, *National Symposium on Urban Hydrology and Sediment Control*, July, 1975.
4. Poertner, H. G., "Design Criteria, Procedures and Techniques," *Practices in Detention of Urban Storm Water, Special Report No. 43*, American Public Works Association, 1974.
5. Rao, G. V. V., "Methods for Sizing Storm Water Detention Basin—A Designer's Evaluation," *National Symposium on Urban Hydrology and Sediment Control*, July, 1975.

Debris Flow on Prismatic Open Channel[a]

Errata

The following corrections should be made to the original paper:

Page 384, Caption of Fig. 2: Delete "$d = 5$ mm";

Page 387, Eq. 18, left hand side: Should read "$\frac{|h - h_\infty|}{h_\infty}$" instead of "$\frac{|h - h_\infty}{h_\infty}$"

Page 387, paragraph 1, lines 1 and 2: Should read "moving at velocity V" instead of "moving at velocity v"

Page 388, Caption of Fig. 5: Delete the last equation "$\rho = 1.0\ \mathrm{g/cm^3}$"

Page 393, Eq. 32, left hand side: Should read "$\frac{d^2y}{dt^2}$" instead of "$\frac{d^2u}{dy^2}$"

Page 393, Eq. 33a, right hand side: Should read

"$$\frac{2}{1+r}\,\frac{(0.5r^{1/3} + 0.5 + \lambda^{-1})^2(r^{1/3} + \lambda^{-1})^3}{(1+\lambda^{-1})^5}$$" instead of

"$$\frac{2}{1+r}\,\frac{(0.5r^{1/3} + 0.5 + \lambda^{-1})^2(r^{1/3} + \lambda^{-1})}{(1+\lambda^{-1})^5}$$"

Submerged Radial Hydraulic Jump[b]

Errata

The following corrections should be made to the original paper:

Page 357, Eq. 11: Should read "$\frac{\Delta E}{E_1} = 1.0 - \left[\frac{0.5F_1^2 + r_0^2 y_0^3}{(r_0 y_0)^2(0.5F_1^2 + S)}\right.$" instead of "$\frac{\Delta E}{E_1} = 1.0 - \frac{S + 0.5F_1^2 - r_0^2 y_0^3}{(r_0 y_0)^2\,[0.5F_1^2 + S]}$"

Page 363, Eq. 22: Should read "$y_p = \frac{\frac{p}{\gamma} - y_1}{y_2 - y_1}$" instead of "$y_p = \frac{\frac{p}{\gamma} - y_1}{r_2 - r_1}$"

---

[a] March, 1980, by Tamotsu Takahashi (Proc. Paper 15245).

[b] March, 1980, by John A. McCorquodale and Abdelkawi M. Khalifa (Proc. Paper 15250).

Cavitation Induced by Turbulence in Stilling Basin[a]

Discussion by Ryszard Błazejewski[2]

The procedure of estimating minimal values of the fluctuating pressure causing a cavitation of the stilling basin bottom, presented by the author seems oversimplified. The author assumes a hydrostatic distribution of the mean static pressure while results of the writer's experiments indicate that pressure values at the bottom of the stilling basin closely to the sluice exceed the value $p_a + \rho g y_m$ (sometimes even by 20%).

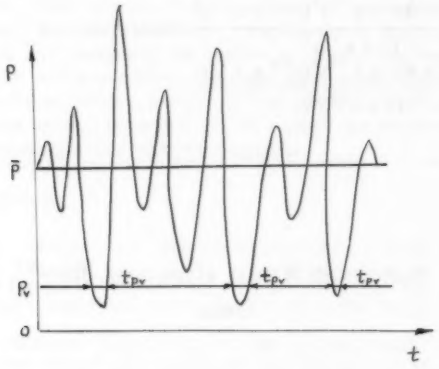

FIG. 3.—Pressure at Stilling Basin Bottom

What deserves, however, even more serious objections is the author's very estimation of the influence of fluctuating pressures, p, upon the cavitational process. In this writer's opinion, the duration of instantaneous pressure below the level p_v should also be taken into consideration. According to Johnson (7), the appearance of bubbles in the process of cavitation requires the time $t_{cr} = 10^{-2}$ sec + 10^{-5} sec. An estimation of this critical time is still an open question. The mean value of the duration of instantaneous pressure below the level p_v (Fig. 3) may be obtained from the following formula:

[a]April, 1980, by Rangaswami Narayanan (Proc. Paper 15305).
[2]Lect., Dept. of Reclamation, Agric. Academy, Poznań, Poland.

$$\bar{t}_{p_v} = \frac{\int_0^{p_v} f(p)dp}{P(p_v)} \quad \ldots\ldots\ldots\ldots\ldots\ldots\ldots\ldots\ldots\ldots\ldots\ldots\ldots\ldots (5)$$

in which $\int_0^{p_v} f(p)dp$ = the intermittency factor (see Fig. 4); and $P(p_v)$ = the mean number of runs below the level p_v, per unit time.

For stationary Gaussian functions

$$P(p_v) = \frac{1}{2\pi} \exp\left[\frac{-(\bar{p} - p_v)^2}{2\sigma_p}\right] \frac{\sigma_a}{\sigma_p} = \frac{1}{2\pi} \exp\left[\frac{-(\bar{p} - \bar{p}_v)^2}{2\sigma_p}\right] \omega_o \quad \ldots\ldots (6)$$

in which σ_a = the root mean square value of $a = dp/dt$; σ_p = the root mean square value of fluctuating pressure p; and ω_o = the mean frequency of pressure fluctuations. Naturally, the cavitation will appear when $\bar{t}_{p_v} \geq t_{cr}$.

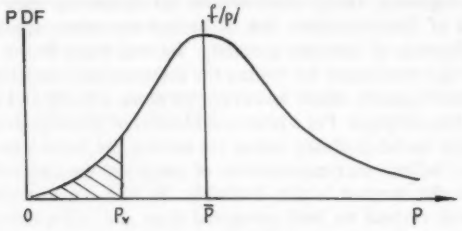

FIG. 4.—Skewed Distribution for Pressure

It is worth mentioning here that the probability distribution of pressure is Gaussian (normal) and usually positively skewed ($As_p > 0$, Ref. 1). This positive skewness cannot remain without influence on the intermittency factor since in the case of consideration the intermittency should be lower than that calculated by the author for $As_p = 0$. Assuming

$$p = Cu^2 = C(\bar{U} + u')^2 \quad \ldots\ldots\ldots\ldots\ldots\ldots\ldots\ldots\ldots\ldots\ldots\ldots (7a)$$

$$\bar{p} = C(\bar{U}^2 + \overline{u'^2}) \quad \ldots\ldots\ldots\ldots\ldots\ldots\ldots\ldots\ldots\ldots\ldots\ldots\ldots\ldots (7b)$$

it is easy to demonstrate that As_p is always positive if the probability distribution of the fluctuating velocity (u') is Gaussian:

$$M_{3c} = \overline{(p - \bar{p})^3} = 8c^3 [3\bar{U}^2(\overline{u'^2})^2 + (\overline{u'^2})^3] \quad \ldots\ldots\ldots\ldots\ldots\ldots (8)$$

otherwise $As_p = (M_{3c}/\sigma_p^3) > 0$.

Finally, the writer would like to draw the reader's attention to calculational errors in the example provided by the author since for $F = 15$, $V_1 = 60$ m/s the values of y_1, y_2, y_m and k should respectively be 1.63 m, 33.79 m, 6.71 m, and 1.84.

APPENDIX.—REFERENCE

7. Johnson, V. E., "Mechanics of Cavitation," *Journal of the Hydraulics Division*, ASCE Vol. 89, No. HY3, Proc. Paper 3530, May, 1963, pp. 251–275.

Laboratory Verification of a Dam-Break Flood Model[a]

Discussion by Nikolaos D. Katopodes[2] and David R. Schamber,[3]
Associate Members, ASCE

In comparing computed and measured data, one is commonly obsessed by the idea that if there is some kind of discrepancy between the two, the mathematical model must be adjusted or calibrated so that it finally agrees with the laboratory or field observations. The method of characteristics, in particular, has been known to be a rigorous, nearly exact scheme for computing open channel flow in the absence of discontinuities, but of limited use when applied to natural streams and channels of complex geometry. Its real value lies in the fact that it can serve as the touchstone for testing the accuracy and consistency of other more approximate models, which however, are more tolerant and reliable when applied to real life problems. For a prismatic channel of rectangular cross section, the characteristic model is ideally suited for solving the Saint-Venant equations and the writers believe that introduction of empirical parameters or arbitrary assumptions to the method is not desirable. In fact, experience shows that best results with respect to both measured data and self-consistency of the model are obtained when the purity of the method is preserved.

During the numerous tests of the five dambreak models developed by Strelkoff and the writers in Ref. 11, it was believed that measurements of the Waterways Experiment Station on the smooth channel were the easiest to reproduce, primarily because of the rigorous estimation of the hydraulic resistance. The characteristics model, XTICSDAM, on a variable grid using 21 computation nodes with maximum node spacing of 20 ft and a maximum time step of 2 sec, predicted the rate of advance of the surge on the dry channel within 1% of the WES data corresponding to the first series. The stage hydrographs also agreed favorably with the experimental data for these runs. In all cases, the volume error was less than 0.5% until recession began, increasing up to 2% thereafter due to the neglected volume of the trailing edge.

The author has assumed an existing base flow in his simulation of the dambreak floodwave in a dry channel with apparent success. The generality of such fictitious initial and boundary conditions is questionable, however, in the light of evidence that numerical experiments using progressively smaller base flows as initial conditions do not produce results converging towards the dry bed solution. In the presence of channel resistance, the extremely small depth computed at the shock front, due to downstream depths that are close to zero, results in very large values for the S_f term in the governing equations and in fact renders the entire model meaningless, unless unreasonably small values of Δt

[a]April, 1980, by Cheng-Lung Chen (Proc. Paper 15324).
[2]Asst. Prof. of Water Resources and Civ. Engrg., Univ. of Louisville, Louisville, Ky. 40208.
[3]Asst. Prof., Dept. of Civ. Engrg., Univ. of Utah, Salt Lake City, Utah.

are used to carry out the computations. Whitham's assumption (12) in effect removes this singularity quite successfully and, in addition, eliminates the need for having to guess the initial conditions. Apparently, there exists a small hypothetical value of base flow which produces results in agreement with the dry bed computations and the experimental data depending, however, on dam height channel geometry and resistance characteristics. Therefore, one would have to determine empirically the appropriate base flow size for each case, which reduces substantially the predictive ability of the method.

In addition, the writers would like to express their concern with regard to the use of an arbitrary base flow and a Manning n given by Eq. 5 for WES run 1.2. The resistance characteristics of this case are shown in Fig. 1 and the test was intended to be under dry bed conditions. However, water trapped between the 3/4-in. angles used for roughening the surface, created a still-water

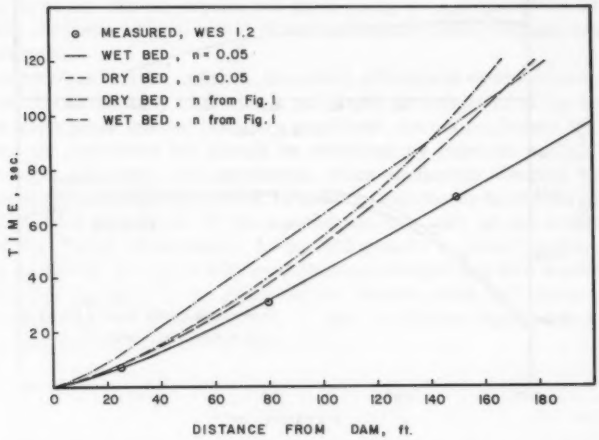

FIG. 14.—Advance Trajectories for WES Case 1.2 under Various Channel Conditions

"base flow" condition of an average depth of 0.06 ft. Advance curves are shown in Fig. 14 for both dry and wet bed conditions corresponding to two different modes of evaluating channel resistance. Note that the small depths encountered near the wave front are way out of the range of Fig. 1 (or Eq. 5), which after all was obtained under conditions of steady uniform flow. The computed advance trajectories indicate that satisfactory agreement with the experimental data can be obtained if one uses an existing depth condition of 0.06 ft downstream of the dam and a constant Manning n value of 0.05 (which corresponds to a depth of 0.24 ft that is most representative of the depths encountered over the entire length of the wave).

Another interesting point arises from observation of Figs. 4 and 5. At the negative wave the depth and velocity profiles approach the horizontal tangentially, which is of course incorrect, since the negative wave front represents a

discontinuity in the slope of forward characteristics emanating from the undisturbed zone in the reservoir. The depression wave front is therefore a discontinuity in the slope of the depth and velocity profiles too, and interpolation across it is strictly prohibited. The so-called "numerical noise" in Fig. 5 may very well have been the light penalty for this violation.

At the other end of the computational domain, the oscillations in the velocity profiles and hydrographs may simply be the consequence of the abrupt change in grid spacing near the wave front associated with the method of characteristics on a fixed grid, which results in a numerical diffraction-like effect at the interface between computational cells differing too much in size. The message related by these "wiggles" is that a variable, moving grid should be used, especially under conditions of high resistance (11).

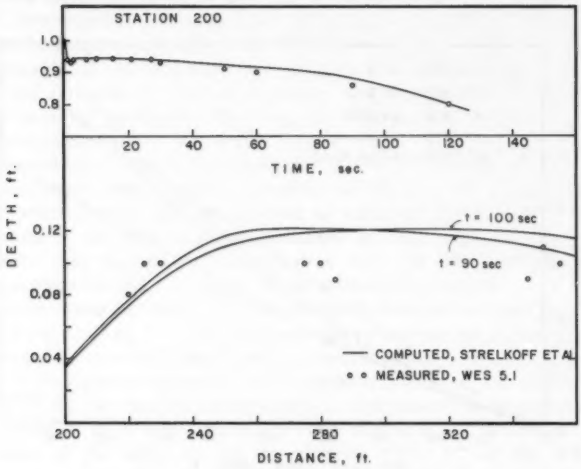

FIG. 15.—Comparison of Computed and Measured Results for WES Case 5.1

For the simulation of partial breach conditions the author has introduced an arbitrary parameter, α, determined by trial and error, which besides reducing the method of characteristics to a semi-empirical model, is unnecessary. Physical observation and two-dimensional computations show that the so-called "conveyance width" has no physical meaning in the flow through a partially breached dam (11). In fact, its use together with some questionable internal boundary conditions, have led the author to the conclusion that the characteristic model fails as the size of the breach decreases, which contradicts the most basic principles of open channel flow. Strelkoff et al., (11) have shown that conservation of mass and energy at the breach section are the appropriate conditions for the free-flowing breach. A solution exists only if both sides of the breach are initially occupied by simple waves, i.e., regions of uniform flow, and the breach itself is treated as a discontinuity in depth and velocity. Fig. 15 shows the results of XTICSDAM for WES case 5.1, corresponding to the author's computa-

tions in Fig. 7. The hydrograph at station 200 (which by inference to the original experimental data appears to be just upstream of the breach), is in satisfactory agreement with the measured data. A profile is shown on the downstream side of the breach in order to eliminate the author's doubts about the accuracy of the WES data, which, incidentally, remain constant for the period between 90 sec and 100 sec. The hydrograph shown in Fig. 7 (STA 200) is 37% too low if compared to the high side of the discontinuity or 400% too high if compared to the low side. The fundamental assumption in the free flowing breach is that the flow passes through critical there at *all* times. During the early stages of dambreak this is true for even complete breach, but thereafter, due to slope and resistance effects, the critical section is not necessarily at the dam site. Imposition of critical conditions at the breach section for nearly complete failure undoubtedly is in error, since the breach will not be small enough to choke the upstream flow and create the assumed critical conditions. For smaller breach widths, however, this assumption will more nearly be appropriate for all times and thus, the computational results should agree more closely with experimental measurements.

For submerged breach conditions, the author, although no results are presented, suggests that "continuity of discharge and depth on both sides of the breach" are the appropriate internal boundary conditions. Across the breach the depth may not be continuous but should be computed by judicious application of conservation of energy and momentum (when applicable), coupled with the appropriate characteristic equations. In addition, one should distinguish between conditions of submergence of the supercritical flow only on the downstream side of the breach discontinuity, which still permits a critical section in the breach, and conditions of full submergence, where the upstream flow is completely coupled with the downstream computations. Results under both these circumstances have been presented in Ref. 11 and are further explored in a paper to be published in this journal by the writers.

Turbulence Prediction in Open Channel Flow[a]

Discussion by Darrel M. Temple,[4] A. M. ASCE

The authors are to be commended for their development of a straightforward approach to the complex problem of turbulence prediction and analysis. The results presented (described by the authors as preliminary) show this approach is deserving of consideration in future investigations. However, their model contains an inconsistency in its assumptions that should be recognized and

[a]April, 1980, by Ruh-Ming Li, James D. Schall, and Daryl B. Simons (Proc. Paper 15347).

[4]Research Hydr. Engr., United States Dept. of Agr., Science and Education Administration, Agricultural Research, Southern Region, Water Conservation Structures Lab., Room 227, Agr. Hall, P.O. Box 551, Stillwater, Okla. 74074.

corrected in future applications. This inconsistency is a result of using Eq. 12 to evaluate the viscous term in Eq. 10.

Eqs. 11 and 12 are statements of Prandtl's "universal velocity defect law." The assumptions classically used to analytically derive this velocity distribution are presented by Schlicting (9) and may be summarized as: (1) The viscous stress is negligible; (2) Prandtl's mixing-length hypothesis is applicable and the mixing length is proportional to the distance from the solid boundary; and (3) the shear stress is constant over the entire flow depth.

Since the region of applicability of Eq. 12 is limited to that portion of the flow field where the viscous stress is much less than the turbulent stress, its use to evaluate the viscous term in Eq. 10 is, at best, questionable. Also, if the first assumption is applied to Eq. 9, the result is a linear variation of shear stress with y, rather than the constant required by the third assumption.

TABLE 3.—Influence of Viscous Term on Computed Value of $E(U_iV_i)$

Variable (1)	Data (2)	(3)	(4)	(5)	(6)	(7)	(8)
y_i/h	0.0001	0.001	0.01	0.1	0.5	0.9	1.0
$\left\lvert \frac{\left(\frac{\nu u_*}{\kappa y_i}\right)}{E[U_iV_i]} \right\rvert$	0.333	0.026	0.0025	0.0003	0.0001	0.0003	1.000

Note: $u_* = 0.30$ m/s $= 1.0$ ft/sec; $h = 0.30$ m $= 1.0$ ft; $\nu = 9 \times 10^{-7}$ m^2/s $= 10^{-5}$ sq ft/sec; and $\kappa = 0.4$.

The error resulting from these inconsistencies will depend on the relative magnitudes of u_* and h. Table 3, constructed using Eq. 13 for "typical values" of u_*, h and ν for flume data, shows the influence of the computed viscous term is small over most of the flow depth, suggesting that the results presented by the authors are valid. It is evident, however, that the use of Prandtl's logarithmic velocity profile prevents the turbulent stress, computed by Eq. 10, from satisfying the physically imposed boundary conditions of $E(UV) = 0$ at $y = 0$ and at $y = h$. Since this behavior is primarily a consequence of applying the first assumption, results resembling those presented in Table 3 would be obtained for other logarithmic mean velocity profiles derived by varying the second and third assumptions.

If that portion of the flow field near the solid boundary is excluded from consideration (as must be the case when a logarithmic mean velocity profile is assumed), the turbulence-prediction model may be made consistent by dropping the viscous term entirely from Eq. 10. The means of computing the time-averaged velocity profile then takes on secondary importance, although maintenance of a consistent set of assumptions is desirable. If the primary interest is in turbulence-parameter prediction near the solid boundary, the solution is not as clear. Possibilities warranting further investigation include two layer, time-averaged velocity distribution models with the viscous term handled consistently within each layer, and empirical curve fit models that force the first derivative $(d\bar{u}/dy)$ to fit the boundary conditions, as well as forcing the time-averaged velocity profile to be reasonably predicted.

Linear Reservoirs and Numerical Diffusion[a]

Discussion by Witold G. Strupczewski[2] and Zbigniew W. Kundzewicz[3]

There is a tendency in a part of hydrology literature to consider the conceptual flood routing models as inherently combined with the finite difference method of solution. By manipulating with the parameters of difference schemes one can achieve effects absent in original models. The author introduced a parameter, C (Courant number) by combining a conceptual parameter (K) and a numerical parameter (Δx). Depending on the value of the parameter, C, the model of a single linear reservoir produces amplification (for $C > 2$), attenuation (for $C < 2$), or conservation (for $C = 2$). According to the author, for the case of $C < 2$ "numerical diffusion is introduced in the computations in order to simulate the physical diffusion process." However, the need for numerical introduction of diffusion effects to the model of a cascade of linear reservoirs is questionable. The model itself is a fair approximation of the diffusion analogy (this statement can be illustrated by the compatibility of impulse responses of both models).

The finite difference approach is not the only method of solution of a differential equation of a conceptual model. By using the impulse response function of a cascade of linear reservoirs (Eq. 1) one can conveniently determine the response of the model to an arbitrary input signal, making use of the following well known integral operator

$$y(t) = \int_0^{\infty} Q(\tau)\, x\ (t-\tau)\, d\tau = y_o(t) + \int_0^{t} Q(\tau)\, x\ (t-\tau)\, d\tau \quad \ldots\ldots\ldots \quad (22)$$

in which x = input signal; y = output signal; Q = impulse response; and y_o = term responsible for the impact of initial condition upon the output signal in the time, t.

For the case of an initially relaxed system Eq. 22 is reduced to the form of convolution equation [i.e., $y_o(t) \equiv 0$ for all t].

In the routing example considered by the author one can, making use of integral operators, determine the model responses analytically. The pulse response of the cascade of linear reservoirs can be found by integrating the impulse response of the model

$$y_{\text{pulse}}(t) = S(t) - S(t-t_o) = \int_0^{t} Q(\tau)\, d\tau - \int_0^{t-t_o} Q(\tau)\, d\tau = \int_{t-t_o}^{t} Q(\tau)\, d\tau \quad (23)$$

[a]May, 1980, by Victor Miguel Ponce (Proc. Paper 15393).

[2]Head of Div., Inst. of Geophysics, Polish Academy of Sci., Warszawa, Poland.
[3]Research Hydro., Inst. of Geophysics, Polish Academy of Sci., Warszawa, Poland.

in which t_o = duration time of rectangular pulse input signal; and S = unit step response of the model (S-hydrograph). The values of the integrals from Eq. 23 can be determined analytically for integer values of the parameter n, with the help of the following equation (12).

$$\int x^n e^{ax} dx = \frac{1}{a} x^n e^{ax} - \frac{n}{a} \int x^{n-1} e^{ax} dx \quad \ldots \ldots \ldots \ldots \ldots \ldots \quad (24)$$

The theoretical solutions prove that the model acts in a diffusionlike manner, whereas amplification or conservation of the amplitude are not inherent properties of the model and result from the numerical method of finite differences.

In the general case of real value, n, and of an arbitrary input signal, analytic evaluation of the integral from Eq. 24 is not possible. However even then simulation can be easily performed with the help of a pocket-sized calculator. Study of more sophisticated convolution models solved with the help of a programmable calculator was presented by Keefer (15).

Integral operators enable calculation of the model response for any number of linear reservoirs directly from the input signal. One does not have to calculate the transformation of the flow in intermediary reservoirs.

Assuming the kernel function is properly defined, routing by convolution is always stable. Therefore the choice of the time interval, Δt, is not constrained by any stability condition. The time step, Δt, warranting the proper accuracy of the numerical convolution routine depends upon the dynamics of the input signal and of the system impulse response function.

If the convolution integral is evaluated by the following discrete representation

$$y_n = \sum_{i=1}^{n} h_i x_{n-i+1} \Delta t \quad \ldots \ldots \ldots \ldots \ldots \ldots \ldots \ldots \ldots \ldots \quad (25)$$

then the value of the time step Δt (or – of the analogate of the Courant number $C = \Delta t / K$) should be sufficiently small to ensure that all discrete moments approximate well the moments of respective continuous time functions. In particular, the continuity condition

$$\left| \sum_{i=1}^{\infty} h_i \Delta t - 1 \right| = \left| \sum_{i=1}^{\infty} KCh_i - 1 \right| \leq \epsilon_1 \quad \ldots \ldots \ldots \ldots \ldots \quad (26)$$

and the condition of compatibility of the time step chosen and of the dynamics of the input signal

$$\left| \sum_{i=1}^{n} x_i \Delta t - \int_0^t x(t')dt' \right| = \left| \sum_{i=1}^{n} KCx_i - \int_0^t x(t')dt' \right| \leq \epsilon_2 \quad \ldots \ldots \ldots \quad (27)$$

should be fulfilled.

It is easy to see that large values of C are not of concern in convolution modelling, since in such a case the bulk of the impulse response function (or range in which variations of input signal occur) may be skipped over.

The formula for the parameter Δx (reach length corresponding to a linear reservoir, i.e., the so-called characteristic reach length) was obtained by Ponce by setting $x = 0$ in Eq. 8 for a physical interpretation of the parameter x of the Muskingum model. The physical sense of the parameter Δx can be found

more directly by: (1) Simplifying the hydrodynamical equation of flow (14); and (2) comparison of impulse responses of the conceptual model of cascade of linear reservoir and of the linearized Saint Venant equations [moment matching method (13)].

Another point that in the writers' opinion deserves discussion is the author's attitude with respect to off-centering of the difference schemes for the Muskingum model and for the kinematic wave approach. If the Muskingum model has to approximate the kinematic wave model one has to use the value of parameter x equal to 0.5 (17).

As will be shown later a cascade of Muskingum models with parameter $x = 0.5$ gives better approximation of the kinematic wave model. Let us apportion the overall modeled reach of the length L into n subreaches, each of the length ΔL. Let us consider the cascade of n Muskingum models, each having the parameters $x = 0.5$ and $K = \Delta L/c = L/(nc)$, in which c = the constant wave celerity. If n tends to infinity, the cascade of Muskingum models tends to the kinematic wave model. This can be clearly demonstrated by means of the transfer function approach. The transfer function for a multiple Muskingum model reads

$$H(s) = \left(\frac{1 - \frac{Ks}{2}}{1 + \frac{Ks}{2}}\right)^n = \left(\frac{1 - \frac{1}{n}\frac{Ls}{2c}}{1 + \frac{1}{n}\frac{Ls}{2c}}\right)^n \quad \ldots\ldots\ldots\ldots\ldots\ldots \quad (28)$$

As can be proved with the help of the de L' Hôspital theorem, this transfer function tends for $n \to \infty$ to the transfer function of the kinematic wave model

$$H(s) = e^{-Ks} = e^{-Ls/c} \quad \ldots\ldots\ldots\ldots\ldots\ldots\ldots\ldots\ldots\ldots \quad (29)$$

As shown in Ref. 16 the values of the parameter x different from 0.5 are the consequence of hydrodynamics; thus, the off-centering of the scheme for the Muskingum model is physically interpretable.

Appendix.—References

12. Bronstejn, J. W., and Semendajev K. A., *Spravocnik po Matematike dla Inzenerov i Ucascikhsja vtuzov*, 11th ed., Nauka, Moskva, U.S.S.R., 1967.
13. Dooge, J. C. I., "Linear Theory of Hydrologic Systems," *Technical Bulletin No. 1468*, Agricultural Research Service, United States Department of Agriculture, Washington, Feb., 1973.
14. Kalinin, G. P., and Miljukov P. I., "Približennij Rasčot Neustanovivšegosja Dvizenija Vodnikh Mass," *Trudy CIP*, Vol. 66, Leningrad, U.S.S.R., 1958.
15. Keefer, T. N., "Desktop Computer Flow Routing," *Journal of the Hydraulics Division*, ASCE, Vol. 100, No. HY7, Proc. Paper 10669, July, 1974, pp. 1047–1058.
16. Strupczewski, W., and Kundzewicz, Z., "Muskingum Method Revisited," *Journal of Hydrology*, Vol. 48, No. 3/4, Nov., 1980.
17. Strupczewski, W., and Kundzewicz, Z., "Translatory Characteristics of the Muskingum Method of Flood Routing—A Comment," *Journal of Hydrology*, Vol. 48, No. 3/4, Nov., 1980.

Hydrographs by Single Linear Reservoir Model[a]

Discussion by James M. Stubchaer,[4] F. ASCE

The authors discuss the theory of the linear hydrograph method and correctly state its limitations. They point out that many urban watersheds are within these limitations. The writer has found that there are many practical applications for a similar method (17) published in 1975 in the analysis and design of urban and some rural drainage systems.

The comparative advantage of single linear reservoir model (SLR) as used in the Santa Barbara Urban Hydrograph (SBUH) method is the ease of application and the few parameters required. In the SBUH method, K is calculated as the time of concentration of the watershed, as in the "Rational Method," and therefore most civil engineers are already familiar with the procedure. The time of concentration in most practical applications can be estimated from the physical characteristics of the watershed and, unlike K in Eq. 15, is independent of storm characteristics. The writer believes that the assumptions necessary to apply Eq. 23 to real watersheds, which do not have planar surfaces or constant rainfall intensities, are no more accurate than approximations used in estimating times of concentration.

The SLR model and SBUH method require little computational effort compared with other hydrograph methods. Routing rainfall excess through a linear reservoir does not require a computer, and can even be done graphically (20). A step by step procedure for calculating a hydrograph by the SBUH method follows:

1. The storm rainfall amount and distribution are determined. The storm is divided into time periods (t), each with a duration of the time interval (Δt) selected. The appropriate amount of rainfall is assigned to each time period [$P(t)$].
2. The impervious portion of the watershed (Imp) which is effectively hydraulically connected is estimated.
3. The pervious infiltration rate in inches per time increment (f) is determined.
4. The watershed area in acres (A) and the time of concentration in hours (Tc) are determined.
5. Runoff depths for each time period (t) are calculated:

$$\text{Pervious area runoff,} \quad R0 = (1 - \text{Imp})[P(t) - f] >= 0 \quad \ldots\ldots\ldots \quad (25)$$

$$\text{Impervious area runoff,} \quad R1 = \text{Imp}\, P(t) \quad \ldots\ldots\ldots\ldots\ldots\ldots \quad (26)$$

[a]May, 1980, by John T. Pedersen, John C. Peters, and Otto J. Helweg (Proc. Paper 15430).

[4]Engr.-Mgr., Santa Barbara County Flood Control and Water Conservation District, 123 E. Anapamu St., Santa Barbara, Calif. 93101.

Total runoff depth for each time period, $R(t) = R0 + R1$ . . . . . (27)

6. The "Instantaneous Hydrograph" ordinates $[I(t)]$ in cubic feet per second for each time period (t) are obtained by multiplying the runoff depths for each time period by the drainage area and a conversion factor:

$$I(t) = \frac{1.008\, R(t) A}{\Delta t} \quad \ldots\ldots\ldots\ldots\ldots\ldots\ldots\ldots\ldots\ldots \quad (28)$$

7. The final hydrograph ordinates $[Q(t)]$ in cubic feet per second are obtained by routing the instantaneous hydrograph through a single linear reservoir with a time delay equal to the time of concentration

$$Q(t) = Q(t-1) + C_1\,[I(t-1) + I(t) - 2\,Q(t-1)] \quad \ldots\ldots\ldots\ldots \quad (29)$$

in which $$C_1 = \frac{\Delta t}{2\,\mathrm{Tc} + \Delta t} \quad \ldots\ldots\ldots\ldots\ldots\ldots\ldots\ldots\ldots\ldots \quad (30)$$

Note that Eq. 29 is applied only once for each time period.

In addition to the author's and writer's work, the SLR model as used in the SBUH method has been tested against observed data in Florida by Golding (19) with good results. The writer believes the method is appropriate in many practical cases where complete hydrographs are required, such as design of stormwater retarding basins. Therefore, it is important to emphasize how easy it is for a nonspecialized engineer to apply so that the model may be used more widely.

Appendix I.—References

19. Golding, B. L., "Hydrograph Synthesis by the HNV-SBUH Method," presented at the June 19–20, 1980, SWMM Users Group Meeting, held at Toronto, Canada.
20. Wilson, W., "A Graphical Flood Routing Method," *Transactions of the American Geophysics Union*," Vol. 21, Part 3, 1941, pp. 893–898.

Appendix II.—Notation

The following symbols are used in this discussion:

A = drainage area, in acres;
f = infiltration rate on pervious area, in inches per time period;
$I(t)$ = instantaneous hydrograph ordinate, in cubic feet per second;
Imp = hydraulically connected impervious portion of watershed decimal;
$P(t)$ = rainfall in time period, t, in inches;
$Q(t)$ = final hydrograph ordinate for time period t, in cubic feet per second;
$R0$ = pervious area runoff, in inches;
$R1$ = impervious area runoff, in inches;
$R(t)$ = runoff depth for time period, t, in inches; and
Tc = time of concentration, in hours.

Curve-Number Procedure as Infiltration Method[a]

Discussion by Richard H. Hawkins[2]

The author has innocently credited the originality of Eq. 4 to Smith (8). The basic authorship might more appropriately be attributed to Cheng-lung Chen, who first derived the expression in 1975 (9,10). This mixup is due in large part to oversights by the writer in review stages of Hjelmfelt's manuscript. While exposed to Chen's 1975 work several times, the writer was not fully conscious of the presence of Eq. 4, and thus overlooked correcting to the earlier dated citation. In fact, several other papers by the writer (2,11,12,13) between 1975 and the present contain the same equation—or near equivalents—without reference to Chen's work. Thus, in a spirit of honest embarrassment, apologies are extended here to Chen for slighting his earlier contributions. Hjelmfelt's paper has served as a vehicle to promote this recognition.

Future researchers probing curve number algebra would do well to study Chen's pioneering work in detail. Lacking an even earlier dated claim, perhaps it would be appropriate hereafter to refer to Eq. 4—and closely allied forms—as "Chen's Equation," i.e.

$$f(t) = \frac{dF}{dt} = \frac{S^2}{(P - I_a + S)^2} \frac{dP}{dt}; \quad P > I_a \quad \ldots\ldots\ldots\ldots\ldots\ldots \quad (11)$$

It should be noted that the foregoing equation is a correction of what is probably a typesetting error in the published paper. The exponent 2 should refer to the entire denominator, and not just S.

Appendix.—References

9. Chen, C. L., "Urban Storm Runoff Inlet Hydrograph Study," *Soil-Cover-Moisture Complex: Analysis of Parametric Infiltration Models for Highway Sideslopes, Publication PRWG 106-5,* Vol. 5 Utah Water Research Laboratory, Logan, Utah, 1975.
10. Chen, C. L., "Urban Storm Inlet Hydrograph Study," *Soil-Cover-Moisture Complex: Analysis of Parametric Infiltration Models for Highway Sideslopes, Federal Highway Administration Report FHWA-RD-76-120,* Vol. 5, Federal Highway Administration, 1976; available from U.S. National Technical Information Service, Springfield, Va., as *PB 263989.*
11. Hawkins, R. H., "Effects of Rainfall Intensity on Runoff Curve Number," *Hydrology and Water Resources of Arizona and the Southwest,* Vol. 8, 1978, pp. 53–64 (AWRA and AAAS Arizona Meeting, Flagstaff, Ariz., April 14–15, 1978).
12. Hawkins, R. H., "Inferring Curve Numbers from Simulator Data," *Proceedings of the Rainfall Simulator Workshop,* Tucson, Ariz., March, 1979; USDA, *SEA Pub. ARM-W-10,* pp. 65–78.
13. Hawkins, R. H., "Infiltration and Curve Numbers: Some Pragmatic and Theoretic Relationships," *Symposium on Watershed Management,* 1980, Vol. II, ASCE, 1980, pp. 925–937.

[a]June, 1980, by Allen T. Hjelmfelt, Jr. (Proc. Paper 15449).

[2]Prof., Dept. of Forestry and Outdoor Recreation (Watershed Science Unit), and Dept. of Civ. and Environmental Engrg., UMC 52, Utah State Univ., Logan, Utah 84322.

Steady-State Estimation of Cooling Pond Performance[a]

Discussion by E. Eric Adams,[3] A. M. ASCE

The authors have presented several useful models for predicting the steady-state performance of cooling ponds with different spatial structure. In their last paragraph they suggest that the general use of these models will be for the estimation of average, such as monthly, performance conditions. This use will provide a basis for comparing initial pond designs, design modifications, etc.

They also suggest that steady-state models can be employed with shorter-term data to approximate the transient response of ponds. However, because the response of a pond to transient meteorological input is governed by its depth, the appropriate time interval for averaging input data is of the order of $\rho c_p H/K$ rather than the residence time as implied. In fact, assuming linear heat transfer and constant station operation, the correct transient solution may be viewed (6) as a time series of steady-state solutions evaluated with an exponentially filtered time series of T_E, using a filter parameter $\rho c_p H/K$. An approximately correct transient response is obtained if one averages meteorological input data over a time interval, $\rho c_p H/K$. The value of $\rho c_p H/K$ is typically between 1 day and 1 week which, coincidentally, is in the same range as typical pond residence times given by $A_p H/Q_o$.

It is also noted (6), that the maximum intake temperature predicted with a steady-state model can be as sensitive to the averaging interval as to the spatial structure assumed for the pond (e.g., longitudinally dispersive versus laterally recirculating, plug flow versus well-mixed, etc.). This suggests that the transient response of a pond is an important consideration, even at the design stage.

Appendix.—Reference

6. Adams, E. E., and Koussis, A., "Transient Analysis for Shallow Cooling Ponds," *Journal of the Energy Division*, ASCE, Vol. 106, Proc. Paper 15737, Oct., 1980, pp. 141–153.

[a]June, 1980, by Gerhard H. Jirka and Masataka Watanabe (Proc. Paper 15449)

[3]Lect. and Principle Research Engr., Ralph M. Parsons Lab. for Water Resources and Hydrodynamics, Dept. of Civ. Engrg., Bldg. 48-325, Massachusetts Inst. of Tech., Cambridge, Mass. 02139.

Technical Papers

Original papers should be submitted in triplicate to the Manager of Technical and Professional Publications, ASCE, 345 East 47th Street, New York, N.Y. 10017. Authors must indicate the Technical Division or Council, Technical Committee, Subcommittee, and Task Committee (if any) to which the paper should be referred. Those who are planning to submit material will expedite the review and publication procedures by complying with the following basic requirements:

1. Titles must have a length not exceeding 50 characters and spaces.

2. The manuscript (an original ribbon copy and two duplicate copies) should be double-spaced on one side of 8-1/2-in. (220-mm) by 11-in. (280-mm) paper. Three copies of all figures and tables must be included.

3. Generally, the maximum length of a paper is 10,000 word-equivalents. As an *approximation*, each full manuscript page of text, tables or figures is the equivalent of 300 words. If a particular subject cannot be adequately presented within the 10,000-word limit, the paper should be accompanied by a rationale for the overlength. This will permit rapid review and approval by the Division or Council Publications and Executive Committees and the Society's Committee on Publications. Valuable contributions to the Society's publications are not intended to be discouraged by this procedure.

4. The author's full name, Society membership grade, and a footnote stating present employment must appear on the first page of the paper. Authors need not be Society members.

5. All mathematics must be typewritten and special symbols must be identified properly. The letter symbols used should be defined where they first appear, in figures, tables, or text, and arranged alphabetically in an appendix at the end of the paper titled Appendix.—Notation.

6. Standard definitions and symbols should be used. Reference should be made to the lists published by the American National Standards Institute and to the *Authors' Guide to the Publications of ASCE*.

7. Figures should be drawn in black ink, at a size that, with a 50% reduction, would have a published width in the *Journals* of from 3 in. (76 mm) to 4-1/2 in. (110 mm). The lettering must be legible at the reduced size. Photographs should be submitted as glossy prints. Explanations and descriptions must be placed in text rather than within the figure.

8. Tables should be typed (an original ribbon copy and two duplicates) on one side of 8-1/2-in. (220-mm) by 11-in. (280-mm) paper. An explanation of each table must appear in the text.

9. References cited in text should be arranged in alphabetical order in an appendix at the end of the paper, or preceding the Appendix.—Notation, as an Appendix.—References.

10. A list of key words and an information retrieval abstract of 175 words should be provided with each paper.

11. A summary of approximately 40 words must accompany the paper.

12. A set of conclusions must end the paper.

13. Dual units, i.e., U.S. Customary followed by SI (International System) units in parentheses, should be used throughout the paper.

14. A practical applications section should be included also, if appropriate.